

# JMIR

JOURNAL OF MARITIME RESEARCH  
Spanish Society of Maritime Research

A. Moreno, D. Moreno, D. Chaos and J. Aranda

HARDWARE IN THE LOOP SIMULATION BENCHMARK  
FOR AUTONOMOUS MARINE VEHICLES

A. López, J.A. Somolinos, L.R. Núñez and M. Santamaría

MODELLING AND SIMULATION OF MOORED DEVICES  
FOR OCEAN CURRENTS ENERGY HARNESSING

R. Ferreiro and F. J. Pérez

DEVELOPING MAGNETIC BEARINGS FOR SUBSEA  
OCEANIC ENVIRONMENTS

F. Fernández, E. Besada, D. Sanchez and J. A. López-Orozco

EXPERT GUIDANCE SYSTEM FOR UNMANNED AERIAL  
VEHICLES BASED ON ARTIFICIAL NEURAL NETWORKS

F. Bonin, A. Burguera and G. Oliver

IMAGING SYSTEMS FOR ADVANCED UNDERWATER  
VEHICLES

M.I. Zamanillo, J.M. Zamanillo, E. Revestido and F. J. Velasco

SIDESCAN SONAR IMAGERY PROCESSING SOFTWARE  
FOR UNDERWATER RESEARCH AND EDUCATION  
PURPOSES

**Carlos A. Pérez Labajos**  
Editor

**Amable López Piñeiro**  
Assistant Editor

**Alberto Pigazo López**  
Associate Editor

**Ana Alegría de la Colina**  
**Marlén Izquierdo Fernández**

**Kenneth Friedman**

**Sean Scurlfield**

**Gema Diego Hazas**

Language Revision Committee

**Antonio Trueba Cortés**

**Andrés Ortega Piris**

Navigation

**Francisco Correa Ruiz**

**Máximo Azofra Colina**

**Diana Díaz Guazo**

Marine Safety

**Francisco J. Velasco González**

Automation in Marine Systems

**Beatriz Blanco Rojo**

**José R. San Cristobal**

Shipping Business

**Julio Barros Guadalupe**

**Víctor M. Moreno Sáiz**

**Alberto Pigazo López**

**Ramón I. Diego García**

Electronic and Electrical Systems

#### **UNIVERSITY OF CANTABRIA**

Escuela Técnica Superior de Náutica  
c/ Gamazo nº1, 39004 SANTANDER  
Telfno (942) 201362; Fax (942) 201303  
e-mail: info.jmr@unican.es  
<http://www.jmr.unican.es>

**Layout:** JMR

**Printed by:** Gráficas Ebro, S.L.

**ISSN:** 1697-4840

**D. Legal:** SA-368-2004

#### **EDITORIAL BOARD**

##### **University of the Basque Country**

---

Fernando Cayuela Camarero

Escuela Técnica Superior de Náutica y Máquinas  
Navales

Miguel Ángel Gomez Solaetxe

Dep. de Ciencias y Técnicas de la Navegación,  
Máquinas y Construcciones Navales

##### **University of Cantabria**

---

Carlos A. Pérez-Labajos

Escuela Técnica Superior de Náutica

Félix M. Otero González

Dep. de Ciencias y Técnicas de la Navegación  
y de la Construcción Naval

##### **University of Oviedo**

---

Rafael García Méndez

Escuela Superior de la Marina Civil

Daniel Ponte Gutiérrez

Dpto. de Ciencia y Tecnología Náutica

##### **University of La Coruña**

---

Álvaro Baaliña Insúa

Escuela Técnica Superior de Náutica y Máquinas

José A. Orosa García

Dep. de Energía y Propulsión Marina

Santiago Iglesias Boniela

Dep. de Ciencias de la Navegación y de la Tierra

##### **University of Cádiz**

---

Juan Moreno Gutiérrez

Facultad de Ciencias Náuticas

Francisco Piniella Corbacho

Dep. de Ciencias y Técnicas de la Navegación  
y Teoría de la Señal y Comunicaciones

##### **The Polytechnic University of Catalonia**

---

Santiago Ordás Jiménez

Facultad de Náutica

Francesc Xavier Martínez de Osés

Dep. de Ciencia e Ingeniería Náuticas

##### **University of La Laguna**

---

Alexis Dionis Melian

E.T. S. de Náutica, Máquinas y Radioelectrónica Naval

Isidro Padrón Armas

Dep. de Ciencias y Técnicas de la Navegación

Pedro Rivero Rodríguez

Dep. de Ingeniería Marítima

---

## C O N T E N T S

<b>Hardware in the Loop Simulation Benchmark for Autonomous Marine Vehicles</b> A. Moreno, D. Moreno, D. Chaos and J. Aranda	3
<b>Modelling and Simulation of Moored Devices for Ocean Currents Energy Harnessing</b> A. López , J.A. Somolinos, L.R. Núñez and M. Santamaría	19
<b>Developing Magnetic Bearings for Subsea Oceanic Environments</b> R. Ferreiro and F. J. Pérez	35
<b>Expert Guidance System for Unmanned Aerial Vehicles Based on Artificial Neural Networks</b> F. Fernández, E. Besada, D. Sánchez and J. A. López-Orozco	49
<b>Imaging Systems for Advanced Underwater Vehicles</b> F. Bonin, A. Burguera and G. Oliver	65
<b>Sidescan Sonar Imagery Processing Software for Underwater Research and Education Purposes</b> M.I. Zamanillo, J.M. Zamanillo, E. Revestido and F.J. Velasco	87





## **HARDWARE IN THE LOOP SIMULATION BENCHMARK FOR AUTONOMOUS MARINE VEHICLES**

**A. Moreno<sup>1,2</sup>, D. Moreno<sup>1,3</sup>, D. Chaos<sup>1,4</sup> and J. Aranda<sup>1,5</sup>**

Received 10 December 2010; in revised form 17 February 2011; accepted 18 March 2011

### **ABSTRACT**

The use of autonomous vehicles is becoming ubiquitous due to the versatility and flexibility that they display in the execution of individual and cooperative task, coupled with the fact that their use avoids placing human lives at risk. Closely related to these autonomous systems are the simulation tools. These tools are essential to test the correct design and behaviour of the modelling and control algorithms theoretically. A poor design could have dramatic consequences to the vehicle itself, the rest of vehicles and even the environment in a real scenario. In this work a benchmark for unmanned vehicles is presented. The main objective is to have a generic framework in which to develop and test control algorithms for coordinated and cooperative tasks between different kinds of vehicles. The tool is constructed in a modular way, so as any kind of vehicle can be simulated (or tested) with a slight modification of the program. The benchmark can run continuous and discrete (DEVS and non-DEVS) simulations and it is constructed over LabVIEW as Hardware-In-The-Loop (HIL) simulation platform. Using the same system for simulation and real experiments reduces the cost of hardware tests and facilitates enormously the portability of the theoretical design to the real world. This tool is oriented both for researchers and students, to test their own control algorithms both theoretically and experimentally.

**Key Words:** benchmark, simulation, control, autonomous vehicles, DEVS, LabVIEW.

<sup>1</sup> Universidad Nacional de Educación a Distancia, Calle Juan del Rosal 16, 28040 Madrid, Spain. <sup>2</sup> PhD Student, Email: amoreno@bec.uned.es, Tel. +34 913987147, Fax. +34 913987690. <sup>3</sup> PhD Student, Email: dmoreno@dia.uned.es, Tel. +34 913987942, Fax. +34 913987690. <sup>4</sup> PhD Student, Email: dchaos@dia.uned.es, Tel. +34 913987157, Fax. +34 913987690. <sup>5</sup> Full Professor, Email: jaranda@dia.uned.es, Tel. +34 913987148, Fax. +34 913987690.

## INTRODUCTION

The use of autonomous vehicles in different research and commercial areas has been increasing in the last few years for reasons that have to do with autonomy, flexibility, and the new trend in miniaturization. Moreover, their use in collaborative tasks allows for the realization of complex missions, often with relatively simple systems; see for example the many works related in the robotics field, (Yamaguchi, 2003) for example.

Closely related to these autonomous systems are the simulation tools. These tools are essential to test the correct design and behaviour of the control algorithms theoretically, as many of these autonomous systems has delicate and expensive instrumentation or are working on dangerous conditions. For example, a poor control design of a vehicle could have dramatic consequences to the system itself, other vehicles and even the environment in which it works. For this reason, coupled with the fact that real tests have high cost on time and money, construction of a test bed satisfies the need for a simulation environment that researchers and students can use to implement and analyse cooperative and non-cooperative control algorithms for different kind of unmanned vehicles (aerial, terrestrial and marine) theoretically and experimentally.

There are many works related with the development of tools for simulation in the autonomous vehicles or robotics field. In (Rasmunsens & Chandler, 2002) a simulator for aerospace vehicles is constructed in MATLAB/Simulink to test cooperative control algorithms. The vehicles are 6 DOF and with embedded flight software. In (Luke et al, 2005) a single-process, discrete event simulation core and visualization library written in Java is developed, designed to be flexible enough to be used for a wide range of simple simulations, but with a special emphasis on swarm multi-agent simulations of many agents (up to millions). (Vaughan, 2005) proposes a simple benchmark for multi-robot simulator performance. For a deeper survey in existent simulation environments, the readers are referred to (Craighead et al, 2007) which presents a survey of computer based simulators for unmanned vehicles, covering a wide spectrum of vehicles. This report surveys 14 widely available simulators, showing the main characteristics for an adequate simulation environment.

These works deal with the simulation field, without testing the actual systems. The aim of our work is to have a modular and easily reconfigurable test bed, so as any kind of vehicle can be simulated and tested with a slight modification of the program by hardware-in-the-loop (HIL) simulations. In this sense there exist some works that include hardware-In-The-Loop (HIL) simulations to test the actual hardware and software with the same tool, without the need of field experimentation. In (Jung and Tsiotras, 2007) the modelling and experimental identification results for a small unmanned aerial vehicle (UAV) are presented. A hardware-in-the-loop (HIL) simulation environment is developed to support and validate the UAV autopilot hardware and software development in MATLAB/Simulink. In (Ridao et al, 2004) a multi-

vehicle, real-time, graphical simulator based on OpenGL that allows hardware-in-the-loop simulations is developed for unmanned underwater vehicles (UUV).

Based on previous works, the software framework presented in the current document is expected to be a modelling and control simulation benchmark for unmanned aerial vehicles (UAVs), unmanned marine vehicles (UMVs) and autonomous underwater vehicles (UAVs), that allows the end user to define and customize models and controls of the overall simulation or instead exchange them by hardware such as real vehicles (HIL simulations). Therefore we have the same tool for simulation and real experiments, facilitating enormously the portability of the theoretical design to the real world and reducing significantly the costs of real tests.

The benchmark runs continuous and discrete (DEVS and non-DEVS) simulations to overcome all the spectrum of possible designs. One step forward respect to previous simulations tools for autonomous vehicles is this possibility of running DEVS simulations. The DEVS M&S formalism (Zeigler et al., 2000) provides several advantages to analyse and design complex systems: completeness, variability, extensibility, and maintainability. Furthermore, in a near future will offer options to include environmental disturbances within the simulation. The recreation scenarios vary from unique vehicle to multi-vehicle study. These scenarios are designed to test bottom-line challenges of control of autonomous vehicles. Hereafter, they are described and divided among two different control layers: individual and multiple vehicle autonomous control.

## **SIMULATION PLATFORM**

As it has been commented, the autonomous vehicle simulation platform runs simulations based on discrete events (DEVS and Non-DEVS) along with continuous simulations. Moreover, these simulations can be performed centralized, distributed, remotely within real or virtual time context. In this section we explain the platform architectural and conceptual design, starting from the base on which is built, stepping in the architecture and communication protocol, and ending with the system modelling and configurations.

### **Basis**

As if it was a building, the construction materials are made of DEVS models (also non-DEVS and continuous models, as well as Hardware) and both the simulations protocol and models follow rules based on its formalism. The platform is built with LabView programming tools.

### ***DEVS***

The Discrete Event System Specification is a general formalism for discrete event system modelling based on set theory (Zeigler et al., 2000). It allows representing any

system by three sets and five functions: input set ( $X$ ), output set ( $Y$ ), state set ( $S$ ), external transition function ( $\delta_{\text{ext}}$ ), internal transition function ( $\delta_{\text{int}}$ ), confluent function ( $\delta_{\text{con}}$ ), output function ( $\lambda$ ), and time advanced function ( $ta$ ). The DEVS M&S formalism provides several advantages to analyse and design complex systems: completeness, verifiability, extensibility, and maintainability. DEVS can reproduce Discrete Time System Specifications (DTSS) and approximate continuous modelling paradigms (Differential Equation System Specification (DESS)). That is, DEVS is able to describe discrete event, discrete and continuous systems. Thus, simulation tools based on DEVS are potentially more general than other tools including continuous simulation tools (Kofman, 2004). Furthermore, DEVS conceptually separates models from the simulator, making possible to simulate the same model using different simulators working in centralized, parallel or distributed execution modes. Recently, a working group of the Simulation Interoperability Standards Organization has developed a standard (Zeigler et al., 2008) to support interoperability of DEVS models implemented in different platforms as well as with legacy simulations.

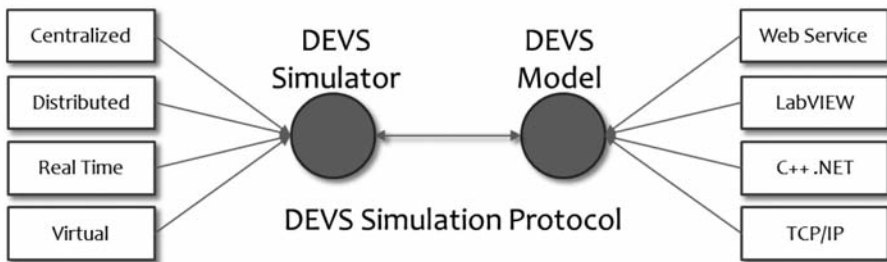


Figure 1: Conceptual Architecture of the Standard.

### **LabVIEW**

LabVIEW's virtual instrument (VI) is a graphical programming language specifically designed for developing instrumentation, diagnostics, and data acquisition systems. Many engineering and scientific disciplines, both professional and academic, have adopted LabVIEW, which has resulted in a broad collection of libraries and legacy code.

Next, we highlight the characteristics of National Instruments software LabVIEW that convinced us to select LabVIEW as our software development framework:

- Hardware integration (HIL).
- Visualization and graph management.
- Real Time.
- Management of communication interfaces (USB, BT, TCP/IP, WS, etc.).
- Data display and user interfaces.

- Multicore programming.
- Multiple Targets and OSs.
- Multiple Programming approaches and interoperability with other languages, applications and paradigms (MATLAB/Simulink, DLL, .NET, ActiveX, etc.).

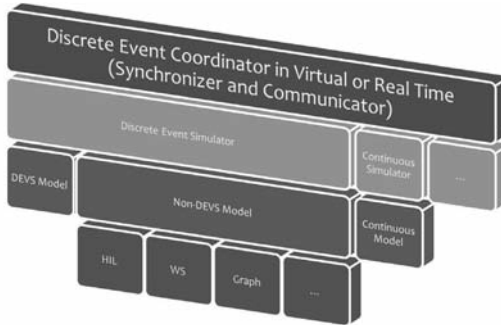


Figure 2: Architecture.

**Architecture**

The architecture is made of three layers: coordination, simulation and modelling. Each layer interacts with the upper or lower layer depending on the simulation protocol step. As seen on Figure 3 the coordinator synchronizes and communicates the simulators that may simulate discrete models, sample a continuous model or other action. A discrete event simulator can simulate a

DEVS or a Non-DEVS model. A non-DEVS model can perform any action discretely, such as Hardware or remote Communication via USB, BT, WS or TCP/IP. While a continuous simulator samples a continuous model at discrete intervals.

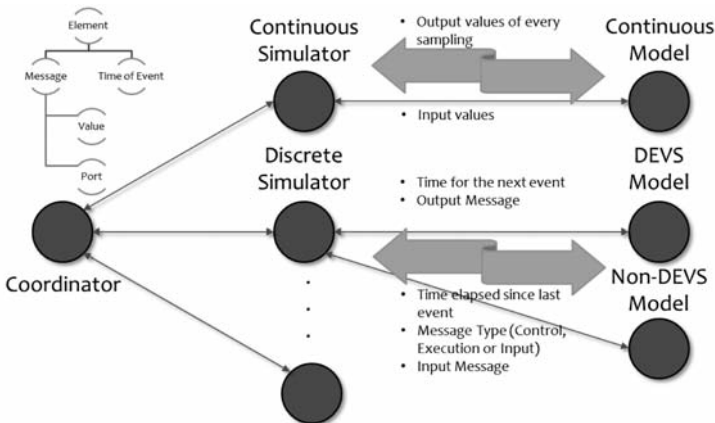


Figure 3: Communication Protocol.

**Communication Protocol**

The communication between coordinator and simulators is achieved by a common structure given by a message and a time event that indicates the time of execution of the next event. In summary, the coordinator communicates with the simula-

tor to send incoming messages, run by time or by a control message and associated event time. Whereas, simulators communicate with the coordinator to send outgoing messages with the time of the next event. Figure 4 illustrates this message exchange protocol with more detail.

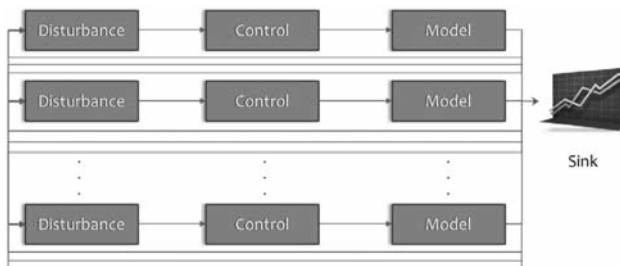


Figure 4: System Modelling.

### System Modelling

The system modelling of an autonomous vehicle experiment scenario is achieved by defining three types of models per individual. A model that prototypes a UAV, UMV, or an AUV through a discrete event or continuous

paradigm. It can also communicate with a real vehicle. The control module performs an intelligent navigation control depending of the overall control strategy over the previous model. Finally, the disturbance model injects alterations in the communications and bounds the field of vision of the vehicle.

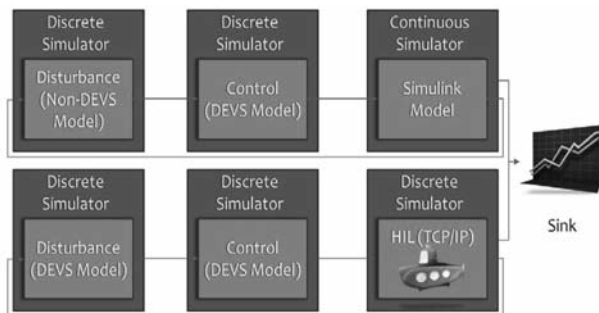


Figure 5: Example Configuration.

### Possible Configurations

Each simulation component may be defined by a DEVS model, non-DEVS model, continuous model, or an interface that interacts with hardware, MATLAB Simulink, DLL, NET, etc. An example configuration is depicted by Figure 6. Also, a model can be built by the user according to

a specific interface for each type. Therefore, a simulation module can behave in any manner while meeting the constraints of the simulation protocol that has been defined. Soon, our tool will provide customized interfaces for automatically link modules to standard communication interfaces such as SOAP Web Services.

### GRAPHICAL USER INTERFACE

One key point of the simulation framework is providing a visual environment that meets the following characteristics; high degree of usability, wide functionality, and offer a pleasant and customizable interface. The platform GUI is divided in two

modules. On the one hand, a scenario editor, which provides a graphical interface for configuring an autonomous vehicle experiment. On the other, the simulation graphical environment, that illustrates the on-going experiment results.

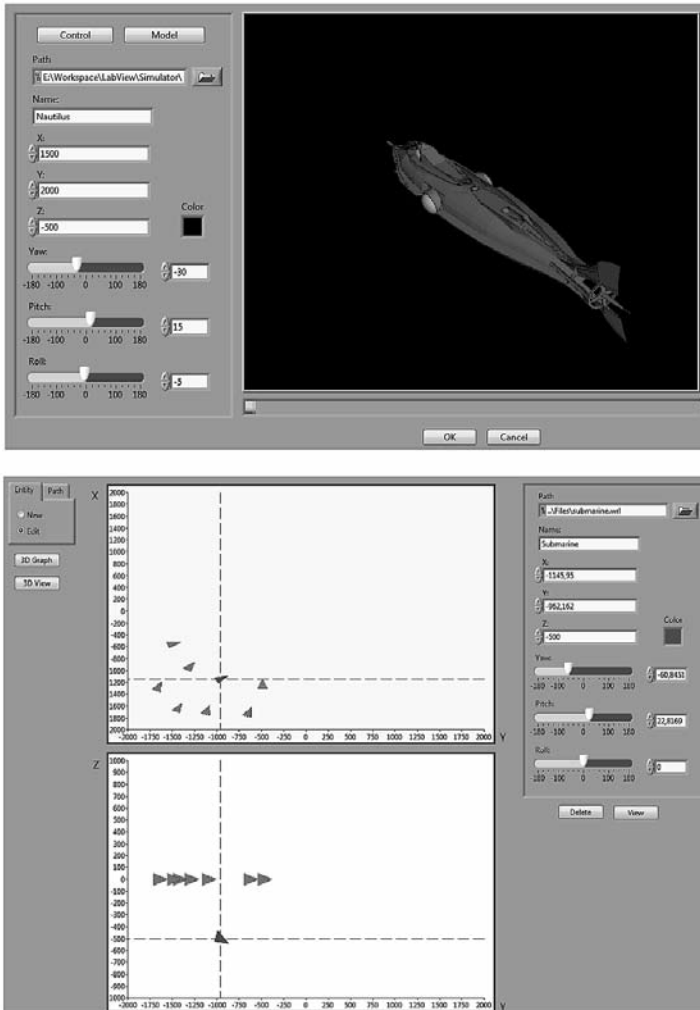


Figure 6: Scenario editor captures (a) and (b).

### Scenario Editor

This tool offers the end user a wide range of possibilities to configure each autonomous vehicle entity. First, select and customize the vehicle's model and control strategy. Secondly, tweak the initial conditions parameters, as seen on Figure 6.a, coor-

dinates (X, Y, and Z) and Euler angles (yaw, pitch, and roll). Besides, it doesn't merely allow the user to configure each vehicle individually, but also gives an overall perspective of the world dimensions and the other vehicles of the mission (Figure 6.b).

### **Simulation Environment**

The goal of this module of the graphical interface is to symbolize the outcomes of the simulation in progress. That is, two and three dimensional graphs that represent each vehicle's trajectory and current position over the simulation world, Figure 7.a. Additionally, illustrates a 3D environment with the autonomous vehicles 3D models aimed to denote reality in a more reliable manner, Figure 7.b. The sea surface effects have not been plotted to allow the visualisation of the AUV model in the Figure 7.b.

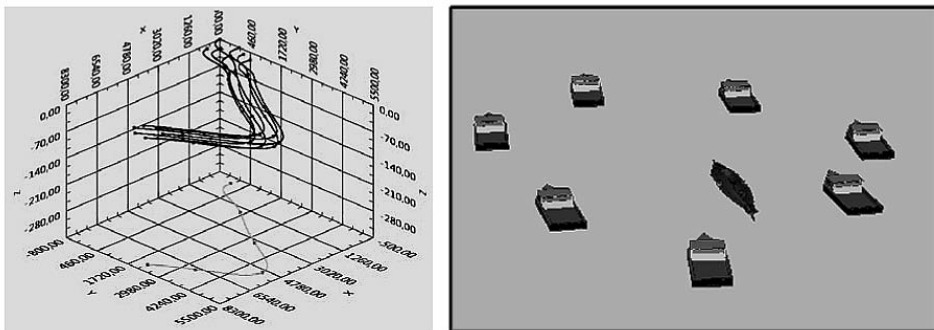


Figure 7: Simulation results (a) and capture of the simulation (b).

## **RUNNING OF THE SIMULATOR TEST BED**

This section describes the results of simulations and real tests that illustrate the potential of the test bed developed for coordinated and cooperative control of unmanned vehicles. The first example shows how the tool developed allows the simulation of multiple and different vehicles for cooperative missions. The second example shows how the “hardware in the loop” allows the immediate conversion of a simulation example into a real test, substituting the vehicle model by the input and output interface of the vehicle.

### **Coordinated control of multiple unmanned vehicles**

The formation control or swarm control is one of the most emerging topics in robotics field. In this example we consider an arbitrary number of underactuated surface marine vessels that must keep a certain formation during the tracking of an underwater target. For the sake of simplicity we consider a centralized strategy where each agent measures the range from the target to itself. The localization of the underwater

vehicle is done via trilateration algorithms (Alcocer, 2009). The formation control is based on a coordinated path following approach in which some time restrictions, maintained by the advance speed control, are introduced. For target trajectory prediction, an Information Filter is used, as defined in (Bar-Shalom et al., 2001). The details are omitted.

The desired positions for the agents depend on the formation required for the task. As it was mentioned, the objective in the underwater target tracking task is to keep the AUV localized by a mobile surface sensor network. As (Moreno-Salinas et al, 2010) describes, the vehicles must keep a regular distribution around the target, the size of which depends on the target depth. The agents can take any position around the target whereas they keep the desired regular formation. This characteristic provides more flexibility to the formation control and allows a simpler tracking control.

The simulation results are shown in Figure 7. We can observe how the regular formation is maintained along the target tracking task keeping the target projection in the centre of the vehicle formation, and therefore keeping the optimal formation to obtain the best accuracy possible, as described in (Moreno-Salinas et al, 2010).

From this example it is clear that with the developed simulator it is easy to carry out complex simulations where a high and arbitrary number of vehicles of different nature are involved in a cooperative and/or coordinate task.

### **Hardware in the loop: Tracking control of a hovercraft.**

An interesting problem arises when any theoretical control that works fine in simulation must be tested in a real scenario. For this purpose, our simulator allows the hardware in the loop simulations, so with an immediate step we can change the simulation scenario by a real scenario, using a real vehicle instead of a theoretical dynamic model.

In this example a non-linear tracking control law for a hovercraft is used. This kind of vehicle is non holonomic, and its study is very interesting from a theoretical point of view, as its behaviour is very similar of a surface craft. This non linear control law is used to follow a circular trajectory, first in a simulation scenario, where a model of the hovercraft is run (from a previous identification process, see (Chaos, 2010)). Then it is tested in a real scenario, where the theoretical model is substituted by the vehicle communication interface in the simulator. The details of the control law are omitted due to space considerations, for a deeper analysis see (Chaos, 2010). This control law is used only as an illustrative example, because, as it was commented in previous sections, any control law (designed or existing) can be implemented for any vehicle, using the control law editor.

In Figure (8.a) we can observe the simulation results, how the hovercraft makes the trajectory tracking with high accuracy with the control law designed. In Figure

(8.b) the results in the real scenario are shown, where we can notice that the behaviour of the hovercraft is similar to the theoretical one. In Figure 9 a capture of the simulation environment is shown.

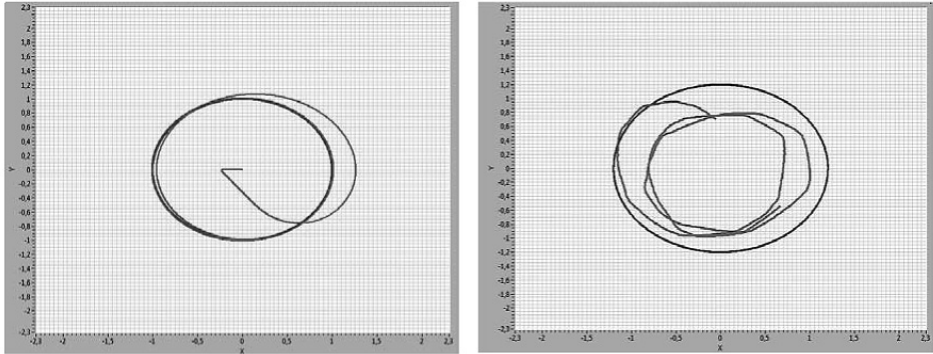


Figure 8: Simulation and HIL simulations results for tracking of a hovercraft.

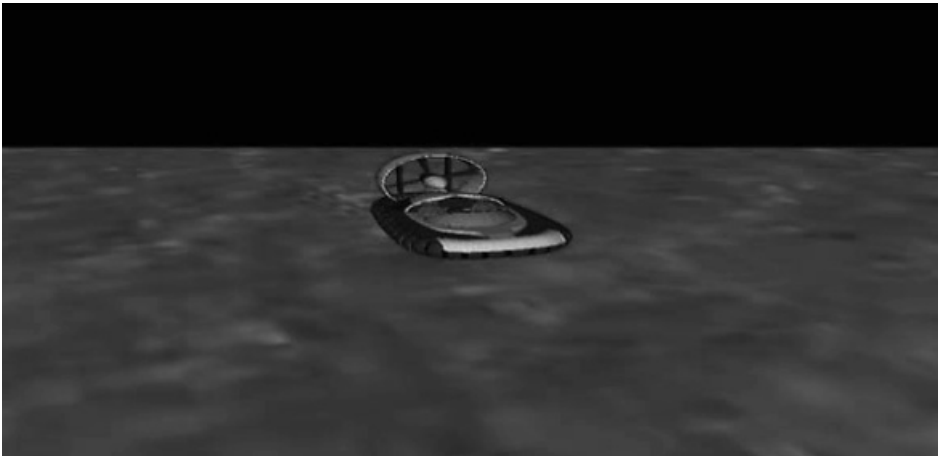


Figure 9: Capture of the simulation environment.

Therefore, we can test our control laws or models both in a theoretical and in a real framework in simple and fast way, without the need of implementing different systems or programs.

## CONCLUSIONS

In the present work a modular and easily reconfigurable test bed have been developed, so as any kind of vehicle can be simulated (and tested) with a slight modification of the program. The test bed runs continuous and discrete (DEVS and no-

DEVS) simulations to overcome all the spectrum of possible designs. One step forward respect to previous simulations tools for autonomous vehicles is the possibility of running DEVS simulations. It is constructed in LabVIEW to allow HIL simulations. Therefore the same tool is used for simulation and real experiments, facilitating enormously the portability of the theoretical design to the real world and reducing significantly the costs of real tests.

Future work will aim at: i) extending the vehicle models to a higher variety of vehicles used in cooperative and coordinated tasks, ii) including in the simulator environmental perturbations, as winds, currents, waves, etc, to improve the simulation platform as well as new control problems, as collision avoidance, fail detection, localization, etc, iii) extending the tool to construct a remote laboratory via web for educational purposes, in which the students could interact with indoor vehicles together with the simulation platform.

## REFERENCES

- Alcocer, A. (2009). Positioning and Navigation Systems for Robotic Underwater Vehicles. PhD Thesis, Instituto Superior Tecnico, Lisbon, Portugal, 2009.
- Bar-Shalom, Y., Li, X. R., & Kirubarajan, T. (2001). Estimation with Application to Tracking and Navigation. John Wiley, New York, NY; 2001.
- Jung, D. and Tsiotras, P. (2007). Modeling and Hardware-in-the-Loop Simulation for a Small Unmanned Aerial Vehicle. American Institute of Aeronautics and Astronautics, Conference and Exhibit, 7 - 10 May 2007, Rohnert Park, California.
- Craighead, J., Murphy, R., Burke, J. and Goldiez, B. (2007). A Survey of Commercial & Open Source Unmanned Vehicle Simulators. 2007 IEEE International Conference on Robotics and Automation, Roma, Italy, 10-14 April 2007.
- Chaos, D. (2010). Nonlinear control of underactuated nonholonomic marine vehicles. PhD Thesis. Department of Computer Science and Automatic Control.
- Kofman, E. Discrete event simulation of hybrid systems. SIAM Journal on Scientific Computing, vol. 25, no. 5, pp. 1771-1797, 2004.
- Luke, S., Cioffi-Revilla, C., Panait, L., Sullivan, K. and Balan, G. (2005). MASON: A Multi-agent Simulation Environment. Journal Simulation, Volume 81, Issue 7, July 2005.
- Moreno, D., Pascoal, A. M.; Alcocer, A; Aranda, J. (2010). Optimal Sensor Placement for Underwater Target Positioning with Noisy Range Measurements. 8th IFAC Conference on Control Applications in Marine Systems, CAMS 2010, Rostock, Germany, September 2010.
- Rasmussen, S.J., Chandler, P.R. (2002). MultiUAV: a multiple UAV simulation for investigation of cooperative control. Winter Simulation Conference (WSC'02), vol. 1, pp.869-877
- Ridao, P., Batlle, E., Ribas, D. and Carreras, M. (2004). NEPTUNE: A HIL Simulator for Multiple UUVs. OCEANS 04 Conference, 524 - 531 Vol.1, 9-12 Nov. 2004
- Risco-Martín, J. L., Moreno, A., Cruz, J. M., and Aranda, J. 2009. Interoperability between DEVS and non-DEVS models using DEVS/SOA. Spring Simulation Multiconference.
- Vaughan, R. (2005). Massively multi-robot simulation in stage. Swarm Intelligence, Volume 2, Numbers 2-4, 189-208, Springerlink.
- Yamaguchi, H. (2003). A distributed motion coordination strategy for multiple nonholonomic mobile robots in cooperative hunting operations. Robotics and Autonomous System, 43, pgs 257-282, 2003 Elsevier Ltd.
- Zeigler, B. P., Kim, T., and Praehofer, H. (2000). Theory of Modeling and Simulation: Integrating Discrete Event and Continuous Complex Dynamic Systems. Academic Press, 2000.
- Zeigler, B. P., Mittal, S. and Hu, X. (2008). Towards a formal standard for interoperability in M&S/System of Systems integration. GMU-AFCEA Symposium on Critical Issues in C4I, 2008.

# **HARDWARE EN EL PUNTO DE REFERENCIA DE SIMULACIÓN DE LOOP PARA VEHÍCULOS AUTÓNOMOS MARINOS**

## **RESUMEN**

El uso de vehículos autónomos está presente en numerosas áreas de robótica debido en parte a la versatilidad y flexibilidad que demuestran en la ejecución de diversas tareas de forma tanto individual como cooperativa, junto al hecho de que su uso evita el poner vidas humanas en peligro para la realización de tareas que entrañen cierto peligro. Estrechamente ligado a los vehículos autónomos se encuentran las herramientas de simulación. Estas herramientas son esenciales a la hora de comprobar el correcto diseño y funcionamiento, tanto de los algoritmos de control como de los modelos usados, de una forma teórica. Esta etapa de simulación es totalmente necesaria en el desarrollo de algoritmos de control, ya que un diseño deficiente puede provocar consecuencias dramáticas para el vehículo, los vehículos vecinos o el medio en donde se desarrolle la tarea. En este sentido en este trabajo se presenta un banco de pruebas, que pueden ser tanto teóricas como experimentales, para vehículos autónomos. El principal objetivo es tener un marco en el cual desarrollar y probar diferentes algoritmos de control para tareas cooperativas y coordinadas entre diferentes clases de vehículos. La herramienta está construida de forma modular de tal manera que cualquier clase de vehículo autónomo pueda ser simulado sólo con ligeras modificaciones del programa principal. Los procesos a simular podrán ser continuos, y discretos (DEVS y noDEVS), estando construido sobre el programa gráfico LabVIEW como una plataforma de simulación “hardware-in-the-loop”. De esta manera se usa el mismo sistema para simulación y tests reales, reduciendo el coste de las pruebas sobre el hardware y facilitando enormemente la portabilidad de los diseños teóricos al mundo real. La herramienta esta orientada para su uso tanto por investigadores como estudiantes, de forma que puedan probar sus propios algoritmos de control de forma teórica y experimental.

## **MÉTODOS**

El software desarrollado en el presente trabajo pretende ser una herramienta de simulación para modelado y control de diferentes clases de vehículos autónomos. Puede ejecutar simulaciones continuas y discretas (DEVS y noDEVS). Una ventaja adicional frente a otros simuladores es la posibilidad comentada de realizar simulaciones DEVs. El formalismo DEVs proporciona diversas ventajas para analizar y

diseñar sistemas complejos como integridad, variabilidad, extensibilidad y mantenibilidad. La recreación de escenarios varía desde un solo vehículo a múltiples vehículos de diferentes clases. Las características principales de la plataforma de simulación son:

**Arquitectura:** La arquitectura del sistema se compone de tres capas: coordinación, simulación y modelado. Cada una de las capas interactúa con las otras dependiendo del paso del protocolo de simulación. El coordinador sincroniza y comunica los simuladores. Los simuladores discretos podrán ejecutar simulaciones DEVS y no-DEVS.

**Protocolo de comunicación:** la comunicación entre el coordinador y simulador es realizada mediante una estructura común dada por un mensaje y tiempo de un evento que indica el tiempo de ejecución del próximo evento. En resumen, el coordinador se comunica con el simulador para mandar mensajes de entrada, por tiempo o por mensajes de control y tiempo de evento asociado. Mientras tanto, los simuladores se comunican con el coordinador para mandar mensajes de salida.

**Modelado:** el sistema de modelado de un escenario experimental de un vehículo autónomo está basado en tres tipos de modelos. Un modelo para el vehículo a través de paradigmas discretos o continuos, o la comunicación con el vehículo real (simulaciones HIL). El módulo de control que implementa el control de navegación dependiendo de la estrategia de simulación deseada a priori. Finalmente, el modelo de perturbación que introduce alteraciones en las comunicaciones y limita el campo de visión de los vehículos.

**Configuraciones posibles:** cada componente de la simulación debe ser definido como un modelo DEVS, no DEVS o continuo, o como un interfaz de comunicación para interactuar con el hardware, MATLAB, DLL, .NET, etc.

**Interfaz de usuario:** la interfaz de simulación debe poseer las siguientes características: alto grado de usabilidad, alta funcionalidad, y ofrecer una interfaz agradable y fácil de manejar. La interfaz está dividida en dos módulos. El editor de escenarios que proporciona un interfaz gráfico para la configuración del experimento y el entorno gráfico de simulación que va mostrando en tiempo real el resultado de la simulación mediante modelos en 3D.

## CONCLUSIONES

En este trabajo se ha desarrollado un banco de pruebas modular y fácilmente reconfigurable, de tal manera que se pueda simular diferentes clases de vehículos autónomos simplemente con ligeras modificaciones del programa. El programa ha sido construido de una forma jerárquica, con las comunicaciones entre vehículos modeladas de forma explícita, incluye herramientas gráficas y los datos son salvados para un posible estudio de los mismos "fuera de línea". La herramienta puede ejecutar simulaciones tanto continuas como discretas (DEVS y noDEVS), de forma que se

abarque todo el espectro de posibles situaciones de diseño. Un elemento diferenciador respecto otros simuladores de vehículos autónomos es este hecho de poder hacer simulaciones DEVS. Además ha sido construido sobre LabVIEW para permitir simulaciones “hardware-in-the-loop”. De esta manera tenemos una única herramienta para la simulación teórica y los test experimentales sobre los componentes hardware, facilitando enormemente la portabilidad de los diseños teóricos al mundo real y reduciendo significativamente los costes de los tests experimentales.





## MODELLING AND SIMULATION OF MOORED DEVICES FOR OCEAN CURRENTS ENERGY HARNESSING

A. López<sup>1,2</sup>, J.A. Somolinos<sup>2</sup>, L.R. Núñez<sup>2</sup> and M. Santamaría<sup>2</sup>

Received 03 February 2011; in revised form 09 February 2011; accepted 15 March 2011

### ABSTRACT

The main objective of this paper is the presentation of modelling solutions of floating devices that can be used for harnessing energy from ocean currents. It has been structured into three main parts.

First, the growing current interest in marine renewable energy in general, and in extracting energy from currents in particular, is presented, showing the large number of solutions that are emerging and some of the most significant types.

GESMEY generator is presented in second section. It is based on a new concept that has been patented by the Universidad Politécnica de Madrid and which is currently being developed through a collaborative agreement with the SOERMAR Foundation. The main feature of this generator is that on operation is fully submerged, and no other facilities are required to move to floating state for maintenance, which greatly increases its performance.

Third part of the article is devoted to present the modelling and simulation challenges that arise in the development of devices for harnessing the energy of marine currents, along with some solutions which have been adopted within the frame of the GESMEY Project, making particular emphasis on the dynamics of the generator and its control.

**Key words:** Marine renewable energy, ocean current turbines, modelling and simulation

<sup>1</sup> Catedrático Universidad. <sup>2</sup>Univ. Politécnica de Madrid, Email: amable.lopez@upm.es, Tel. 91 336 7212, ETSI Navales, Departamento de Sistemas Oceánicos y Navales, Ciudad Universitaria s/n, 28040 Madrid, Spain.

## INTRODUCTION. INTEREST OF MARINE RENEWABLE ENERGY USE

The growing energy demand of the world, the variable cost of oil and the Kyoto and followings agreements to decrease the CO<sub>2</sub> emissions, have made the engineers and scientifics to study alternative ways of obtaining energy. By considering the ocean as one of the most important renewable energy resource (Bedard, 2008), different technologies have appeared for extracting energy from it.

Energy from the sun and the moon is captured and stored by the ocean water in different ways. That is the main reason because different marine renewable energies (MRE) are being developed (Huckerby et al., 2008) which can be classified as:

- Wind offshore: currently, has a large increase on installed power with larger units (80 m diameter rotors) than land ones by the lesser value of surges but with bigger costs of installation, maintenance and line transmission.
- Wave power: there exist a large number of projects at different stages. They offer a great variety of possible operating locations near the coast all over the World, but the proposed devices must be improved to withstand the storms of the sea (Perera et al., 2010).
- Tidal height (potential energy), a more experienced ERM with a limited future due to the negative environmental impacts of the necessary dams.
- Tidal flow and current (kinetic energy), with a similar number of designs to those of the waves. (King et al, 2009).
- Thermal gradient (OTEC) and salinity gradient, with few and high cost research projects.
- Submarine geothermal energy and marine biomass, currently limited expectations.

Marine currents are the one of the most promising MRE –with wind and waves energy– and are originated by several causes. The mains are: tides, winds, different density between waters and the Coriolis forces of the Earth. They key current source are the tides and only in those areas where the average velocity of the streams can be high is possible to obtain enough kinetic energy to be considered as an important source of renewable energy. The main advantages for harnessing the tidal energy are:

- There are many locations in the oceans with high energy density.
- It is possible to obtain a reliable long-term prediction of speed and power.
- Better relationship between mean and nominal power than other MREs.
- Very low environmental impact.
- High reliability compared to wave devices.

The quantification of the energy that could be extracted from sea and ocean currents is estimated at more than 800 TWh/year -about 4% of global electricity consumption- (Soerensen, 2008), but currently it is not possible to exploit the most important part of this huge energy potential since most of this energy is concentrated inside areas with depths over 40 meters. Then, it is necessary a new generation of converters capable of extracting this energy from these high depth sites.

## STATE OF THE ART AND MOST SIGNIFICANT TYPES OF DEVICES

Nowadays the tidal stream development technology is still in the beginning of its life and there are only some devices used more as a test to learn and improve the technology, than to generate and sell electricity. Currently, there are over seventy devices into the tidal stream generation technology, and most of these concepts use an horizontal axis rotor as first converter, without any sign that the industry is going to converge towards a single configuration now. There is only one machine connected to the electrical network and this is the Marine Current Turbine's Sea Gen with 1,2 Mw generation power, which is located into the sea at the Strangford Narrows. (Fraenkel, 2010).

The other technological concepts are in different stages of development but not on industrial exploitation, and none of them, Sea Gen included, are capable to exploit currents that are at more of 40 meters depth sites.

While the development of devices for the stream exploitation, usually called Tidal Energy Converters (TEC), is focusing on the so-called "first-generation" (fixed to the bottom of the sea, and suitable for sites with depths below 40 m), there are a small

number of "second generation" developments (anchored with cables and suitable for depths over 40m). The four most common kinds of TECs are displayed in figure 1:

- Devices with open rotors: a good example is the Gen Sea, above mentioned.
- Turbine type devices with closed conduit: like the Open Centre Turbine.
- Devices with blades rotating about an axis perpendicular to the current: like Enermar.
- Devices with oscillating or linear displacement blades: the Pulse Stream is shown.



Figure 1. Sea Gen, OCT, Enermar & Pulse Stream TECs.

## GESMEY PROJECT DESCRIPTION

### Objectives

The initial goal of GESMEY Project (Spanish acronym from Submarine Electrical Generator with Y shape Framework) was to develop a specially designed device to harnessing the currents of the Strait of Gibraltar. This Strait is the natural way of connection between the Mediterranean Sea and the Atlantic Ocean. It has a very irregular

bathymetric profile, with an average depth of 550 m in the main channel, and with zones between 90 m and 960 m depth. The energetic resource that the Strait offers is made up by a double current, a superficial one from the Atlantic to the Mediterranean and the other one that go by the bottom from the Mediterranean to the Atlantic.

The principal part of the energy associated to these tides is into the upper Atlantic water currents and they are going along an hypothetical channel surrounded by the sea surface and the low level that is situated over 100 meters depth. On the Strait there are several places with a “mean spring tide” speed up 2 m/s but normally they are in deep waters, usually on 80 to 100 meters depth locations.

By this, the GESMEY project main objective was to develop a device with a low cost of life cycle, designed for the Strait of Gibraltar and others World sites with water depths over 40 m where the current devices (first generation devices) cannot operate. It should be noted that second-generation devices (Black & Veatch, 2004) allow access to 80% of the oceans currents energy. The goals that the GESMEY design can be resumed as:

- Simplified deployment
- Minimum environmental impact
- No surface elements on operation
- Robust and simple construction
- Easily scalable (depth, stream, speed, nominal power)
- Use of mature commercial off-the-shelf (COTS) technologies

### **Project methodology and stages**

During the development of a MRE device, a five stages protocol (U. Southampton, 2008) can be used as guideline to reduce costs and ensure development quality. The use of this protocol on the GESMEY project is summarized below.

The starting point of GESMEY Project was a Universidad Politécnica de Madrid (UPM) patent (Lopez, 2007) which has received an award from the Madrid Regional Administration. The Project is been developed in collaboration between a research team from the E.T.S. Ingenieros Navales (ETSIN) of the UPM and other one from the SOERMAR Foundation Technological Centre.

The Project Stage 1 has been supported by funds from The Spanish National Research Program 2008/2011 (Subprogram of Industrial Applied Research, Call 2008, Ministry of Science and Innovation) and was developed between 2008 and 2009. During 2010, new funds have been obtained from the Spanish Ministry of Industry, Tourism and Commerce to develop Stages 2 and 3 of the MRE protocol.

Over the basic concept of GESMEY generator (Lopez, 2007), there were a lot of design options and it was necessary to make a feasibility study to choose the best option as a starting point to perform the device functional design. This proposed specific methodology to carry out this task is shown in figure 2.

### Device description

As a result of the study of alternatives, we choose the GESMEY design drawn in figure 3 (left). It can be seen that the GESMEY TEC comprises the following elements:

- Rotor: With fixed pitch blades to improve efficiency and reliability.
- Central POD: Power Take-Off (PTO) components and ancillary systems, based on COTS elements.
- Columns: Main structural parts and ancillary ballast tanks.
- End Torpedoes: Main ballast tanks. They provide stability during operation (asymmetric load) and on flotation (like a semi-submersible platform).

An important portion of the inner volume of the columns and torpedoes is used as water ballast tanks. The changes on their ballast volume lets handle its floatability and then the position and/or the orientation of the device are controlled. More details of the design, distribution of elements, location of components, and dimensions are described in (Núñez et al., 2010).

### Operational states

On operation, as is showed on figure 3 (right), the device is maintained on position by mooring systems adapted to location environmental condition and controlling the ballast water level on torpedoes (the uppers with net buoyancy and the lowers with net weight) an adequate stability is achieved to keep the device vertical with reduced heel and trim angles on despite the torque produced by the rotor.

For maintenance, decommissioning or when it is necessary to extract the device form water, the procedure is very simple (see figure 4). First, when a rope is detached and some ballast removed, the device goes up to surface smoothly. When it reaches the sea surface, a new change on ballast tanks produces a self rotation. And finally the de-

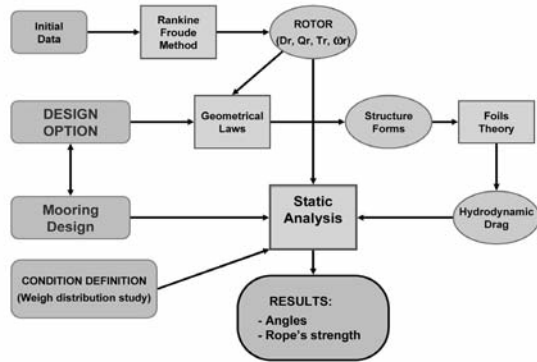


Figure 2: Flow diagram of the used methodology.

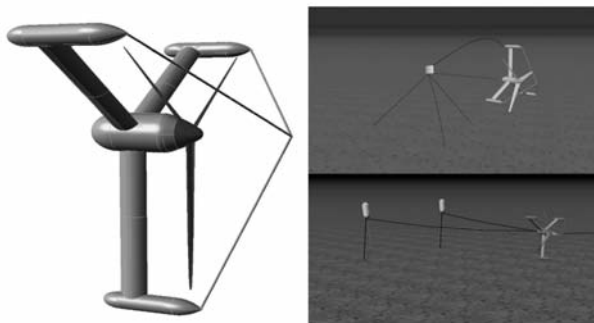


Figure 3: GESMEY device and two mooring alternatives.

vice floats on sea surface with the rotor outside water, ready for first level maintenance or transport. The device is self supported for transport.

For installation of the device or going back to operation state after a maintenance procedure, it can be used the reverse sequence. The whole procedure can be fully automatized with a supervisory control from the tidal farm operators.

**MODELING AND SIMULATION OF MOORED TECs**

At the first phase of the GESMEY Project, it was found that there was no turnkey design and calculation tools that can solve the design, calculation, analysis and simulation needs for a device like the proposed one, which should work submerged like a submarine and stand with a different orientation when it is on the sea surface.

Therefore in the definition stage a set of tasks for the analysis and adaptation of existing tools –for models development, calculation and simulation, etc.– were carried out. These methods and tools can be applied to other submerged and moored MER devices. Next subsections are devoted to present some of the most significant aspects of the carried out analysis for modelling and simulation.

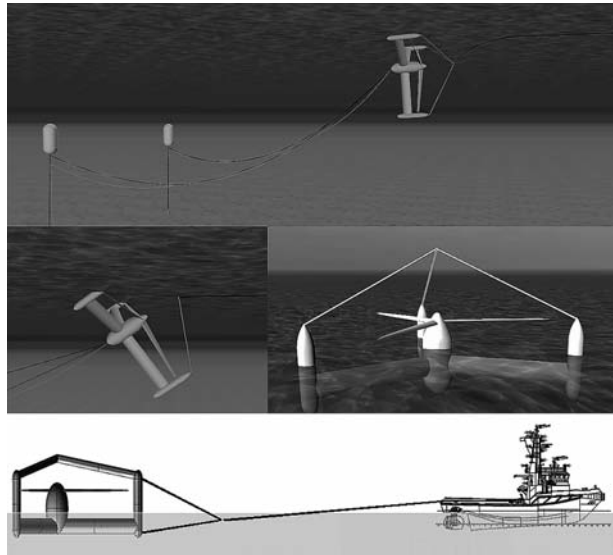


Figure 4: GESMEY procedures for maintenance and transport.

**Hydrodynamic behaviour**

The key element of a TEC is the rotor. It is the component that converts the water kinetic energy into mechanical energy. As it was described above, in most cases the rotor is similar to the one from a wind generator or from a hydro turbine, but in the case of the TECs, as an additional feature normally it should work in both directions.

The models and tools used for the design of ships propellers are not suitable for the analysis of TECs rotors because of their different shape and because they work in the reverse sense, that is, by absorbing energy instead of transfer it to the water. Therefore the typical propeller curves ( $K_t(J)$  and  $K_q(J)$ ), where  $K_t$ ,  $K_q$  and  $J$  are the thrust, torque and advance coefficients cannot be used.

Instead of these curves,  $C_p$  (Power Coefficient),  $C_t$  (Thrust Coefficient) and  $C_q$  (Torque Coefficient) defined all of them as function of  $\lambda = \text{TSR}$  (Tip Speed Ratio) are used. They are defined as:

$$TSR = \frac{\omega \cdot R}{V} \tag{1}$$

$$C_p = \frac{P}{0,5 \cdot \rho \cdot A \cdot V^3} \tag{2}$$

$$C_t = \frac{T}{0,5 \cdot \rho \cdot A \cdot V^2} \tag{3}$$

$$C_q = \frac{Q}{0,5 \cdot \rho \cdot A \cdot R \cdot V^2} \tag{4}$$

Being:

- $\rho$  Water density (1025 kg/m<sup>3</sup> for salad water)
- $\omega$  Angular speed of the rotor
- A Useful area of the rotor
- R Rotor ratio (to blade tip)
- V Water current velocity (free waters measured)
- P, T, Q Power, Thrust and Torque on the rotor shaft.

For rotor modelling,  $C_p(\lambda)$  and  $C_t(\lambda)$  are needed - $C_q$  can be obtained from  $C_p$  and they can be obtained from hydrodynamic test canal experiments (Bahaj et al., 2007) or from numerical computerized models. The general aspect of both curves can be seen from figure 5.

When a propeller works at its optimum point, the energy extraction coefficient ( $C_p$ ) which measures the ratio between shaft power and the mass of water flowing through the device is between 0.4 and 0.5, being the theoretical maximum achievable known as the “Betz limit”  $C_p < 0.59$ .

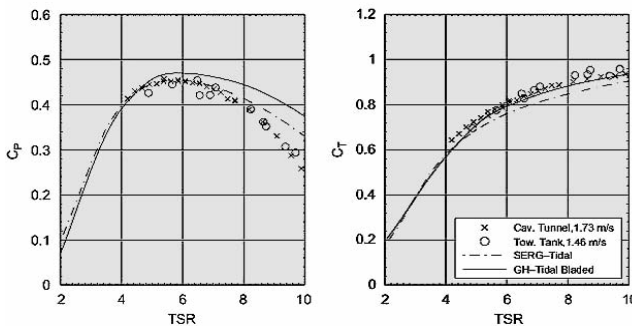


Figure 5. Tip cal  $C_p$   $C_t$  curves for a TEC rotor.

Within the GESMEY Stage 1, the propeller has been tested in a towing tank and computational fluid dynamics (CFD) simulations have been carried out in order to optimize its structure design with constructible shapes (figure 6).

**Device in operation**

In operation (producing energy) a moored submerged TEC works practically in steady state due the slow variation of current velocity. Disturbances came from the turbulence in the current profile if the device is very close to the bottom and that can be wave-induced if it is near the surface. Under these limit conditions, such efforts will produce large fluctuations in the blade’s root, but the torque and thrust oscillations transmitted to the PTO is reduced if the rotor has three or more blades.



Figure 6. Preliminary physical and CFD models of the GESMEY rotor and structure.

This greatly simplifies the analysis of the behaviour of TEC in operation, and it can be done using simple static models. The objectives of this analysis are to know the device forces, torques and orientation angles, allowing to adjust the ballast tanks level.

Therefore, two mathematical sub models are necessary: the mechanical and the hydrodynamic ones. Both of them have been developed in basis the similar ones used in naval architecture design. The “hydrodynamic model” developed is based on first, segregating the device structure into different elements and, second, computing their drag as function of their respective speed, according with the formulae:

$$Fd = 0,5 \cdot Cd \cdot \rho \cdot A \cdot V^2 \tag{5}$$

Where  $F_d$  denotes the drag of each element,  $A$  is its significant surface,  $V$  represents the water speed and  $C_d$  is the form coefficient -Reynolds Number dependent- that has a small change with velocity because of the huge dimensions of the elements.

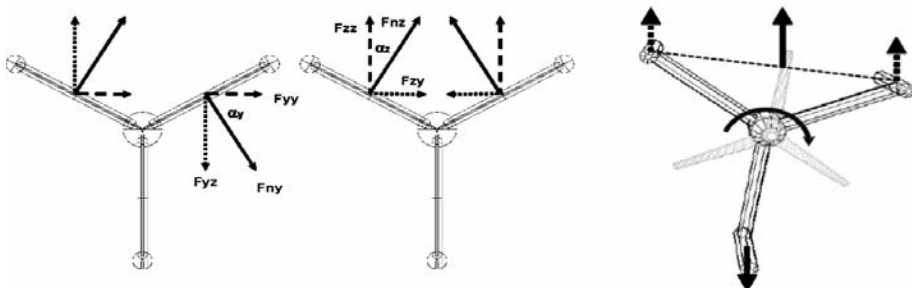


Figure 7. Basic elements forces. Hydrostatic equilibrium.

The values of the forces along the three principal axes are calculated and applied in the centre of each element (see figure 7 left & centre). The model neglects the lift forces because all the elements are disposed in a symmetric way with respect to the direction of the flow, and the mooring system lets the device automatically orient in the flow direction.

All the volumes are computed, and then, buoyancy forces are applied over each of these elements. On the other hand, all the weights are computed too, and gravitational forces are obtained. The “hydrostatic forces” are obtained by composing both forces.

Once all the hydrodynamic, hydrostatic and rotor forces have been computed, they are integrated into the “mechanical model” together, in order to get essentially the heel and trim angles values obtained from the device “metacentric height” (GB), the definition of the mooring points and the torque from the rotor.

During the Project Stage 1, different possibilities for making a computerized tool which facilitates the calculations seen above were considered. The final developed tool HACERIC (Spanish acronym from: tool for the analysis of radial bodies inside currents flow) lets the user enter data (sizes, weight...) corresponding to the device under analysis and adjust different ballast tanks levels, obtaining as results the most significant forces, torques, and orientation angles of the device.

When GESMEY is operating at 2 m/s, HACERIC shows these results: 14 degrees of heel angle; negligible trim and yaw angles (see figure 7, right) and a total force of 1.0 MN over the mooring ropes. Also we checked -with the Orcaflex tool, showed below- that the effects of 4 m height waves into the device movements are minimal.

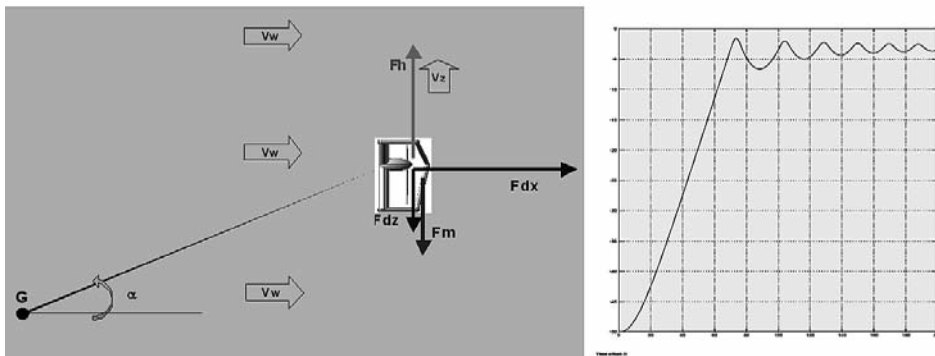


Figure 8. Basic modelling and simulation results of GESMEY emersion.

### Emersion and immersion manoeuvres

All TEC that works underwater, must be designed so that they can perform the manoeuvres of immersion and emersion in a controlled way. These manoeuvres are necessary during the device installation and decommissioning operations, and every time it is necessary do maintenance tasks.

These processes are clearly dynamics, being necessary to develop behaviour models and adapt existing simulation tools. Within these processes, there are two very different phases: first when the TEC is totally submerged (for example, during the emersion of GESMEY device, the objective is to maintain the vertical orientation) and the second when the TEC goes out of water (partly) appearing a free surface (in the case of GESMEY corresponds to the rotation showed in figure 4).

For modelling the first phase (figure 8) the model must represent the main forces and moments: restorative (buoyancy and weight), dissipative (resistance and lift) and inertial (actual and added masses). The problem is that many of these forces are not linear, being particularly complex the modelling of the added mass (Korotkin, 2009).

A simplified 2D model has been implemented under the Simulink-Matlab environment. Details of the used model can be seen from (López et al., 2009) and depth of the device as function of time when an emersion procedure is ordered can be seen from figure 8. It can be clearly appreciated the non linear and with small damped behaviour response when the device reaches the water surface.

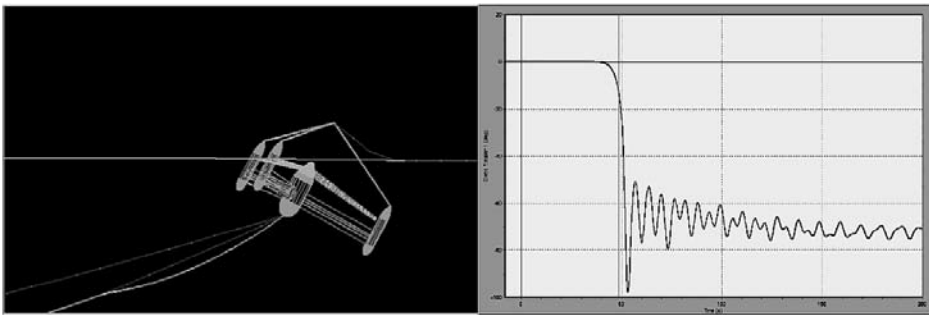


Figure 9. GESMEY surface turn modelling and simulation with Orcaflex.

An additional problem that arises when modelling the behaviour of moored bodies is to characterize the behaviour of ropes. This is a widely studied and complex hydro-elastic problem, and however, very difficult to implement in tools such as Simulink-Matlab. In order to solve this handicap, the use of the simulation tool (3D) Orcaflex was decided. Orcaflex is considered as the main reference mooring design tool in the field of offshore marine systems. Working with this tool presents two problems:

- To model complex bodies, as they are the TECs, it is necessary to define the body like a set of elements (8 in the case of GESMEY) and for each to put in a set of parameters like volume, weight and hydrodynamic drag, added mass etc. To solve this problem, we have generated a parametric calculus procedure.
- It is difficult to implement in the model the control systems necessary to simulate the automatic operation of the TEC. So far we have solved this problem by simulating processes (Figure 9) with model predictive control, being planned in the future to develop an interface between Simulink and Orcaflex.

### Power electromechanical system (PTO)

Because the speed of ocean currents cannot be considered constant, GESMEY has been designed and configured as a variable-speed turbine in order to capture the maximum amount of power over a wide range of water speeds. By this, is necessary the use of active control systems that meet different objectives depending upon the water speed.

The PTO consists on a set of components from the propeller to the electronic converter. The main elements of the PTO are: the rotor, the mechanical gearbox, the synchronous generator, the breaking system and the electronics converter.

The proposed dynamic model can be see at (Somolinos, 2010) and a voltage controller has been implemented for simulation of this turbine in the Matlab-Simulink software. Some simulated results are obtained under different changing conditions of the water currents and under a step increment of the voltage reference input.

Figure 10.a shows the speed of the current input. It has been obtained in a synthetic way, adding an step increment of (-1.3 m/s at instant  $t = 20$  s), and a limited bandwidth white noise. The reference signal for the controlled system is the desired voltage of the load. Its starting value is 1900 V and after 10 seconds, the desired voltage is changed to 2100 V with a step signal increment of +200 V.

Figure 10.b shows the electrical torque. Figure 10.c shows the angular speed of the PTO (high speed shaft). It can be observed the generator speed evolution when the input reference changes. Finally, figure 10.d shows the real voltage response of the system and the voltage reference input signal.

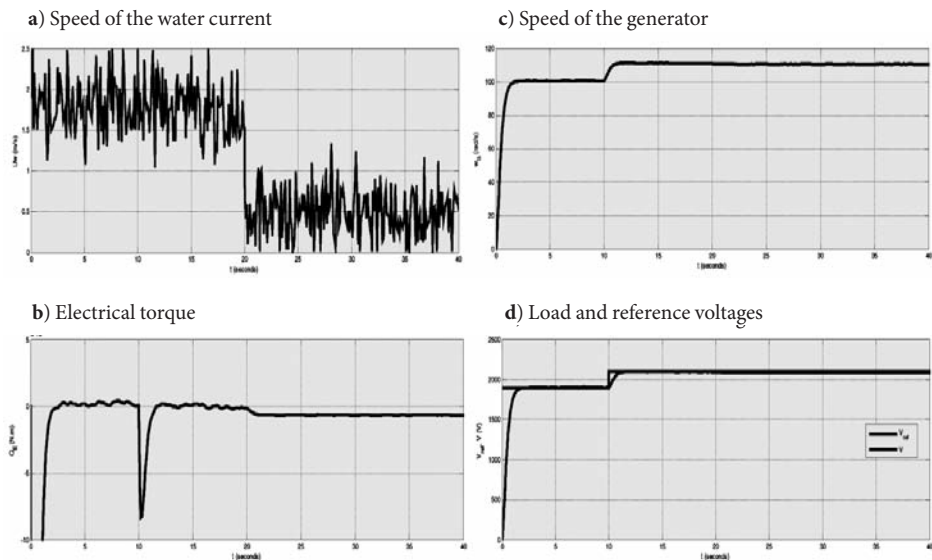


Figure 10. PTO response curves for a simulated operation.

## CONCLUSIONS

From the analysis of the state of the art of the Marine Renewable Energies and from the GESMEY Project experience, it is found that the extensive development that will take in the coming years in this area is an opportunity for industry and for R&D. In order to reach the success, projects must follow an established development stages protocols and must be supported by consolidated groups that are able to solve the financial, technological and scientific challenges that will take place.

Among the scientific challenges to the case of moored TECs it is needed to develop new models and calculation and simulation tools. Within GESMEY project these problems are been addressing. Solutions with a right balance between scientific rigor, the precision of the results and cost (acquisition, development and use) of the models and tools have been found.

The taken steps thus far, would have shown the feasibility, performance and ease of operation and maintenance of GESMEY device, and they have proven to be possible to develop the basic tools at a reasonable cost.

Next steps will focus, from the technological point of view, on the development of an experimental prototype of 10 kW and a detailed project of a 1 MW generator. From the scientific viewpoint, the validation and calibration of the tools developed, through a testing program in test channel is needed, and a detailed study of the control of the procedures of immersion and emersion have to be improved and tested.

## REFERENCES

- Bahaj A. et al. (2007): Experimental verifications of numerical predictions for the hydrodynamic performance of horizontal axis marine current turbines. *Renewable Energy* 32. October, [www.elsevier.com/locate/renene](http://www.elsevier.com/locate/renene).
- Bedard, R. (2008): Technology characterization: Ocean wave and tidal energy. *Global Marine Energy Conference*. April, New York
- Black & Veatch (2004): Tidal stream energy resource assesment. The Carbon Trust, September, London.
- Fraenkel, P.: Development and testing of marine current turbine's SeaGen 1.2MW tidal stream turbine. 3rd International Conference on Ocean Energy, October, Bilbao, Spain.
- Huckerby, J. et al. (2008): Implementing Agreement on Ocean Energy Systems. 3rd International Seminar on Ocean Energy. May, Bilbao, Spain.
- King, J. et al. (2009): Tidal Stream Power Technology – State of the Art. OCEANS-2009-Europe Conference. May, Bremen, Germany.
- Korotkin, A. (2009): Added Masses of Ship Structures. e-ISBN 978-1-4020-9432-3. Springer Science + Business Media B.V.
- López, A. (2007): Patent nº P200700987 UPM. OEPM Spanish Patent and Trademark Office. April, Madrid.
- López, A. et al. (2009): Modelado y simulación de la operación de un generador para el aprovechamiento de las corrientes del estrecho de Gibraltar. XXX Jornadas de Automática. CEA-IFAC, September, Valladolid, Spain.
- Núñez, L.R. et al. (2010): The GESMEY Ocean Current Turbine. A proposal for marine current energy extraction on deeper waters. 3rd International Conference on Oceanic Energy. October, Bilbao, Spain.
- Perera et al. (2010): Evaluation of the Energetic Potential of Swell for the Canary Island. *Journal of Maritime Research*, Volume 7, Number 2. August, Santander, Spain.
- Soerensen, H. et al. (2008): Ocean Energy: Position paper for IPCC. IPCC Scoping Conference on Renewable Energy. January, Lübeck, Germany.
- Somolinos, J.A et al. (2010): Automatic System for Underwater Ocean Current Turbines. Application to GESMEY. 3rd International Conference on Oceanic Energy. October, Bilbao, Spain.
- University of Southampton (2008): Tidal-current Energy Device. Development and Evaluation Protocol. IEA-OES Guidelines for Development and Testing of Ocean Energy Systems Task 2.2.

## **MODELADO Y SIMULACIÓN DE DISPOSITIVOS FONDEADOS PARA EL APROVECHAMIENTO DE LA ENERGÍA DE LAS CORRIENTES MARINAS**

### **RESUMEN**

En este artículo, tras presentar el estado actual del aprovechamiento de las energías renovables marinas (MRE), y en especial los dispositivos para el aprovechamiento de la de las corrientes (TECs), se describe el generador GESMEY en desarrollo entre la UPM y SOERMAR y los modelos y simulaciones desarrollados para él y que son utilizables en otros TECs fondeados.

### **INTRODUCCIÓN. INTERÉS DEL USO DE LAS MRE**

Entre las fuentes de MRE: viento, olas, corrientes, altura de mareas, gradientes térmico y salino, etc., las tres primeras son las que tienen un mayor potencial. La energía de las corrientes (mayoritariamente de las mareas) se estima en 800 TWh/año, existiendo bastantes lugares en el mundo, donde se concentra. Sus principales ventajas son su predictibilidad, alto factor de utilización, fiabilidad y bajo impacto ambiental.

### **ESTADO DEL ARTE Y TIPOS DE TECs REPRESENTATIVOS**

En la actualidad existen más de 70 conceptos de TECs en diversas fases de desarrollo y de distintas tipologías. En la figura 1 se muestran cuatro ejemplos significativos, que corresponden a turbinas de rotor abierto y cerrado con eje horizontal, a una turbina de eje vertical y a un dispositivo de palas oscilantes. Entre todos los proyectos, puede considerarse que el de referencia es el Sea Gen, cuyo prototipo comercial de 1,2 MW, lleva más de un año entregando energía a la red.

### **DESCRIPCIÓN DEL PROYECTO GESMEY**

Aunque el objetivo inicial del proyecto GESMEY (Generador Eléctrico SubMARino con Estructura en Y), es el aprovechamiento de la energía de las corrientes en el Estrecho de Gibraltar, al ser un dispositivo de 2ª generación (apto para trabajar en lugares con más de 40 m de lámina de agua), es utilizable en otros lugares con esas profundidades, con lo que tiene acceso al 80% de la energía de las corrientes, frente al 20% disponible para los de 1ª generación. Su diseño se ha basado en unos objetivos

ambiciosos (instalación simple, mínimo impacto ambiental, sin elementos en superficie, simple de construcción, basado en elementos estándar y escalable) con objeto de optimizar su ciclo de vida y maximizar su rentabilidad.

En el proyecto GESMEY durante 2008 y 2009 se realizó la fase 1 (diseño funcional) y en la actualidad se están abordando las 2 y 3 (diseños constructivo y operativo con pruebas de un primer prototipo en el mar). En la figura 2 se muestra el proceso seguido para la elección de diseño final entre distintas alternativas.

En la figura 3 se muestra el diseño del TEC GESMEY. Consta de un domo (POD) central en el que va el tren de potencia (PTO) y los equipos auxiliares en cuyo extremo se sitúa un rotor de tres palas de paso fijo (para simplificar la construcción y aumentar la fiabilidad). Del centro del domo salen tres brazos (en cuyo interior van tanques de lastre). En el extremo de cada brazo se dispone un cuerpo en forma de torpedo, en cuyo interior van los tanques de lastre principales.

En operación produciendo energía (figura 3, derecha), el dispositivo está unido a una serie de cables de fondeo, que lo sujetan al fondo, a través de una serie de boyas sumergidas, permitiendo que se oriente automáticamente en la dirección de la corriente. La diferencia de llenado entre los tanques de lastre superiores e inferiores, produce una altura metacéntrica suficiente para estabilizar el generador en vertical, frente al par producido por el rotor.

Cuando se desea sacarlo a la superficie (figura 4), basta con liberar alguno de los cables y vaciar de forma controlada uno de los tanques, lográndose que el dispositivo suba en vertical de forma suave. Cuando emerge una parte, se vacían, de forma secuencial, el resto de los tanques de lastre, girando y quedando flotando en horizontal y dispuesto para las tareas de mantenimiento de primer nivel o el transporte.

## MODELADO Y SIMULACIÓN DE TECS FONDEADOS

El elemento fundamental de un TEC es el rotor, que se modela a través de las curvas de potencia y empuje ( $C_p$  y  $C_t$  en función del TSR), tal como se ve en la figura 5. Dentro de GESMEY se ha ensayado un modelo a escala y se han realizado simulaciones con CFDs.

Al no existir herramientas adecuadas para el análisis de TECs sumergidos, se ha desarrollado la aplicación HACERIC que integra modelos hidrostáticos, hidrodinámicos y mecánicos originales, permitiendo calcular las fuerzas de fondeo y los ángulos de operación. Los modelos se basan (figura 7) en la descomposición del TEC en una serie de cuerpos simples, que son estudiados por separado, integrándose sus fuerzas y momentos para analizar el comportamiento del conjunto.

Para el estudio y simulación de las maniobras de emersión e inmersión se han utilizado las herramientas Simulink y ORCAFLEX que es la de referencia dentro del campo offshore para sistemas fondeados. Con ambas (figura 8) se han logrado unos buenos resultados en la fase sumergida, pero Simulink presenta problemas en cuanto

hay parte del dispositivo fuera del agua. Por ello, para las fases de giro el trabajo se ha centrado en ORCAFLEX (figura 9), habiéndose desarrollado métodos originales para el cálculo de los parámetros hidrodinámicos que hay que incorporar al modelo.

Dado que GESMEY utiliza un sistema de paso fijo en el rotor, el generador tiene que trabajar a velocidad variable, en función de la velocidad del agua. En la referencia (Somolinos, 2010) se describe el sistema de control desarrollado.

## **CONCLUSIONES**

El desarrollo de las MRE en los próximos años supone un reto tecnológico y financiero y una oportunidad para el desarrollo de nuevos proyectos de I+D. Los modelos y herramientas desarrollados dentro del proyecto GESMEY han demostrado su utilidad para su uso por otros TECs de segunda generación, siendo necesario trabajos complementarios de desarrollo, validación y calibración que se van a abordar próximamente.



## DEVELOPING MAGNETIC BEARINGS FOR SUBSEA OCEANIC ENVIRONMENTS

R. Ferreiro<sup>1,2</sup> and F. J. Perez<sup>1,3</sup>

Received 04 February 2011; in revised form 15 February 2011; accepted 16 March 2011

### ABSTRACT

The article deals with the set-up environment especially designed and implemented to improve vibration attenuation of rotating machines installed on subsea environments. Active Magnetic Bearing Control (AMBC), including vibration attenuation or suppression associated to the passive magnetic bearings (PMB) design for subsea oceanic gas compressors and motors is the aim of the article. Gas production forecast and production was the motivation for subsea gas compression using High-speed Variable Speed Drives (VSD) in order to keep the actual gas production volume at the initially forecasted levels using underwater compressors and motors equipped with active magnetic bearings (AMB).

Robust control algorithms for AMBC using the most efficient technologies to ensure performance are demanded. With the developed test-rig, the improvement of vibration control algorithms to be applied on subsea motors and compressors equipped with hybrid magnetic bearings (HMB), (consists of active and passive magnetic bearings) is the objective of the work. The implemented test-rig provides us a test environment which can be modified to support different scenarios with regard to structural components, loads and severe operating conditions.

**Key words:** Active magnetic bearings, Passive magnetic bearings, Subsea rotating machines, Vibration control.

<sup>1</sup> University of a coruña, ETSNM, Paeo de Ronda 51, 15011 A Coruña, Spain. <sup>2</sup> Head of research group, Email: ferreiro@udc.es, Tel. +34981 167000, Fax. +34981 167101. <sup>3</sup> Member of research group, Email: javierpc@udc.es, Tel. +34981167000, Fax. +34981167101.

## SUBSEA TECHNOLOGICAL BACKGROUND

Producing oil and gas from reservoirs located at long distances from land is a costly proposition that presents many challenges to offshore operators. Going subsea with long reach from shore or remote platform can be a very cost-efficient solution as it may eliminate the need for a fixed or floating topside installation. To help operators achieve efficient electric power supply and control at long step-out distances, some developers and manufacturers offers technical solutions of highly developed electrical products and associated services tailored for subsea production applications.

The objective of subsea gas exploitation using subsea compressors and related equipment is to minimize big investments and operational expenses in new off-shore production units by utilizing existing production units as a hub and have a significant part of the gas recompression equipment installed on the sea-bed (for boosting in the wellhead area) by means of long step-out cables. To achieve proposed objectives several technical challenges will be addressed:

High-speed VSD, long step-out power system, a very long umbilical cable between frequency converter and machine/compressor, power rating equipment for step-out system so far, rated for 6-8 MW compressor power and motor supply frequencies of up to 200Hz., and finally the motor and compressor equipped with active or hybrid magnetic bearings (R. Fantoft, 2005) (Raad, R.O.; Henriksen, T.; Raphael, H.B.; Hadler-Jacobsen, A, 1996) (Pyrhonen J., Nerg J., Kurronen P., Lauber U., 2008).

Some of the subsea solutions are based on the standard frequency converters and special designed transformers (Moreno, V. and Pigazo, A., 2007), adapted to meet the stringent requirements of topside or subsea installation.

Many specialised manufacturers are introducing subsea electrical solutions based on the gained experience since they have been involved in the development of subsea electrical equipment for many years. Feasibility studies on subsea components began two decades ago and the first commercial subsea transformer was delivered in the last decade. Since then, such manufacturers has delivered variable speed drive systems and transformers to some of the largest and most advanced offshore developments in the world.

With long experience and in-depth expertise, they offer solutions ranging from straightforward equipment supply, such as redundant monitoring systems (Ferreiro K., Haro, M. and Calvo, J. L., 2009), to full project management of the total subsea electrification network -from fixed or floating production units to subsea pipelines, wellheads or even downhole. With each delivery, the customers gain a highly qualified service and support partner to ensure that the products perform to the customers' expectations throughout the lifecycle of the field.

### The key for subsea applications

For subsea electrical consumption applications, state of the art technology provide topside variable speed drives and transformers designed to extend step-out distances

and reduce subsea cabling. Well proven topside electrification systems ensure reliable, efficient power supply to subsea power consumers and provide substantial cost savings by reducing subsea component and cabling requirements.

### *Topside Variable Speed Drives*

Based on the market-leading AC drives, topside drive systems are air or liquid-cooled and feature high robustness in a compact size. Depending on load characteristics, the topside drive system provides a step-out distance of up to 47 km. All components must be qualified and meet international standards and marine classification requirements. Typical selection of frequency converters includes:

- Drives for load up to 2 MW with 14 km reach-out distance, 11kV transmission voltage
- Drive for 2-4 MW load, 31 km reach-out distance, 25kV transmission voltage
- Drives for 8 MW load, 47 km reach-out distance, 36-52 kV transmission voltage

### *Topside Transformer*

Among the existing input transformers there are some of them that can be for 6, 12 or 24 pulse converter input. The step-up transformer is tuned for optimal voltage in the umbilical. The special developed topside transformer from is combining input and step-up transformer into one single tank. It is of a high temperature design. This gives a significant reduction of weight and volume compared to ordinary transformer solutions. They are delivered with an integrated earth fault monitoring system for the umbilical.

## **Design studies for subsea electrical systems**

Stimulating subsea oil and gas reservoirs effectively through boosting, injection and compression is critical for achieving stable production and extending the feasibility of the field.

For reservoirs with long step-out distances, powering the subsea equipment that performs these functions is a challenger task, requiring electrical equipment that is powerful, rugged and reliable.

Producing oil and gas from reservoirs located at long distances from land is a costly proposition that presents many challenges to offshore operators. Going subsea with long reach from shore or remote platform can be a very cost-efficient solution as it may eliminate the need for a fixed or floating topside installation. To help operators achieve efficient electric power supply and control at long step-out distances, some manufacturer's offers technical solutions comprising highly developed electrical products and associated services tailored for subsea production applications.

Conquering subsea gas resources with the use of cost effective technology requires being part of the world's first full-scale subsea gas compression equipment.

Some manufacturers have submitted subsea electrical equipment for full scale testing, analysis and qualification for a subsea compression application to boost gas production from the North Sea oil and gas fields. Project parameters include a tie-in distance of 47 km, and an 8MW compressor powered by a 200 Hz motor.

### The challenges for subsea compressors and motors set-up

Traditionally an electrical driven gas compressor package contains stand alone electrical motor, couplings, gear box and compressor(s) with shaft seals. A lubrication system is normally required for bearings in rotating parts. In the compact gas compressors external couplings, gearbox and shaft seals are removed, as shown in figure 14.

Magnetic bearings are used instead of lubricating bearings. The magnetic bearings can either be exposed to the transported gas or be separated from it by using a can. The electrical motor is running at the same speed as the compressor and the motor is cooled by pressurized gas alone or in combination with insulating liquid.

Rated motor speed for compact compressors can be up to 12 000 RPM. For a 2-pole motor this means a supply frequency slightly above 200 Hz. Motor windage is the highest motor loss component for the electrical motor in a compact gas compressor. It increases with speed and pressure. The loss in the long step-out power system does also increase with increased frequency. From an energy efficiency point of view, it is preferred to reduce the rated motor speed. Reduced speed will however increase the size of the compressor. In the technology qualification program, compressors with rated speed 9500 RPM and 11200 RPM have been tested. Operating speed is typically in the range of 30-100% of rated speed.

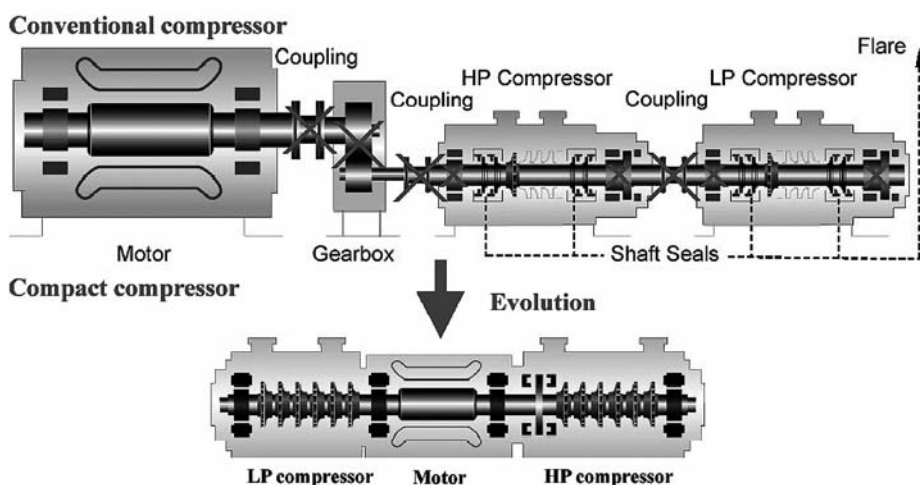


Fig. 1. The evolution of a conventional gas compression station to a compact subsea gas compression station.

Motor rotor in compact compressors can either be of solid metal design with or without a copper squirrel cage or a laminated rotor design with a copper squirrel cage.

From a rotor dynamical point of view, solid rotor is preferable. A solid rotor has a high degree of nonlinear magnetic property.

Motors that are cooled by pressurized well stream gas only, can have either conditioned gas, semi-conditioned gas or use the same gas that is going through the compressor. Compatibility between the cooling gas and the insulation material in motor and magnetic bearings is a critical success factor for the qualification of compact compressors on wet gas.

Motors that are cooled by pressurized gas and insulated liquid, separates the stator from the gas. Motor stator is then cooled by insulated liquid.

The pressure inside the motor will be slightly above gas compressor inlet pressure (any gas leakage will go from motor through labyrinths to the compressor).

Magnetic bearings have been considered as the very suitable solution for subsea applications as a lube oil system can then be omitted. In figure 1 (Gerald Scheuer et al. 2005) it is shown the evolution from a conventional gas compression station to a compact actual compression station equipped with active magnetic bearings for subsea applications.

Among the key technical items focused in the design of a gas compression module is a set of reliable components such as seals and bearings needing special attention.

Active magnetic bearings applied on motors and compressor requires also a position control system capable to support shaft unbalance and inherent vibration dynamics. Although passive magnetic bearings don't need position control, in practical applications vibration control to compensate unbalance and cavitations disturbances is required.

With the aim of improve reliability and efficiency on subsea magnetic bearings applications, next section is devoted to the description of the necessary basic equipment (test rig) to develop passive magnetic bearings and in section 3 vibration attenuation by means of a vibration control system is described.

## **PROPOSED PMB STRUCTURES.**

Magnetic bearings allow contact-free levitation. This is an attractive feature which offers some interesting advantages, such as no friction, no lubrication, low maintenance cost, long life, etc. In recent years, magnetic bearings have found applications in flywheels, pumps, compressor drives, and so on.

There are mainly two types of magnetic bearings: the active magnetic bearings and the passive magnetic bearings. The passive magnetic bearings don't need active control and extra input energy, so they are more compact and easy to use.

There are several ways to achieve passive magnetic bearings: superconductor, diamagnetic, eddy current, and permanent magnet. The simplest type of passive

magnetic bearing is only using permanent magnets. This type has the advantages of potential to miniaturization, high stiffness, reliability, and cost effectiveness. Although Earnshaw's theorem states that there is no stable and static configuration of levitating permanent magnets, permanent magnet can be used as either axial magnetic bearing or radial magnetic bearing. Actually, lots of practical magnetic bearings consist of active magnetic bearing as well as permanent magnetic bearing to obtain total stability and relatively low cost. Common configurations of permanent magnetic bearing are composed of two monolithic permanent magnetic rings with either axial magnetization or radial magnetization.

Magnetic bearings have been widely used due to their advantage of without mechanical wear and noise, which are beneficial to many applications such as subsea pumps and compressors with high speed and power. There are many different types of non-contact rotary machines. It is hopeful of designing a magnetically suspended motor with compact structure and simple control. A new structure of motor with PMB is introduced in this paper and is shown in figure 2.

Although one passive magnetic bearing is unstable, a stable PMB can be constructed by combination of a pair of two passive magnetic rings coupled in opposition

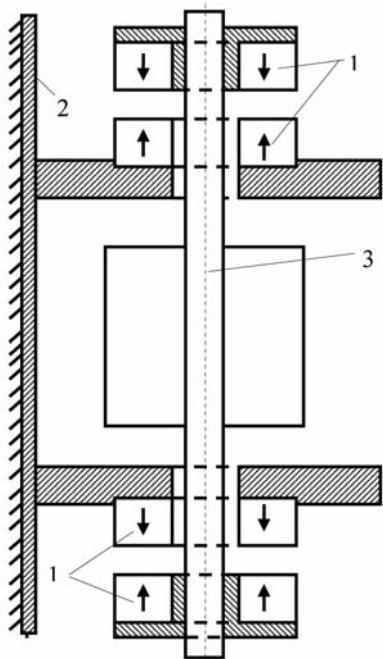


Fig. 2. Structure of a motor rotor equipped with the prototyped PMB. Axial magnetized magnetic rings, 1. Stator support, 2. Rotor body, 3.

between them, which yields the proposed prototype named the inverse PMB (IPMB). As shown in figures 2, 3 and 4 the axially polarized magnetic rings are assembled by pairs of rings in opposition, so that stability of the rotor is inherently ensured. The axial stability of the rotor can be obtained by the radial force of the passive magnetic bearings and by the instinctive behaviour of the IPMB rotor since the axial inverse magnetic forces try to keep the shaft centered with respect to the stator.

In figure 3, three stages axial IPMB is shown. The basic idea is to construct axial IPMB with the required magnetic stages for a particular application. In this prototype the supported load approaches 300 N, which is a considerable force in comparison with the magnetic mass. The axial force is then determined by the size of the magnetic mass of the magnetic rings and the number of magnetic stages.

The layout of a prototyped two stages axial passive magnetic bearing is shown in figure 4. A pair of such an IPMB is necessary at least for every shaft or rotor.

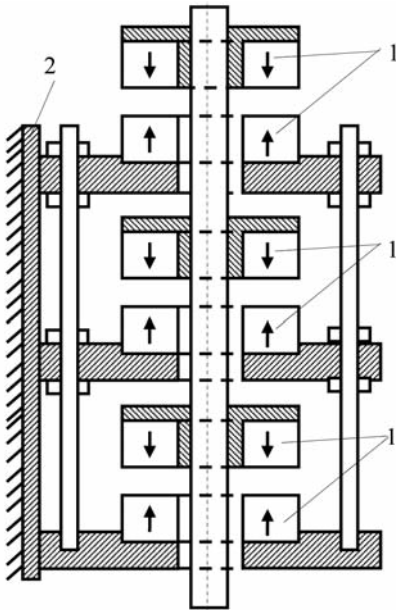


Fig. 3. Structure of a prototyped IPMB of three magnetic stages.

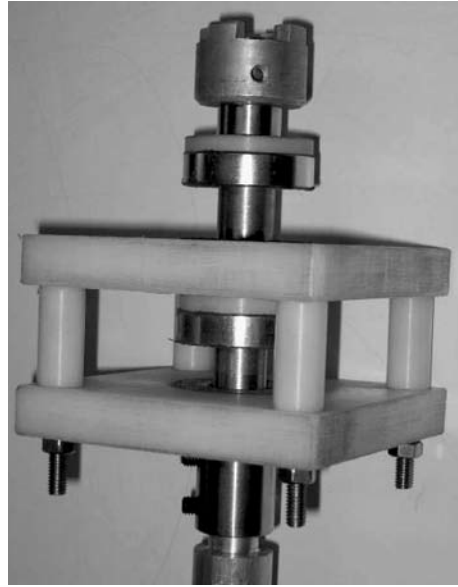


Fig. 4. Prototyped two stages axial passive magnetic bearing.

## VIBRATION CONTROL

### Introduction to Vibration Control

Motors, compressors, and turbines or pumps and blowers including all rotating machinery in general, is commonly used in process industry, including machining tools, power generation, as well as aircraft and marine propulsion among the most important industrial applications. Mass imbalance is commonly responsible for rotating machinery vibration. When the principal axis of inertia of the rotor is not coincident with its geometric axis imbalance occurs. Nevertheless there are some more causes for rotating machinery vibration such as operation near resonant frequencies or critical speeds.

There are two major categories in AVC techniques for rotating machinery:

- Direct active vibration control (DAVC) techniques in which directly apply a lateral control force to the rotor.
- Active balancing techniques which adjust the mass distribution of a mass redistribution actuator. Active balancing isn't under the scope of this work.

The control variable in DAVC techniques is a lateral force generated by a force actuator based on a magnetic bearing. The advantage of DAVC techniques is that the input control force to the system can be changed according to vibration characteristics.

By applying a fast changing lateral force to the rotating machinery, the total vibration, including the synchronous vibration, the transient free vibration, and other nonsynchronous vibration modes of the rotating machinery, can be attenuated or suppressed. The limitation of most force actuators is the maximum force they can provide. In high rotating speed, the imbalance-induced force could reach a very high level. As most force actuators cannot provide sufficient force to compensate for this imbalance-induced force, active balancing methods are well justified. Although active balancing methods can eliminate imbalance-induced synchronous vibration, they cannot suppress transient vibration and other nonsynchronous vibration.

(Maslen and Bielk, 1992) (R. Larsson, 1998) presented a stability model for flexible rotors with magnetic bearings. Besides the flexible rotor model itself, their model included the dynamics of the magnetic bearing and the sensor-actuator noncollocation. This model can be used for stability analysis and active vibration synthesis.

Most recently, an analytical imbalance response of the Jeffcott rotor with constant acceleration was developed by (Zhou and Shi, 2001). They concluded that a satisfactory solution quantitatively shows that the motion consists of three parts:

- the transient vibration at damped natural frequency,
- the synchronous vibration with the frequency of instantaneous rotating speed,
- and a suddenly occurring vibration at damped natural frequency.

Such mentioned technique provides physical insight into the imbalance-induced vibration of the rotor during acceleration. For this reason it can be used for the synthesis of AVC schemes.

For the synthesis of DAVC techniques, most it is common to use simplified low-order finite element models of the rotor system. Although the techniques developed can be extended to a high-order system theoretically, the computational load and consequently the signal-to-noise ratio will have to be higher. The DAVC techniques can be difficult to implement for the high-order system. Therefore, it is conveniently to use a reduced order models to approximate the high-order system models. Applied model reduction techniques have a specific impact on the performance of the DAVC schemes that must be considered if expected performance cannot be achieved.

### **AVC with Magnetic Actuators**

This section presents the test environment for active vibration control of rotating machinery. The principal idea is to control bending vibrations of a flexible rotor, supported by AMBs based on two sets of non-contacting electromagnetic actuators located at both shaft ends as shown in figure 5.

The test environment is composed of the following parts; a rotor test rig, two sets of magnetic actuators assembled to operate as both electromagnetic actuators and

AMBs, and a programmable control unit (C.R. Fuller, S.J. Elliot, and P.A. Nelson, 1996), (C.R. Knospe, et.al, 1997), (S.J. Elliot, 2001) to be applied on vibration attenuation or vibration suppression by means of feedback control applied to decrease the dynamic response of the rotor assumed as active magnetic dynamic damping. The main studies to be carried out on the described test rig deals with the dynamic response in the range of

velocities of interest, especially near the resonant frequency region which can be reduced with a conventional velocity-feedback controller, or alternatively feedback filtering based control (K. Tammi (a), 2003)

The use of a velocity feedback controller decreases the response of the rotor significantly. The active control brings the possibility to run the rotor across the critical speed. A feedforward system, based on an adaptive finite-impulse-response filter (K. Tammi (b), 2003), may also be designed to compensate disturbances caused by the mass imbalance if a reliable model of imbalance is available.

As shown in figure 6, every degree of freedom to be controlled requires a feedback control loop. The control system applies the force commands to attenuate shaft vibration while keeping the shaft into the radial position centre. The implementation of a shaft end vibration and position control scheme is shown in figure 6. It consists in an Agilent Technologies based hardware programmed under Matlab-Simulink V.9(a).

Every shaft end should be equipped with a control system comprising at least the parts shown in figure 5. It consists in two independent closed loop controllers to attenuate or suppress the shaft vibration in the normal plane of the shaft. The other shaft end should be equipped with a similar system.

### Control Loop hardware

Control loops accessories such as data acquisition and final control elements or actuation devices are implemented with specifically designed hardware based components.

Radial displacement is sensed by means of a data acquisition system which is based on a set of Eddy current probes. Axial displacement is measured under the same technology. Eddy Current Probe (ECP) systems are integral components,

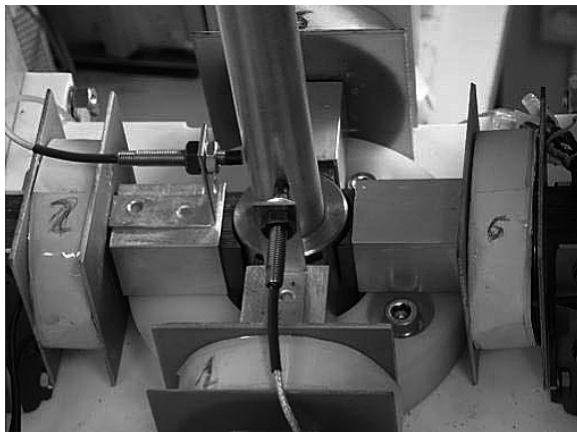


Fig. 5. A detail view of the test-rig electro-magnetic actuators for vibration control.

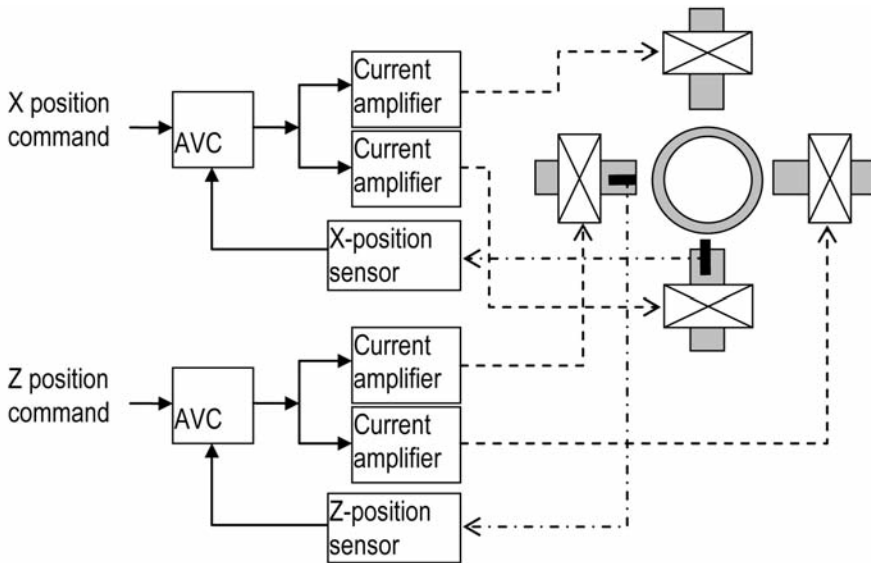


Fig. 6. Control structure for every shaft end

which typically consists of a non-contacting probe, an extension cable and a driver. An ECP typically senses mechanical movement and converts this movement (displacement) into a usable electrical signal.

**THE AVC UNDER UNBALANCE INFLUENCES**

To initiate the discussion, it is appropriate to consider the traditional diagram of a Jeffcott rotor as shown in figure 10 (a).

At very low speeds, unbalance forces are negligible. The shaft turns around bearing centreline and all rotating elements are concentric. This condition is depicted in the detail (b) of figure 10. As rotor speed increases, the straight shaft will deflect into the predictable mode shape shown in figure 7.

The only driving force in the system is the centrifugal force due to the unbalance mass  $M$ .

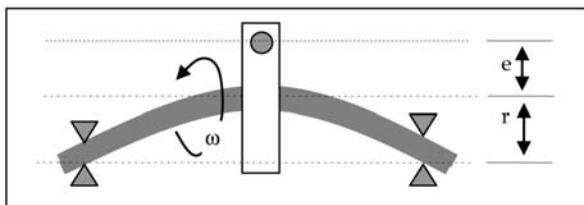


Fig.7. Shaft deflection mode under centrifugal forces due to an imbalanced mass.

The maximum bending deflection of the shaft is identified by  $r$  and the mass eccentricity by  $e$ . Furthermore, the rotational speed is indicated by  $\omega$ . By inspection of the figure 11 it can be seen that the shaft and disk are rotating at the

operating speed  $\omega$ . Simultaneously, the deflected shaft is whirling in the magnetic bearings at this speed. The mechanism driving this whirl is the centrifugal force generated by the eccentric mass on the disc. As rotor speed increases, the outward force increases in accordance with the normal centrifugal force  $F_c$  equation

$$F_c = M \cdot (r + e) \cdot \omega^2 \quad (1)$$

With regard to expression (1), the total radius of the mass unbalance  $M$  is composed of the shaft bending  $r$ , and the eccentricity of the mass with respect to the shaft centreline  $e$ . Such centrifugal forces will be compensated as much as possible by the active magnetic forces developed by the control algorithm. Since the shaft speed is squared in expression (1), the shaft rotational speed has a strong influence on the AVC algorithm. Nevertheless, such influence is attenuated due to the inertial effect of the rotor which causes the response magnitude to decrease as rotational speed increases. The developed test rig has been subjected to experimental validation where a feedback control action provided by a PID is implemented. Several controller gains have been applied so that the time response is achieved for variable rotational speeds.

As shown in figure 8 a vibration control test is performed under variable rotational speed. The rotating speed is varying from zero at the start point to 16 rad/sec. in about 50 seconds. At same time, different controller gains have been applied. As consequence, after three tests with different controller gains given as  $K_p= 3, 5$  and  $7$  respectively, three time responses were achieved and shown in figure 9 As depicted in figure 9, analytical or theoretical prediction of the optimum controller gain  $K_p$ , is

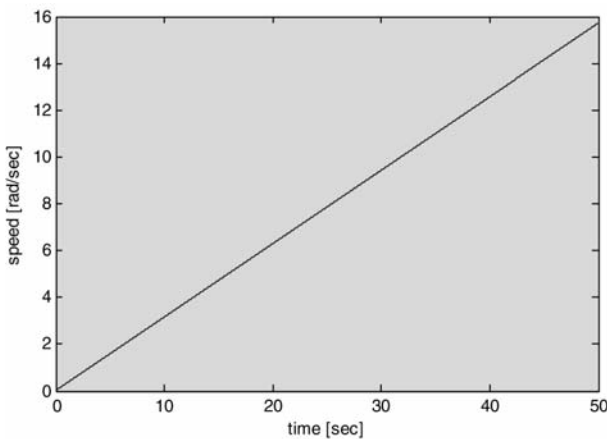


Fig. 8. Rotational speed (Rad/sec) as function of time.

not trivial. Instead, the selection of a controller gain  $K_p$  such that for a known rotating speed the response be acceptable, appears to be a satisfactory solution.

Generally, for very low rotating speeds, a low gain value is better than a high one. As rotational speed increases the effect of varying the controller gain is decreasing. This means that for high frequency vibration the vari-

ation of the AVC algorithm gain is not effective at all. An interesting topic to be taken into account with regard to the vibration attenuation is the vibration effect of the shaft on the shaft support rig. If the rotor mass insignificant with respect to the bedplate mass, then vibration attenuation may be considered effective. On the other hand, shaft vibration is transmitted to the bedplate, with dramatic consequences.

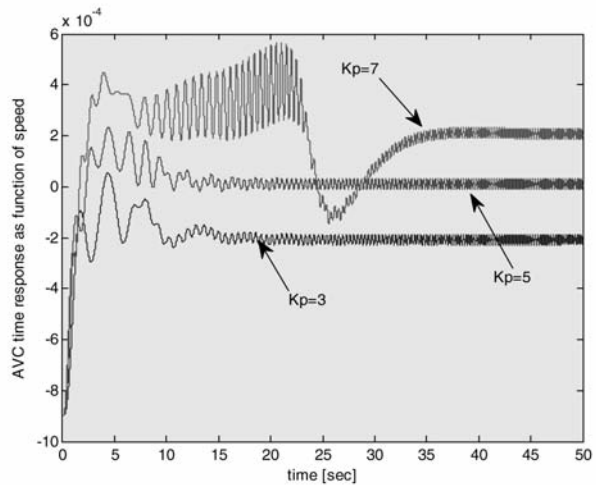


Fig. 9. Time response of the AVC as function of rotation speed.

## DISCUSSION AND CONCLUSIONS

A test rig has been designed and implemented to improve vibration attenuation of rotating machines installed on subsea environments.

Active balancing techniques promise solution to many of these problems and lead to significant economic benefits through increased reliability of machinery and the enabling of other advanced technologies.

Previous state-of-the-art non-adaptive active balancing control methods required extensive *a priori* modelling of system dynamics. Existing adaptive control methods for active balancing were not able to take advantage of the most recent data fast enough to ensure good performance and stability in the event of time-varying or nonlinear dynamics. This means that it is necessary a great research effort on this field, which must be associated to efficient and sophisticated test rigs to accurately improve and verify results.

According our experience, vibrations around the critical can be efficiently damped by velocity feedback control. It provided a possibility to run the rotor at critical speed by virtue of increased damping. It also provided smoother phase characteristics, which made feedforward compensation easier.

Control algorithms based on velocity feedback are one of the simplest examples for active vibration control in general. An important reason for this is the characteristically low damping of mechanical systems; a significant reduction in response can be achieved by a simple controller acting against vibration velocity. According to the literature review, the control method has also been applied to rotors. It has been shown experimentally that the reduction is significant in the resonance region for a rotor with low external damping.

The resonance can also be shifted with the control system by implementing a control force proportional to the displacement of the rotor. A load-carrying function is thus applied. This was briefly tested and found to work in the test environment. However, in heavy rotating machines, very large forces would be required and electromagnet based actuators under such conditions are not useful.

Velocity feedback control can also be successfully associated to feedforward control. Feedforward compensation converges at low frequencies, and outside the range of resonant frequencies, but diverges when the resonance frequencies are approached.

As mentioned, advanced control techniques and algorithms are being applied in order to render efficient productivity under the increasing industrial demands.

A variety of sophisticated control algorithms using the most efficient techniques to identify and estimate the rotating machine parameters, observer design, and advanced filtering is being applied. Nevertheless the AVC continues being an intensive research area. The improvement of control algorithms as well as control strategies will be validated by means of the developed test-rig, which can be modified to support a diversity of scenarios with different loads and changing severe operating conditions.

## REFERENCES

- Ferreiro, R.; Haro, M. and Calvo, J.L. (2009): "On sensor FDI by functional and physical redundancy applied to DP systems," *Journal of Maritime Research*, Vol-VI. No. II, pp. 53-70.
- Fuller, C.R.; Elliott, S. J. and Nelson, P. A. (1996): *Active Control of Vibration*, Academic Press, New York.
- Gerald Scheuer, Bjarne Monsen, Knut Rongve, Tor-Odd Ronhovd, Tor-Eivind Moen, Esa Virtanen and Steve Ashmore (2005): Subsea compact gas compression with high-speed VSDs very long step-out cables. ABB. Switzerland. Statoil Hydro ASA.  
<http://ieeexplore.ieee.org/stamp/stamp.jsp?arnumber=05164879>;
- K. Tammi (a) (2003): Active Vibration Control of Rotor in Desktop Test Environment, VTT -Technical Research Centre of Finland, VTT Publications series 498, Espoo, Finland 2003.
- K. Tammi (b) (2003): Mass imbalance compensation of rotor with adaptive finite-impulse-response filter and convergent control, VTT Industrial Systems, Espoo 2003, pp.23, Research report BTUO57-031122.
- Knospe, C.R.; Tamer, S.M. and Fittro, R. (1997): "Rotor Synchronous Response Control: Approaches for Addressing Speed Dependence," *Journal of Vibration and Control*, 3, 435-458.
- Maslen, E.H. and Bielk, J.R. (1992): "A Stability Model for Flexible Rotors with Magnetic Bearings," *ASME Transactions, Journal of Dynamic Systems, Measurement, and Control*, 114, 172-175.
- Moreno, V.M. and Pigazo, A. (2007): "Future trends in electric propulsion systems for commercial vessels," *Journal of Maritime Research*, Vol-IV. No. II, pp. 81-100.
- Pyrhonen, J.; Nerg, J.; Kurronen, P. and Lauber U. (2008): "High-speed, 8 MW, solid-rotor induction motor for gas compression", 18. International conference on electrical machines, Vilamoura, Portugal, Sep. 2008. pp. 1-6.
- R. Fantoft (2005): FMC Kongsberg Subsea AS. Subsea gas Compression-Challenges and Solutions. Offshore Technology Conference. OTC 17399. Houston, TX, U.S.A. 2-5 may 2005. pp. 1-6.
- Raad, R.O.; Henriksen, T.; Raphael, H.B.; Hadler-Jacobsen, A. (1996): "Converter fed subsea motor drives", *IEEE Transactions on Industry Applications*, 32, 5, Sep/Oct 1996
- R. Larsonneur (1998): "*Design and Control of Active Magnetic Bearing Systems for High Speed Rotation*", PhD Thesis, Swiss Federal Institute of Technology, ETH Zurich, Switzerland..
- S.J. Elliot (2001): *Signal Processing for Active Control (Signal Processing and its Applications)* Ed. Stephen Elliot, Academic Press, London.
- Zhou, S. and Shi, J. (2000): "Active Balancing and Vibration Control of Rotating Machinery: A Survey", Sage Publications, *The Shock and Vibration Digest*, 33, 4, 361-371



## EXPERT GUIDANCE SYSTEM FOR UNMANNED AERIAL VEHICLES BASED ON ARTIFICIAL NEURAL NETWORKS

F. Fernández<sup>1,2</sup>, E. Besada<sup>1,3</sup>, D. Sanchez<sup>1,4</sup> and J.A. López-Orozco<sup>1,5</sup>

Received 10 February 2011; in revised form 16 February 2011; accepted 17 March 2011

### ABSTRACT

This article proposes an expert guidance system for Unmanned Aerial Vehicles (UAVs) for marine rescue missions. The difficulty of the problem, due to the time constraints that the mission has to fulfil are lightened by the use of Artificial Neuronal Networks, taking advantage of their high adaptability, low memory requirements, real time response capability, and extrapolation properties. We use them to implement two different types of behaviours for the two main phases of the task: in prediction mode they are responsible of calculating the displacement that the castaways suffer due to the sea and wind currents and in sensing mode they are in charge of guiding the UAV while it tracks already found shipwrecked and search for new ones. To illustrate the successful behaviour of the expert system embedded in a simulator, some results are shown in the final section.

**Key words:** Castaway, Shipwreck, Artificial Neural Network, Unmanned Aerial Vehicle, Search and rescue.

### INTRODUCTION

The technological advances in unmanned vehicles are being exploited by a growing number of projects of the research areas of control, cooperation and artificial intelligence (ASF, BERK, CALT-Mur, MAGIC, MICA, MIT). The employment of these

<sup>1</sup> Universidad Complutense de Madrid, Av. Complutense s/n, 28040 Madrid, Spain. <sup>2</sup> Phd student, Email: francisco.fernandez.ramirez@gmail.com, Tel. 34913944436, Fax. 34913944687. <sup>3</sup> Assistant Professor, Email: evabes@dacya.ucm.es, Tel. 34913944740, Fax. 34913944687. <sup>4</sup> Phd Student, Universidad Complutense de Madrid, Email: davisanc@fis.ucm.es, Tel.34913944375, Fax. 34913944687. <sup>5</sup> Associated Professor, Email: jalo@dacya.ucm.es, Tel. 34913944436, Fax. 34913944687.

vehicles is extending to multiple civil and military fields too, such as surveillance tasks (Houden, 2008) or reconnaissance missions (Tian, 2006; Besada-Portas 2010).

The demanding time constraints of sea rescue tasks can benefit of the use of these types of vehicles: when a ship wrecks, the time elapsed between the shipwreck, its detection by a rescue centre, and the departure and arrival of a rescue vessel, can't be too long. Finding the castaways quickly is primordial but hard: as time passes the shipwrecked are spread by the sea winds and currents along a wide area, rendering their location difficult. The complementary capacities of Unmanned Air Vehicles (UAVs) and Unmanned Surface Vessels (USVs) can facilitate the rescue task: quickly UAVs can be sent to locate the castaways and precise USVs to perform their rescuing. This paper focuses on the UAV search and tracking side of the sea rescue task.

The capabilities of the UAVs to perform rescue or tracking tasks in designated areas have already been used in other problems (Kamrani and Ayani, 2009; Rubio et al., 2004). In our research, these capabilities are developed by an expert system that is in charge of obtaining the high level commands that will properly guide the UAV towards and inside the rescue area. We assume that the UAV already incorporates a low level stabilization and control system that interprets the high level commands. That is, the high level expert system guides the vehicle, while the low level stabilization and control system drives it. Finally, the time restrictions of the task and the resource constraints of the onboard UAV CPU have to be considered too in the expert system design.

In order to achieve all the necessary requirements, we have designed a guidance expert system based on Artificial Neural Networks (ANNs), which are parallel computing structures for *modelling* and *learning* nonlinear complex behaviours (Haykin, 1999; Patterson, 1996). Their high adaptability, low memory requirements, real time response capability, and easy integrability are also appealing. Our expert system incorporates two types of ANNs: ones to predict the position of the castaways before they are located by the UAV and other to guide the UAV after finding the first shipwrecked. We also learn their behaviours: the prediction ANN parameters are adapted to the sea rescue environment while the sensing ANN behaviour extrapolates the knowledge of an expert to different situations. So, our ANN based guidance expert system adapts to the rescue task. Besides it doesn't require much memory or CPU resources.

The rest of this paper is organized as follows. Section 2 describes and formalizes the sea rescue problem. Section 3 presents the UAV expert system, starting with their differing elements and ending with the whole system. Finally, section 4 shows the results of using the designed expert system in two different simulated rescue tasks.

## PROBLEM DESCRIPTION

Searching and tracking shipwrecked people or items with an UAV is a difficult task due to the dynamics and uncertain behaviour associated to the different elements of

the system. On one hand, the shipwrecked elements are stochastically moved by the sea and wind currents. On the other, the UAV only collects noisy measurements of the shipwrecked positions that are inside the camera field of view or that have been beacons by the UAV when first detected. Then, while no shipwrecked are observed, the UAV needs to find them using a predictive model. Once shipwrecked are found and beacons, it can track them while searching the rest. In both cases, the search is carried out by moving the UAV, whose position is deterministically controlled by high level commands. Hence, the rescue task consists on selecting the commands that let the UAV efficiently find the shipwrecked. In the remaining parts of this section we present the notation and the model of the problem used throughout the paper.

### Notation

In this paper, a capital italic letter ( $V$ ) represents a unidimensional variable, a bold-face capital italic letter ( $\mathbf{V}$ ) - a multidimensional one, and a lowercase roman letter ( $f$ ) a function. Sub-indexes are used to distinguish variables:  $t$  associates the variable to the  $t$ -th timestep and  $i$  - to any of its possible realizations. Super-indexes are used to distinguish the elements of multidimensional variables:  $x$  and  $y$  refer them to Cartesian coordinates,  $r$  and  $\theta$  - to polar coordinates. For example,  $M_{t,i}$  represents the  $i$ -th variable labelled  $M$  at time step  $t$  and  $M_{t,i}^x$  stands for its corresponding  $x$  coordinate. Finally,  $\text{dir}(\Delta X, \Delta Y)$  is the function that calculates the orientation of the vector  $[\Delta X, \Delta Y]$  and  $\text{IsTrue}(\text{BooleanExpression})$  the indicator function that returns 1 when the Boolean expression is true and 0 otherwise.

### General problem Formulation

To model the behaviour of the problem, we assume that the number of elements needing rescue is fixed and equal to  $N$ , and consider the following variables:  $U_t$  to represent the position of the UAV;  $A_t$ , the high level control command applied to the UAV;  $M_{t,i}$ , the real position of the  $i$ -th shipwrecked;  $D_{t,i}$ , the moment the  $i$ -th shipwrecked element was first detected (i.e.: never, just, previously); and  $S_{t,i}$ , the measurement obtained by the UAV for the  $i$ -th detected shipwrecked. Moreover,  $U_t = [U_t^x, U_t^y, U_t^\theta]$ ,  $M_{t,i} = [M_{t,i}^x, M_{t,i}^y]$  and  $S_{t,i} = [S_{t,i}^x, S_{t,i}^y]$ . Finally, the control command  $A_t = [A_t^x, A_t^y]$  indicates the next waypoint that the UAV has to be driven to by the low level onboard UAV controller.

The relationships among all these variables are schematized in figure 1, where variables in circles belong to the hidden state space, variables in squares are observations, and an arrow  $V \rightarrow W$  means that the value of  $W$  depends on the value of  $V$ . In other words, figure 1 represents that  $U_{t+1} = f(U_t, A_{t+1})$ ,  $M_{t+1,i} = g(M_{t,i})$ ,  $D_{t+1,i} = h(D_{t,i}, M_{t+1,i}, U_{t+1})$ , and  $S_{t+1,i} = q(D_{t+1,i}, M_{t+1,i})$ . Function  $f$  deterministically models the UAV evolution, and so it depends on the UAV characteristics. Function  $g$  stochastically models the shipwrecked evolution, and so the sea wind and currents that move the ship-

wrecked elements are included in its definition. The remaining two functions are related with the beacon and camera measurement systems. Function  $h$  models the evolution of  $D_{t,i}$ : from *never* detected to *just* detected when the camera first observes the object falling inside its field of view, and from *just* detected to *previously* detected in the following time step. When the shipwrecked is just detected, function  $q$  behaves as the noisy camera measurement model, and hereafter, as the noisy beacon measurement model.

At each time step, the high level command  $A_t$  applied to the UAV must increment the chances of finding new never detected shipwrecked. Then,  $A_t$  is calculated in closed loop to be able to take into account the current observations and past history.

The way to proceed to obtain  $A_t$  depends on the available information. Before the first shipwrecked is located by the UAV camera system, the UAV can only use the predicted  $M_{t,i}$  and the UAV position  $U_t$  to decide where to go. Once the position of any item is detected, i.e. when the UAV starts collecting  $S_{t,i}$ , the high level command  $A_t$  can directly depend on the shipwrecked measured locations. In short: before finding castaways,  $A_t = r(U_{t-1}, \{M_{t,i} | i = 1:N\})$ ; and afterwards,  $A_t = c(U_{t-1}, \{S_{k,i} | D_{k,i} \neq \text{never}, k \leq t\})$ , where the functions  $r$  and  $c$  represent the high level controllers for the prediction and sensing working modes respectively.

The objective of our research is to find efficient implementations for both high level controllers that let the UAV robustly respond to the evolution of  $M_{t,i}$  or  $S_{t,i}$ .

**UAV CONTROLLERS BASED ON ANNs**

In the following two sections, we present the controllers used in each of the working modes. They fulfil the efficiency and robustness requirements by means of employing properly trained ANNs. Afterward, the whole system, that also includes a manager responsible of selecting the correct controller and handling exceptions, is described.

**Prediction mode**

Before the first castaway is located by the UAV, the UAV can only be driven towards the shipwrecked positions  $M_{t,i}$ . However, as  $M_{t,i}$  belongs to the system state and not

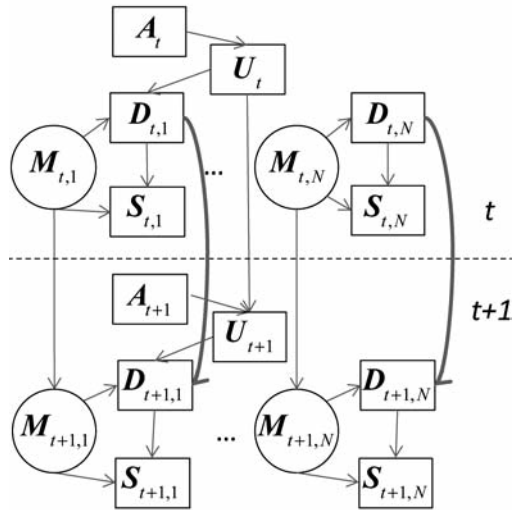


Figure 1. Dependencies of the problem variables.

to the observations,  $M_{t,i}$  has to be calculated too. That is, when the controller is working in this mode, not only does the expert system have to implement the controller  $A_t = r(U_{t-1}, \{M_{t,i} | i = 1:N\})$ , but also a module, called predictor hereafter, responsible for obtaining all  $M_{t,i}$  with the selected  $M_{t+1,i} = g(M_{t,i})$  and the initial location  $M_{0,i}$  where the vessel sunk. Figure 2 shows the connection between both subsystems.

Since the efficiency of the complete prediction controller (which obtains  $M_{t,i}$  and  $A_t$ ) depends on both functions  $g$  and  $r$ , special care should be taken when selecting them.

*Prediction model  $M_{t+1,i} = g(M_{t,i})$*

The prediction  $g$  models usually available in rescue centres, such as the Mercator Ocean (MERCATOR) or the Spanish Project ESEEO (Álvarez, 2005), are too complex and slow for the UAV CPU. Online predictions based on wind and current maps, generated with numerical models such as HIRLAM

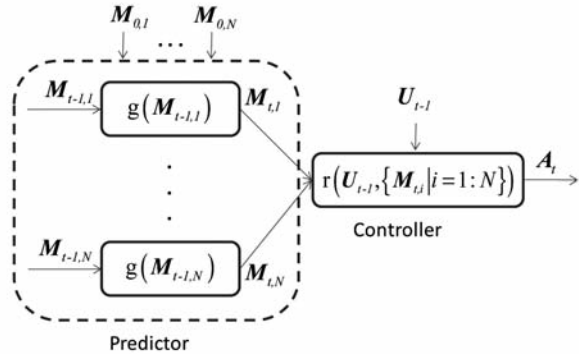


Figure 2. Complete prediction controller.

(High Resolution Limited Area Model, Gómez and Carretero, 2005) or CEPPM (Medium Term Prediction European Center), are not fast enough either because they have to generate dense maps to obtain the wind and current values at every  $M_{t,i}$ , and predict  $M_{t+1,i}$  based on the previous  $M_{t,i}$ . Therefore we opt to implement a prediction model  $g$  with an ANN trained offline at the rescue centre before the UAV starts its mission.

To develop our predictor, we implement the function  $g$  as the incremental model presented in equation (1), where function  $p$  is a feedforward ANN.

$$M_{t+1,i} = M_{t,i} + p(M_{t,i}) \tag{1}$$

This incremental implementation of  $g$  makes  $M_{t,i} = [M_{t,i}^x, M_{t,i}^y]$  the natural input for the ANN, and  $M_{t+1,i} - M_{t,i} = [M_{t+1,i}^x - M_{t,i}^x, M_{t+1,i}^y - M_{t,i}^y] = [\Delta M_{t+1,i}^x, \Delta M_{t+1,i}^y] = \Delta M_{t+1,i}$  its output. Then, since  $\Delta M_{t+1,i} = p(M_{t,i})$ , the ANN is forced to learn the displacement caused to the shipwrecked by the local conditions on each point of the environment.

The pairs of input  $M_{t,i}$  – output  $\Delta M_{t+1,i}$  used to train the ANN are generated with the numerical predictor  $g$  used in the rescue centre. As function  $g$  returns  $M_{t+1,i}$  and the ANN output is  $\Delta M_{t+1,i}$ , this last value has to be calculated to generate the training data pairs. The training data are used to update the weights of the ANN with the Bayesian Regulation Backpropagation algorithm. This algorithm calculates the ANN

parameters, using a method that combines the squared errors and ANN weights in such a way that a well generalizing ANN is usually obtained (MacKay D., 1992). The training phase takes into account the error between the  $\Delta M_{t+1,i}$  obtained with the ANN and the  $\Delta M_{t+1,i}$  obtained after subtracting  $M_{t,i}$  from the output  $M_{t+1,i}$  of the numerical predictor  $g$ . Figure 3 summarizes the complete training task.

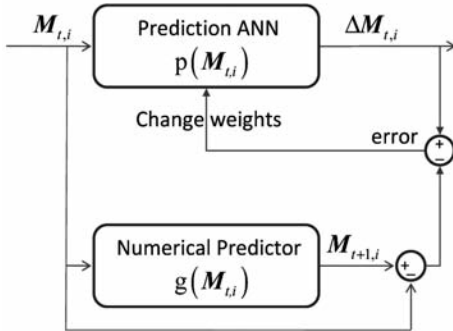


Figure 3. Training step of the prediction network.

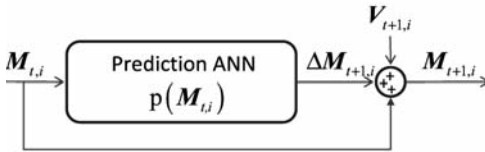


Figure 4. Onboard predictor  $M_{t+1,i} = g(M_{t,i})$

The numerical predictor  $g$  used in our experiments to train the ANN  $p$  predicts the next shipwrecked positions using a grid map of forces caused by the sea winds and currents. The trained ANN generalizes the effects of those winds and currents over the shipwrecked on the points defined by the grid map.

The onboard predictor  $g$ , represented in figure 4, obtains  $M_{t+1,i}$  from  $M_{t,i}$  using the trained ANN  $p$  to generate the displacement  $\Delta M_{t+1,i}$  and an additive Gaussian random variable  $V_{t+1,i}$ , with zero mean and covariance  $Q$ , that models little disturbances not included in the numerical predictor.

The simplicity of the onboard  $g$  depends on the properties of the ANN. To speed up these operations,

we successfully use a feedforward ANN with two inputs  $[M_{t,i}^x, M_{t,i}^y]$ , two outputs  $[\Delta M_{t+1,i}^x, \Delta M_{t+1,i}^y]$ , and three layers with only two neurons in the input layer, four in the hidden and two in the output. Its training time is small too: a convergent ANN is usually available in only 5 minutes using a Pentium Core Duo. Therefore, the offline training step might be carried out while the UAV gets ready for its mission.

Finally, it is worth mentioning that there are other types of ANNs, such as the recurrent ones, that are directly used to predict a sequence (at different time steps) of outputs given the initial conditions (Hontoria et. al, 2001). Our prediction ANN is different (it learns the displacement between two successive points of the sequence), facilitates the learning task, and usually reduces the accumulated error at the end of the sequence.

$$\text{Controller } A_t = r(U_{t-1}, \{M_{t,i} | i = 1:N\})$$

The function that obtains the high level command  $A_t$  based on the predicted positions of the shipwrecked elements  $M_{t,i}$  needs to conduct the UAV towards them as quickly as possible to let the UAV visual system find the first shipwrecked.

An efficient way to achieve an appropriated behaviour consists on generating the high level command that makes the UAV move towards the mean value of  $M_{t,i}$ . So, the controller function  $r$  implements the following equation:

$$A_t = \frac{1}{N} \sum_{i=1}^N M_{t,i} \quad (2)$$

Note that with this way of proceeding the UAV doesn't necessary arrives to the mean value of  $M_{t,i}$  in the following time step, because the high level command only identifies the next waypoint that the UAV has to visit. Besides, the trajectory followed by the UAV to reach the waypoint depends on the UAV and low level controller properties.

In spite of the simplicity of this controller, the UAV can usually intercept the mean predicted trajectory of the shipwrecked by redirecting the UAV while approaching the castaways. However, when the shipwrecked predicted positions are not correct (due to a significant discrepancy on the real and predicted environmental conditions), the UAV can only verify that there are no castaways in the vicinity of the mean expected area and notify it to the rescue centre.

### Sensing Mode

When the vessel wrecks near the rescue centre or sea winds and currents do not disperse the shipwrecked elements far from the wreckage zone, the UAV may find them quickly. However, when the shipwrecked have been dispersed before finding the first, the UAV has to track it and look for the remaining.

In order to facilitate the tracking task, the UAV puts a beacon in each shipwrecked the first time it detects them. So, after the UAV visual system first observes the location  $S_{t,i}$  of any element, the UAV keeps obtaining its new locations  $S_{t,i}$  from its designated beacon. This way of proceeding also favours the search and rescue tasks: the UAV can move freely to search unobserved elements while tracking the already observed that fall outside its field of view, and the vessels in charge of rescuing the shipwrecked can be sent towards the designated beacons.

The searching task requires a function that obtains  $A_t$  taking into account the possible errors of the predictors and the shipwrecked dispersion. The first requirement is fulfilled using (in the controller  $c$  of the sensing mode) the available measurements of the shipwrecked  $\{S_{k,i} | D_{k,i} \neq \text{never}, k \leq t\}$  instead of the predicted position  $M_{t,i}$  (used in the prediction controller  $r$ ). For achieving the second, the sensing controller  $c$  is developed over a feedforward ANN s, which is trained with the behaviours proposed by an expert for different situations.

*Sensing ANN controller*  $A_t = c(U_{t-1}, \{S_{k,l}|D_{k,l} \neq \text{never}, k \leq t\})$

Implementing a sensing controller that uses the available measurements  $\{S_{k,l}|D_{k,l} \neq \text{never}, k \leq t\}$  requires a function  $c$  with an increasing number of inputs. To fix the number of inputs and compact the available information, we select the following four parameters (after checking other possibilities also based on  $\{S_{k,l}|D_{k,l} \neq \text{never}, k \leq t\}$ ) as the best sensing ANN inputs:

- $I_{t,1}$ , the orientation of the mean direction of the previously observed shipwrecked. This variable lets the ANN know the global tendency of the already located shipwrecked elements.
- $I_{t,2}$ , the distance of the UAV to the mean location of the previously observed shipwrecked. This variable lets the ANN know how far the UAV might travel while it still observes castaways and changes the searching radio of the ANN.
- $I_{t,3}$ , the orientation of the mean direction of the shipwrecked that have only been observed twice (because we need two elements to determine a direction). This variable lets the ANN know if the unobserved elements are dispersing and consider new searching directions.
- $I_{t,4}$ , the percentage of already located shipwrecked. This variable adapts the erratic behavior and searching radio of the ANN.

The relationships between the four ANN inputs  $[I_{t,1}, I_{t,2}, I_{t,3}, I_{t,4}]$  and the available measurements  $\{S_{k,l}|D_{k,l} \neq \text{never}, k \leq t\}$  are presented in the following equations:

$$I_{t,1} = \text{dir} \left( \sum_{i|D_{t-1,i} = \text{previously}} (S_{t,i}^x - S_{t-1,i}^x), \sum_{i|D_{t-1,i} = \text{previously}} (S_{t,i}^y - S_{t-1,i}^y) \right) \quad (3)$$

$$I_{t,2} = \sqrt{\left( \frac{\sum_{i|D_{t-1,i} = \text{previously}} S_{t,i}^x}{\sum_{i=1:N} \text{IsTrue}(D_{t-1,i} = \text{previously})} - U_t^x \right)^2 + \left( \frac{\sum_{i|D_{t-1,i} = \text{previously}} S_{t,i}^y}{\sum_{i=1:N} \text{IsTrue}(D_{t-1,i} = \text{previously})} - U_t^y \right)^2} \quad (4)$$

$$I_{t,3} = \text{dir} \left( \sum_{i|D_{t-1,i} = \text{just}} (S_{t,i}^x - S_{t-1,i}^x), \sum_{i|D_{t-1,i} = \text{just}} (S_{t,i}^y - S_{t-1,i}^y) \right) \quad (5)$$

$$I_{t,4} = \frac{\sum_{i=1:N} \text{IsTrue}(D_{t-1,i} \neq \text{never})}{N} \quad (6)$$

Note that to obtain  $I_{t,1}$  and  $I_{t,3}$ , we don't divide the summations between  $N$ , because vectors  $[\Delta X, \Delta Y]$  and  $\left[ \frac{\Delta X}{N}, \frac{\Delta Y}{N} \right]$  have the same orientation. Besides, the summations are over  $D_{t-1,i}$  to ensure that there are at least two observations for the new located elements and more than two for the previously located ones.

The sensing ANN output cannot be directly  $A_t$  since it stores the next waypoint, in global Cartesian coordinates, that the UAV has to reach, and the ANN inputs  $[I_{t,1}, I_{t,2}, I_{t,3}]$  are distances and orientations, which only provide relative information. Therefore, we choose as sensing ANN output  $O_t = [O_t^r, O_t^\theta]$ , a high level command that stores the displacement and orientation that the UAV has to follow to reach the waypoint  $A_t$ . The relationships between  $A_t$  and  $O_t$  are defined by the next expressions:

$$A_t^x = U_t^x + O_t^r \cos O_t^\theta \tag{7}$$

$$A_t^y = U_t^y + O_t^r \sin O_t^\theta \tag{8}$$

Figure 5 presents the complete sensing controller  $A_t = c(U_{t-1}, \{S_{k,l} | D_{k,l} \neq \text{never}, k \leq t\})$ , that consists of the sensing ANN  $O_t = [I_{t,1}, I_{t,2}, I_{t,3}, I_{t,4}]$ , and the input and output translation processes (Equations (3-6) and (7-8)). The simplicity of the translation operations doesn't overload the complete sensing controller. Moreover, the use of a sensing ANN, whose inputs and outputs are relative coordinates, allows the complete sensing controller to extend the behaviour learnt through the information gathered on one point, to the rest of the space. Finally, the selected ANN is a feedforward neural network with four inputs  $[I_{t,1}, I_{t,2}, I_{t,3}, I_{t,4}]$ , two outputs  $[O_t^r, O_t^\theta]$ , and three layers with only four neurons in the input layer, eight in the hidden and two in the output.

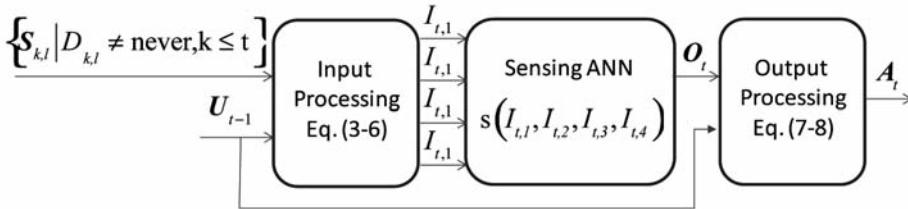


Figure 5. Complete sensing controller  $A_t = c(U_{t-1}, \{S_{k,l} | D_{k,l} \neq \text{never}, k \leq t\})$

### Training

The pairs of inputs  $[I_{t,1}, I_{t,2}, I_{t,3}, I_{t,4}]$  - outputs  $[O_t^r, O_t^\theta]$  used to train the sensing ANN  $s$  are generated according to a set of rules defined for different situations. The next two situations illustrate the followed process:

- When none of the beacons falls inside the UAV field of view, the UAV should return to the observation area. The  $O_t^\theta$  and  $O_t^r$  that will drive the UAV towards it, can be obtained based on  $I_{t,2}$  and  $I_{t,1}$ . Figure 6.a) illustrates this situation.
- When the UAV is flying according to the direction of the already observed shipwrecked and detects a new one that is moving with a different orienta-

tion, the UAV should correct its orientation to search new unobserved ones in the surrounding area of the just observed element. The  $O_t^\theta$  that will drive the UAV towards it, can be obtained based on  $I_{t,1}$  and  $I_{t,2}$ . Figure 6.b) illustrates this situation.

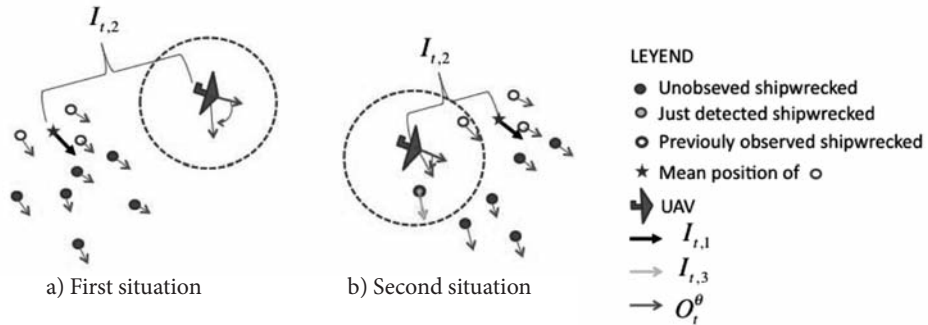


**Figure 6.** Training situations of the sensing ANN.

For each situation, we create a rule based on the parameters that govern it. With the rule, we generate pairs of inputs-outputs that are used to train the sensing ANN. The training step, performed only once for each UAV type, uses the UAV model  $U_{t+1} = f(U_t, A_t)$ .

### The whole system

The onboard UAV controller is implemented as an expert system made up by the two controllers (see previous sections), alongside a manager in charge of the following:

- 1) Deciding in which working mode the expert system is, according to the information provided by the UAV onboard sensors. In particular, before the UAV vision system finds the first shipwrecked the expert system must work in prediction mode; once the first element is detected, it switches to sensing mode.
- 2) Controlling the number of already observed shipwrecked.
- 3) Managing exceptions related with the lapse until a new element is detected. The behaviour depends on the working mode. When the UAV is in prediction mode and no other element is observed for a period of time longer than originally expected, the UAV must send an alarm to the rescue centre requesting orders. When the UAV is in sensing mode and cannot find any new element during a designated period of time, the manager directly modifies the sensing ANN input parameter  $I_{t,2}$ , incrementing its value accordingly to the time that has passed since the last new observation, with the purpose of exploring areas farther away from the mean position of the already located shipwrecked.

The steps carried out after the rescue centre receives an alarm are the following:

- 1) As soon as the alarm is received, the rescue centre runs its numerical predictor  $M_{t+1,i} = g(M_{t,i})$  to generate the data pairs  $M_{t,i}$  and  $\Delta M_{t+1,i} = M_{t+1,i} - M_{t,i}$  used to train the prediction ANN  $\Delta M_{t+1,i} = p(M_{t,i})$ .
- 2) Next, the trained prediction ANN  $\Delta M_{t+1,i} = p(M_{t,i})$  is loaded into the UAV expert system and then, the mission on prediction mode starts.
- 3) While flying in prediction mode, the expert system runs the complete prediction controller, that includes the prediction ANNs and prediction controller, to obtain the high level commands  $A_t$  that drive the UAV towards the mean of the predicted values of the shipwrecked positions.
- 4) Once the first shipwrecked is observed, the expert system stops the complete prediction controller and starts running the complete sensing controller, that includes the sensing ANN  $O_t = s(I_{t,1}, I_{t,2}, I_{t,3}, I_{t,4})$ , and the input and output processing steps. When the UAV does not observe any new shipwrecked for a long period of time, it also modifies directly the input  $I_{t,2}$  of the sensing ANN.

The whole expert system and these main steps are presented in figure 7, which does not include all the variables and connections to make it visually simpler. The missing information can easily be inferred from the previous figures and equations.

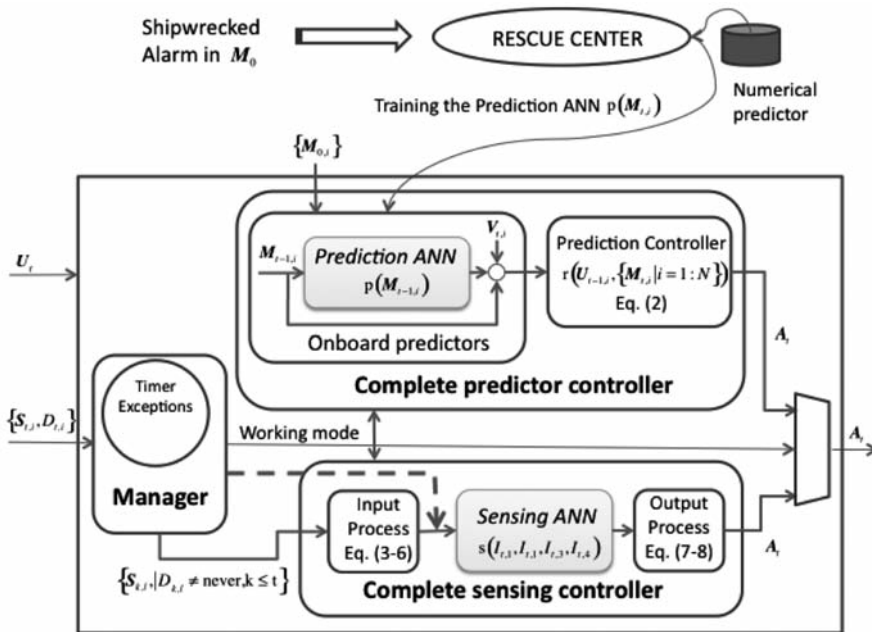


Figure 7. Expert system.

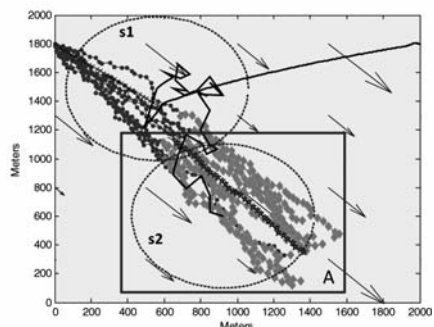
## RESULTS

Next, we show the behaviour of the whole expert system in two simulated sea rescue tasks that differ in the distance that exists between the rescue centre and the wrecked area, and therefore, in the spread of the shipwrecked when the UAV finds the first element. In both cases, the total number of castaways  $N=10$ .

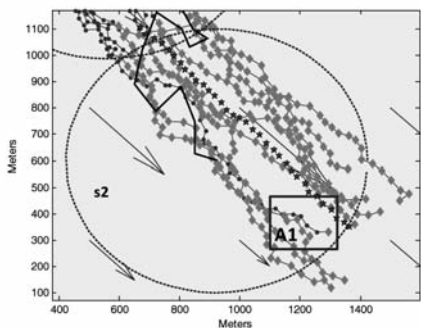
To run the experiments, we include our expert system in a MATLAB simulator that is also responsible of calculating at every time step the 'real' castaways and UAV positions. The shipwrecked movements, simulated during the two phases with the rescue centre predictor instead of the onboard ANN based predictor, are used to obtain the shipwrecked measurements ( $S_{t,i}$  and  $D_{t,i}$ ). The UAV positions ( $U_t$ ) are obtained with a complex model that defines the UAV dynamics and includes an onboard low level controller in charge of stabilizing and driving the UAV towards the high level command positions  $A_{t,i}$  obtained by the expert system. Besides, the simulator also randomly generates the initial positions of the shipwrecked in a small area around the initial wrecked position  $M_{0,i}$ . Therefore, the simulator closes the control loop: from the point of view of the expert system it applies its output ( $A_{t,i}$ ) to the UAV to generate its inputs ( $U_t$ ,  $S_{t,i}$  and  $D_{t,i}$ ) considering the UAV and shipwrecked simulated positions.

The results of the two experiments are presented in figures 8 and 9 using distinct glyphs for different elements and phases, whose meaning is shown at the legend at the bottom of figure 8. The simulated positions of the shipwrecked before each of them is first observed are presented with a dark grey circle and afterwards with a light grey diamond. Besides, to identify which point belongs to each castaway, we join them with a line in order to observe their trajectory too. The mean of the estimated positions of the shipwrecked at each time step before the first is observed is shown with a dark  $x$ . The mean of the observed positions of the detected shipwrecked after the first observation is presented with a dark star. When the shapes are not distinguishable, the differences on the grey levels among all these symbols can be used to identify these elements. The UAV trajectory is presented with a black line and the field of view at the positions when a new unobserved castaway is detected with a dashed circle identified as  $s\#$ . The arrows represent the mean direction of the sea wind and currents. The first graphic inside each figure represents the whole experiment while the others show a zoomed region of the experiment (marked in the first figure with a square). Finally, note that as we draw the trajectories of the simulated shipwrecked and UAV, the represented unobserved simulated elements that fall inside the UAV field of view at a given time  $t$  don't necessarily correspond to any of the simulated position they have at  $t$ . In other words, an unobserved castaway (circle) that is inside a dashed circle doesn't become observed (diamond) unless it was really inside the dashed circle at the correct time step.

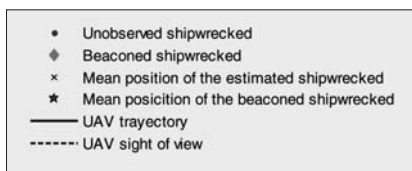
In the first experiment the ship wrecks at the upper left corner of figure 8.a) and the rescue centre is placed only 2000 m apart in the upper right corner. The rescue centre



a) Global view



b) A zone. Sensing mode



c) Legend

Figure 8. First experiment.

of the sensing mode behavior where the following 6 castaways are observed when the UAV fields of view are s2-s7, and so their dark circle glyph becomes a light diamond. In this area the UAV trajectory is close to the mean trajectory of the found castaways (dark stars) because the lapse between two new observations is small. Figure 9.a) and 9.d) show how the behavior changes after observing the 7<sup>th</sup> castaway, because no new observations are obtained for long and the expert system extends the UAV searching zone incrementing  $I_{t,2}$  accordingly with the time without new observations. This allows locating elements that are further away from the mean trajectory of the detected ones. Figure 9.d) shows when the last castaway, moved away from the main

receives the message, trains the onboard prediction ANN for the current sea state, and the UAV starts flying on prediction mode towards the mean estimation obtained by the expert system, while the castaways are adrift by the simulator. Once the UAV has reached the online predicted spot, before the castaways have been significantly spread, it detects simultaneously all but one shipwrecked when its field of view is s1. Then, the UAV starts flying on sensing mode, tracking the 9 observed shipwrecked (light diamonds) while it searches the remaining (dark circles) following a zigzag trajectory close to the mean of the observed castways (dark stars). This behavior, shown in figures 8.a) and 8.b), continues until the UAV field of view becomes s2 and the UAV observes the last item in the A1 region. Then the UAV finishes its mission.

The setup of the second experiment, presented in figure 9, differs from the first on the distance of 10000 meters between the ship wrecked position and rescue centre. Figure 9.b) shows the prediction phase and how this bigger distance lets the sea winds and currents increment the simulated shipwrecked dispersion a lot before the UAV arrives at the online predicted spot and detects the first shipwrecked with the s1 field of view. Figure 9.c) shows the part

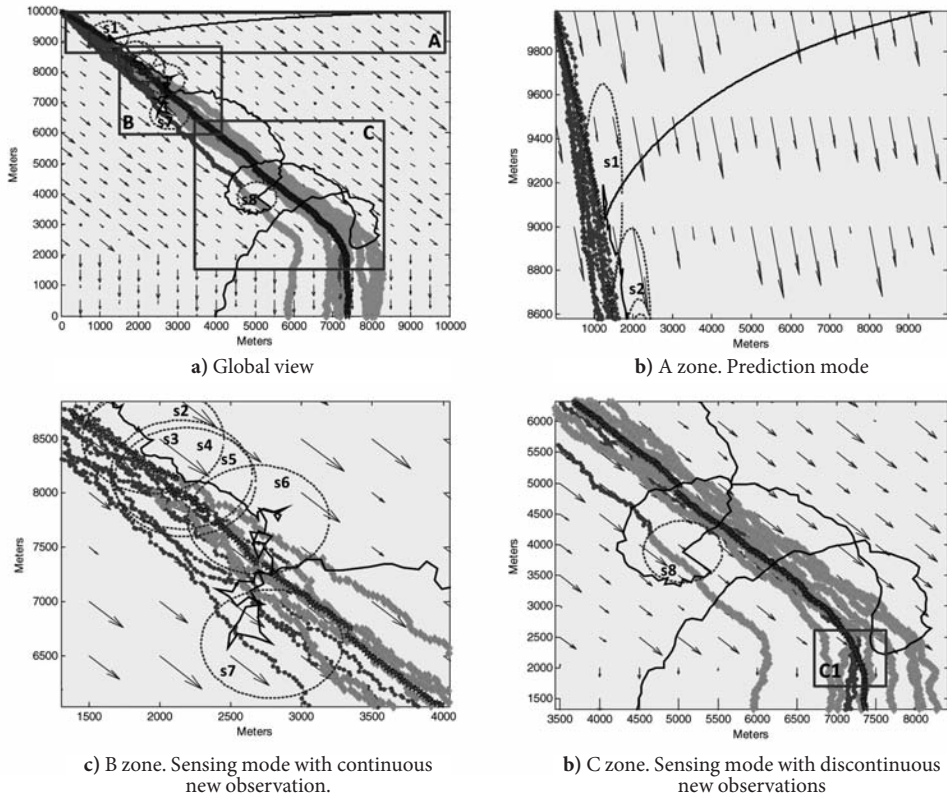


Figure 9. Second experiment.

group, is found at s8. At this moment, the searching radio is reduced to locate closer castaways. As time passes without new findings the searching radio increases again. The remaining two shipwrecked are not found in the represented experiment. Finally, although in region C1 the UAV and unobserved trajectories are really close, the UAV does not find them because their position at the same time step is not.

## CONCLUSIONS

In this paper, we present a new expert system, based on neural networks, to guide a UAV that has to search and locate castaways on a wide area after a shipwreck. The expert system is designed to work in real time on board of any UAV, using the prediction or the measurements of the castaways provided by the UAV. So far, it works successfully with little information about the castaways position and really simple user-defined behaviors. We plan to expand both in the near future, including statistical techniques to tack the observed castaways, incrementing the types of inputs of the sensing ANN and training it with more complex behaviors.

## REFERENCES

- Alvarez Fanjul, E. (2005): Establecimiento de un Sistema Español de Oceanografía Operacional. *Revista de Puertos del Estado*. March 2, 57-64.
- ASF, <http://www.aa.washington.edu/research/asfl> [Accessed 18 December 2010]
- BERK, <http://vehicle.me.berkeley.edu> [Accessed 18 December 2010]
- Besada-Portas, E. de la Torre, L. de la Cruz, J. M. de Andrés-Toro, B. (2010): Evolutionary Trajectory Planner for Multiple UAVs in Realistic Scenarios. *IEEE Transactions on Robotics* 26 (4), 619 – 634.
- CALT-Mur, <http://www.cds.caltech.edu/~murray/projects/darpa01-mica> [Accessed 18 December 2010]
- Farzad Kamrani and Rassul Ayani (2009): UAV Path Planning in Search Operations, Aerial Vehicles, Thanh Mung Lam (Ed.), Available from: [http://www.intechopen.com/articles/show/title/uav\\_path\\_planning\\_in\\_search\\_operations](http://www.intechopen.com/articles/show/title/uav_path_planning_in_search_operations) [Accessed 10 December 2010]
- Gómez Lahoz, M. and Carretero Albiach, J. C. (2005): Wave forecasting at the Spanish coasts. *Journal of Atmospheric & Ocean Science*, 1741-7546, Volume 10 (4), 389-405.
- Haykin, S. (1999): *Neural Networks: A comprehensible Foundation*. Second edition, Prentice-Hall New Jersey, USA.
- Hontoria L., Aguilera J., Riesco J. and Zufiria P. (2001): Recurrent Neural Supervised Models for Generating Solar Radiation Synthetic Series. *Journal of Intelligent and Robotic Systems*, 31 (1-3)
- Howden D. and Hendtlass T. (2008): Collective intelligence and bush fire spotting, in *Proc. Genet. Evol. Comput. Conf.*, pp. 41–48.
- Mackay D.J.C. (1992): Bayesian interpolation, *Journal Neural Computation*, Volume 4 (3), pp. 415 - 447
- MAGIC, <http://magicc.et.byu.edu/cmsmadesimple> [Accessed 18 December 2010]
- MERCATOR, [http://www.mercator.eu.org/html/mercator/index\\_en.html](http://www.mercator.eu.org/html/mercator/index_en.html) [Accessed 18 December 2010]
- MICA, <http://www.darpa.mil/ixo/mica.asp> [Accessed 18 December 2010]
- MIT-How, <http://www.mit.edu/people/jhow> [Accessed 18 December 2010]
- Patterson D.W. (1996): *Artificial Neural Networks. Theory and Applications*, Prentice Hall.
- Rubio J.C., Vagners,J, and Rysdykz R. (2004): Adaptive Path Planning for Autonomous UAV Oceanic Search Missions, *AIAA 1st Intelligent Systems Technical Conference*, 20 - 22 September, Chicago, Illinois, pp 1-10.
- Tian J., Shen L., and Zheng Y. (2006): Genetic algorithm based approach for multi-UAV cooperative reconnaissance mission planning problem, in *Lecture Notes in Computer Science*, vol. 4203. Berlin, Germany: Springer-Verlag, pp. 101–110.

# SISTEMA EXPERTO PARA GUIADO DE VEHÍCULOS AÉREOS NO TRIPULADOS BASADO EN REDES NEURONALES ARTIFICIALES

## RESUMEN

En las tareas de rescate marítimo es crucial alcanzar la zona de la catástrofe en el mínimo tiempo posible, porque según éste aumenta suele crecer la dispersión de los naufragos y la dificultad de su búsqueda. Por lo tanto, el uso combinado de vehículos aéreos y marítimos no tripulados (UAVs y USVs) en este tipo de tareas suele resultar ventajoso, ya que el tiempo de llegada de los primeros es habitualmente mucho menor que el de los segundos. Teniendo en cuenta las capacidades de ambos tipos de vehículos, una distribución conveniente de la tarea de rescate consiste en asignarle a los UAVs las labores de localización y seguimiento de los naufragos, y a los USVs las de rescate de los naufragos localizados. Este artículo se centra en las partes de la tarea de rescate directamente relacionadas con el UAV.

Con este objetivo, se ha diseñado un sistema experto que genera las órdenes de alto nivel que indican al UAV hacia donde debe dirigirse para localizar los naufragos. Este sistema tiene que ser incorporado en un UAV, motivo por el que es conveniente minimizar su coste computacional y de memoria. Por esta razón, se han utilizado como núcleo del sistema experto un conjunto de redes neuronales, ya que además son fáciles de implementar e integrar en la tecnología existente. Por último, sus capacidades de respuesta en tiempo real y su alta adaptabilidad a diferentes situaciones, hacen que resulten elementos apropiados para resolver nuestro problema.

El sistema experto finalmente diseñado consta de dos tipos de redes neuronales: unas encargadas de predecir la posición de los naufragos antes de que estos sean localizados y otras de guiar su búsqueda una vez que el primer elemento ha sido encontrado. El primer tipo de red forma parte del subsistema que funciona durante la fase en la que el UAV sigue, de acuerdo con una ley de control muy sencilla, las posiciones predichas por este tipo de red. El segundo constituye la parte fundamental del subsistema que funciona durante la fase de sensorización y búsqueda. La figura 10 muestra un esquema de todo el sistema, en el que las operaciones primordiales son realizadas por las redes neuronales, explotándose así su eficiencia intrínseca.

Finalmente, queremos hacer notar que los parámetros de las redes neuronales utilizadas son obtenidos de dos procesos de entrenamiento diferentes de forma que las redes neuronales de predicción adaptan su comportamiento al estado de los vientos y corrientes de la zona de naufragio y que las redes neuronales de sensorización lo hacen al comportamiento sugerido por un experto para diferentes situaciones de rescate.



## IMAGING SYSTEMS FOR ADVANCED UNDERWATER VEHICLES

F. Bonin<sup>1,2</sup>, A. Burguera<sup>1,3</sup> and G. Oliver<sup>1,4</sup>

Received 10 February 2011; in revised form 16 February 2011; accepted 19 March 2011

### ABSTRACT

Exploration of the underwater environment either by human operated or by autonomous vehicles can highly benefit from using a visual imaging system. When a vision system for an underwater vehicle has to be designed, some specific characteristics of the image formation in sub-sea conditions should be taken into account. This paper presents an extensive survey of components, techniques and methods used to build underwater vision systems. First, most of the phenomena that affect the image formation in submersed conditions are described; second, some significant illumination techniques and light sources, including laser, are presented; and third, the review follows with a list of relevant underwater visual installations and submarine vehicles with vision-based infrastructures recently developed and commercially available. Furthermore, the paper finally introduces some techniques for improving the quality of underwater images. Among all these techniques, a special attention has been paid to the effect of employing polarized light to overcome the undesired scatter present in images. This last section includes some experiments carried out by the authors to test the usefulness of polarization-based methods in robotic applications.

**Key words:** Autonomous Underwater Vehicles, Robot Vision, Polarization, Underwater Installation.

<sup>1</sup> University of the Balearic Islands, carretera de Valldemossa km 7.5, 07122 Palma de Mallorca, Spain. <sup>2</sup> Researcher, Email: francisco.bonin@uib.es, Tel. 971172813. <sup>3</sup> Researcher, Email: antoni.burguera@uib.es, Tel. 971172911. <sup>4</sup> Director of the group, Email: goliver@uib.es, Tel. 971173201.

## INTRODUCTION

Thanks to recent technological advances, the subaquatic world is more accessible for exploration, scientific research and industrial activity. When the tasks involved in missions are repetitive, hazardous or too long to be carried out by divers or human guided vehicles, the use of unmanned vehicles becomes more suitable. At present, remotely operated vehicles (ROVs) are commonly used in a variety of applications such as surveying, biological, archaeological and geological sampling, rescue operations or infrastructure inspection and maintenance (Ortiz and Antich, 2009). Trying to overcome some of the intrinsic limitations of ROVs, such as their limited operative range or the need of a support vessel, autonomous underwater vehicles (AUVs) are progressively being introduced.

Improving the sensorial capabilities of underwater vehicles is a key point to increase the variety and the feasibility of missions that can be carried out by ROVs and AUVs.

Optical imaging sensors can provide dense information updated at high speed and they are commonly used in many terrestrial and air robotic applications. However, due to the interaction between water and electromagnetic waves, optical imaging systems and vision systems need to be specifically designed to be used in underwater scenarios, whether their output images and videos are going to feed an autonomous system or a human operated one. Sub-sea images have specific characteristics that should be taken into account during the gathering process. Light attenuation and scattering, non-uniform lighting and shadows, colour filtering, suspended particles or abundance of marine life on top or surrounding the target of interest are frequently found in typical sub-sea scenes. Some improvements specifically designed for the described situations, including specialized lighting systems, filtering methods, ultra-sensitive and wide-spectrum cameras or multi-camera systems have been described in the literature. From the image acquisition point of view, research in underwater optical imaging has recently proposed novel solutions that achieve significant advances in image quality (Kocak, et al., 2008). It has also been proved that vision algorithms performance can be improved if the physical process of image formation is appropriately modelled and taken into account (Singh, *et al.*, 2004) (Negahdaripour, 1998). Physics-based image formation models, including information from the radiant source, the nature of the surface of scene objects or the imaging hardware has been extensively studied in recent years (Ortiz and Oliver, 2006)(Ortiz and Oliver, 2010).

This paper focuses its attention on presenting a study of available cameras and different possibilities for illuminating the environment, to get the best image quality and performance in underwater optical imaging systems. Moreover, a list of underwater installations and submarine vehicles recently developed and commercially available has been included as a reference of previous experiences. Besides, among all

the known techniques devoted to improve the image quality, those that use polarized light have been analyzed in detail and experimentally tested.

## UNDERWATER OPTICAL IMAGE FORMATION

When electromagnetic waves propagate in a sub-aquatic medium they interact with water molecules and with dissolved and particulate matter. As a consequence, the distance this radiation travels in the underwater environment is dramatically reduced compared to air. A general exposition of this situation from a physical point of view can be found in (Gordon, 1994) and (Moblely, 1994). Detailed analysis regarding the underwater light propagation problem, focused on computer vision and its applications in robotics are presented in (Ortiz, A., 1998) and (Horgan and Toal, 2009), respectively. Among all the optical issues known, refraction, scattering and absorption seem to play a more significant role in underwater optical image formation and computer vision, thus, they are described below.

Underwater cameras are housed in watertight enclosures including a depth rated lens. Before reaching the sensitive area of the camera, the refraction causes the light rays coming from the scene to bent as they pass from water to glass and then from glass to air. The refraction modifies the apparent size and position of objects. This effect combined with the imperfections of the housing system, including lens defects and misalignments, lead to non-linear image distortion that must be compensated with a proper calibration process.

When a photon hits a particle suspended in the water its original path is deflected. Depending on the angle the light ray is deviated, this phenomenon is known as forward scatter or backscatter. Forward scatter occurs when the angle of deflection is small, resulting in image blurring and contrast reduction. Backscatter occurs when the light from the light source is reflected to the camera before reaching the object to be illuminated. Backscatter may cause bright points in the image usually known as marine snow. However, the main problem of backscatter, also referred to as veiling light,

is that it can highly reduce the image contrast, causing serious problems in underwater imaging systems. The general term for this problem, that also appears in other media than water, is path radiance. The referred effects of backscatter, forward scatter and refraction are illustrated in Figure 1.

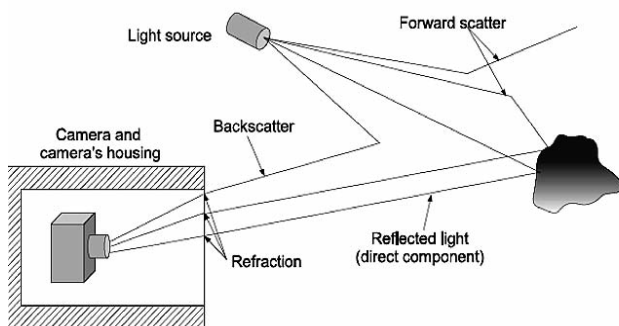


Figure 1: Example of backscatter, forward scatter and refraction.

Both backscatter and forward scatter depend on the volume of illuminated water inside the camera's field of view. In general, this means that the negative effects of scatter in underwater imaging increase with the distance from the camera to the object to be viewed. Moreover, as it will be exposed later, some veiling and snow effect reduction can be obtained increasing the distance from the light source to the camera in an opportune way.

The absorption causes the electromagnetic waves traversing water to be quickly attenuated. Furthermore, the spectral components of light are differently absorbed. Thus, in clear water long wavelength (red light) is lost first. In turbid waters, or in places with high concentration of plankton red light may be better transmitted than blue light. As a consequence, two problems arise as they have important consequences for optical imaging and computer vision systems. First, the use of artificial lighting is needed in most cases and dramatically limits the distance at which objects are perceived. Second, the natural colours are distorted and the perception of the scene can be altered.

The overall effect of absorption, scatter and other phenomena not described in this work such as the fluorescence, produces an attenuation of light. The attenuation factor depends on the specific characteristics of the water, the dissolved components and the particles in suspension. A common measure of this effect is the attenuation length, which is the distance where the intensity of the light has dropped by a  $1/e$  factor. In other words, the attenuation length is the distance after which about the 64% of the light intensity is lost. Visibility in water ranges between one and two attenuation lengths. This means, in general, ranges from 30 to 60 meters in clear waters, from 6 to 15 meters in deep waters and from 1.5 to 6 meters in coastal waters. As it will be shown throughout this document, the visibility range can be significantly increased by using the appropriate illumination and camera.

## **ILLUMINATION TECHNIQUES**

### **Illumination Sources**

Choosing the proper light sources for an efficient underwater visual system becomes an important issue because illumination conditions always determine certain imaging effects and results. Natural light sources, like daylight, can be used at low depths, but they completely attenuate before they reach significant depths. Artificial light is necessary at deeper environments, and since a single visible light source illuminates the scene producing a central bright spot surrounded by a poorly illuminated area, it is common to use different light sources strategically located, specially if they emit structured light.

From the illumination type point of view, underwater visual systems can be classified according to different concepts. In a first approximation, illumination systems can be roughly classified as active or passive. On the one hand, passive illumination

systems image scenes illuminated by some kind of natural lighting source (sunlight or bio-luminescence sources) or by some artificial source non specifically placed to illuminate that environment (light coming from a nearby stations, ships or whatever that is generating and/or consuming energy). Passive imaging is especially attractive for covering operations such as fish seeking prey or in Navy secret inspecting or surveillance tasks. On the other hand, active Illumination and structured lighting systems take advantage of artificially generated light with one or more sources strategically placed and configured, These systems offer substantial benefits for underwater imaging in the sense that the incident light can be either continuously emitted (standard visible light sources), collimated into very narrow or wide beams, be monochromatic (lasers), or can also be flashed and sent in a sequence of very short duration pulses (strobe, pulsed lasers). These more sophisticated lighting systems typically allow imaging at greater ranges and/or higher depths than passive systems. The most significant of the advanced techniques that use the effects of light at specific frequencies to overcome harmful effects as scatter, refraction or absorption, among others, are:

*Synchronous scanning systems:* The illumination source emits a collimated light (rays are nearly parallel) with a minimal beam section. This causes minimum backscatter and it results in high contrast images. To compute target range, triangulation can be used (B. Zheng, *et al.*, 2009).

*Light Stripe Range Scanning (LSRS):* A plane or sheet of light, typically generated by a laser diode, scans the environment or an object to be imaged to obtain its 3D reconstruction (Narasimhan and Nayar, 2005), (Taylor and Kleeman, 2006). In the presence of scattering, the light sheet becomes visible and it makes the detection of the obstacle surface more complicated. This technique reduces backscatter and permits to recover 3D information by means of triangulation.

*Photometric Stereo (PS):* Photometric Stereo techniques are a good alternative to LSRS techniques when the last take too long, for example, in dynamic environments. In the absence of scattering, it is well known that three images obtained illuminating the scene from three different but known directions are enough to reconstruct the surfaces of the different scene objects. The challenging problem arises when it is necessary to determine how many sources are needed to infer the scene features in the presence of scattering (Negahdaripour *et al.*, 2002), (Narasimhan and Nayar, 2005).

*Range Gated Systems:* The source emits a pulse of light and the camera shutter waits for the time the light takes to propagate from the emitter to the target, scatter in the target surface and back again to the camera. Only the light scattered by the target is received and considered for imaging. The main difficulty that these systems entail is that a very precise light gating is needed in the camera receptor.

Obviously, the light pulse is much shorter than the total light propagation time. The cost of these systems is high but they considerably reduce the backscatter and augment the contrast (Han, *et al.*, 2009), (Tan *et al.*, 2006).

### Selection of the light source position

When using conventional illumination systems, the amount of backscatter depends on the volume of water where the light field and the camera's field of view intersect. Because of this, it is common to separate the light source as much as possible from the camera in order to reduce the aforementioned volume of water. Figure (2-a) exemplifies the volume of water producing backscatter when the camera and the light source are close between them, and Figure (2-b) shows the difference when increasing this distance. Jaffe (Jaffe, 1990) emphasizes the importance of this aspect by stating that the basic trade-offs in underwater imaging design are between camera-light separation, contrast and power. As a matter of fact, the rough classification of underwater imaging systems provided in (Jaffe, 1990) is widely referenced by the underwater vision community. According to this classification, underwater imaging systems fall in one of the following three groups:

*Conventional systems:* The light source is placed close to the camera. This configuration makes it possible to obtain images up to 2 attenuation lengths.

*Increased camera/light separation:* The light source is separated from the camera as much as possible in small underwater vehicles (3-5 meters). This configuration allows the acquisition of images up to 3 attenuation lengths.

*Exotic systems:* These systems used range gated or laser based systems, increasing their complexity and price, and also their power consumption.

Thus, increasing the separation between the light source and the camera is a very simple and cheap way to obtain images one attenuation length farther than conventional systems, neither involving major changes in the imaging architecture nor requiring more power. Although this idea has been widely used and is considered common knowledge, very few studies have quantified the effects of such increase in separation. Jaffe models the behaviour of light in water as well as the image formation process and performs several computer simulations in (Jaffe, 1988) and (Jaffe, 1990). These simulations assume a camera pointing to the sea floor and evaluate the image contrast for different separations between the camera and the light source, moving the light source vertically and horizontally.

Simulations show that separating the light source horizontally dramatically increases the image contrast. Separations up to 10 to 20 meters considerably increases the contrast, but it tends to slightly decrease at large distances, mainly due to the light attenuation. For example, for a camera altitude of 40m, increasing the separation 3 to 5 m results in an approximate doubling of the image contrast. The results

provided by (Jaffe, 1990) are summarized in figure 3. The image contrast also increases when separating the light source vertically. This may seem counter-intuitive as this kind of separation does not decrease the volume of water where backscatter may appear. According to Jaffe, this improvement appears because the area directly in front of the camera is not illuminated as intensely as in the case that no separation exists.

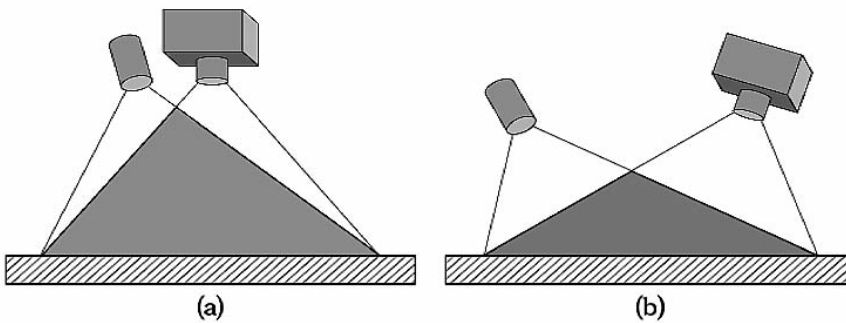


**Figure 2:** (a) Conventional system (b) Increased camera to light source separation.  
The grey area depicts the volume of water where backscatter appears.

Nevertheless, the improvements in image contrast are much smaller when moving the light source vertically than horizontally. For example, for a camera altitude of 60m, there is almost no difference in putting the light source very close to the camera or separating it vertically. Increasing the horizontal separation between the light source and the camera is a worthwhile improvement for some underwater imaging systems, but it can be difficult to apply in vehicles, depending on their shape and size. However, it is always possible to place the light source and the camera in different vehicles and coordinate their navigation (Jaffe, 2007). These systems increase cost and complexity in their coordination and can generate moving shadows in the image.

### **Illuminating Systems**

At the time of choosing a proper light source for an undersea visual installation, one has to search a balance between the cost consumption and the quality of the produced light. These terms are all reflected in the parameter *efficacy* (lumens/Watt). Efficacy is an important term, specially in autonomous vehicles which need to optimize the power consumption to generate the maximum light. Underwater visual systems have progressively evolved towards the use of more effective technology, and that obviously includes the illuminating systems. Different types of light emitters with different levels of efficacy are listed next:

*Halogens:* They use a filament to ignite halogen gas. Halogen lamps are more effective than incandescents since they emit a 30% in average whiter and more brilliant light consuming less watts and irradiating less infrared heat. Halogens do not produce blackening of the bulb glass in usage and they are smaller compared with a standard incandescence emitter. Halogens have a longer live-time than standard incandescence.

*HID (High Intensity Discharge or also know as Xenon):* These lamps use an electrical discharge between two electrodes for igniting xenon gas in a sealed bulb. They emit a blue-white light closer to the natural daylight. This technology improves halogens durability and security in 10 times and also increases efficiency producing much more light (measured in lumens or lux) than halogens with the same power consumption and emitting much less heat. HID's emit light that penetrates darkness better than halogens. HID's are extensively used in underwater applications such as ROVs (where the power can be supplied via its umbilical) or static underwater stations.

*HMI (Hydrargyrum medium-arc Iodide lamp):* In this lamps, bulbs are filled with mercury vapor which is excited by creating an electrical arc between two electrodes. They are useful in imaging systems that need a long time light exposure. They are typically used in the film industry, but since 1996 they have been used in underwater photography. They are usually expensive and high power consumers (more than 600watts) although some manufacturers are beginning to produce low consumption HMI lights. They produce extraordinary illumination quality and are used in some ROVs for underwater filming at high depths.

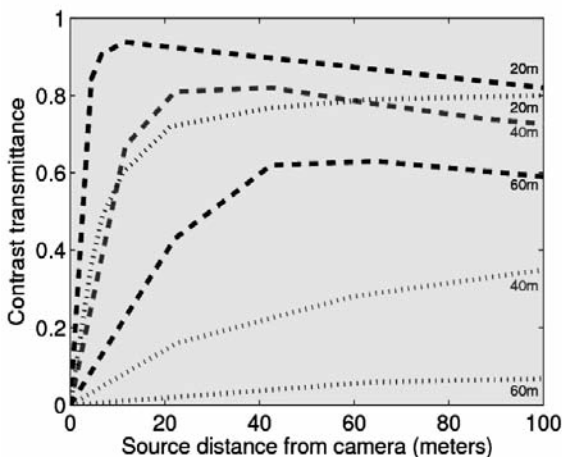


Figure 3: Contrast transmittance vs. separation. (...) Vertical separation. (---) Horizontal separation. Source: Jaffe, 1990.

*HIF (High Intensity Fluorescent):* In many cases, these systems are more energy-efficient than HID solutions. They generate lower lumen depreciation rates, present better dimming options and reduce the glare. They are able to illuminate a more extensive area than HID lamps do. Fluorescent solutions are applied in underwater for attracting fish but rarely for underwater vehicles.

*LEDs:* These systems are supplied with direct and continuous current, (12V or 24V). The

power consumption is 4 times less, in average, than the halogens. LEDs can emit light in a wide range of wavelengths, they have a small spectral bandwidth, their live time is much longer than halogens and, in general, they have a higher efficiency than HIDs. Although they can be expensive, LEDs have become specially important and suitable for underwater autonomous vehicles equipped with batteries since they considerably reduce the power consumption.

*Infrared:* Light is considered to be infrared for wavelengths in the 700nm-1mm range. Infrared imaging is extensively used for night vision and in some underwater applications. Infrared light emitting must be accompanied with the use of cameras with infrared receivers (IR cameras). Infrared light is very useful for filming marine fauna, since it can be used to remotely determine the temperature of targets and it is no visible. Infrared light penetrates shallower than orange, yellow or green light, but it has been demonstrated to still be suitable for some underwater imaging applications (Lam *et al.*, 2007), (Sedlazeck *et al.*, 2009). In some cases, the undesired scatter can be filtered-out in the receptor if the wavelength of the received energy is different than the emitted one.

*Laser:* Laser usual operation wavelength is in the 350nm-630nm range. Laser are usually used in underwater extended range techniques, since it permits to illuminate at further distances than light with lower or higher wavelength. Laser permits also to calculate distances and object sizes with a high degree of precision. Laser has two main problems: a) emitters are considerable more expensive than HID, LEDs or infrared, and b) emitters generate a very narrow beam which makes necessary to scan the environment to take an image, delaying the process and reducing the frame rate.

Although these systems are considerably more expensive than the rest, they deserve and special attention for the wide range of benefits that offer.

## **LASER-BASED TECHNIQUES**

Techniques using laser emitters and receptors are intended to considerably extend the range of the captured scenes thanks to the laser scattering and absorption properties, improving contrast and resolution beyond that offered by other means such as infrared or systems with visible light (Funk *et al.*, 1972). Laser emitters concentrate intense light over a very small and narrow area, but this light propagates longer. Although laser-based solutions are of difficult implementation, they need an important post-processing software, and can be more expensive than standard solutions. They are the best choice for long range imaging since they can be effective up to 5,6 or 7 attenuation lengths, while with visible light images are clear up to 2-3 attenuation lengths. The most outstanding techniques involving laser infrastructures are detailed next.

### **Laser Range-Gating (LRG) Methods**

These systems scan the scene with laser pulses emitted at frequencies lower than 100Hz (short pulses of approximately 6ns). Special cameras must be provided with ICCD sensors that are able to synchronously capture laser light in time gates. Knowing the speed of light in water and the distance to the target, the time that the light pulses need to go from the emitter to the target and return to the receptor can be easily calculated. Therefore, using a gateable receiver with a sufficiently high temporal resolution the most of the undesired scatter can be filtered out leaving only the signal returned by the target. In 1994, Range-Gating was already a consolidated technique for extending underwater imaging range (Swartz, 1994) (Weidemann *et al.*, 2005). More recently, Shan *et al* proposed a new method for the synchronization control of the laser emitter and the camera receptor in a LRG system. Improving the synchronization between the emitter and receiver helped to precisely improve the image resolution (He *et al.*, 2009).

Recently, Wu *et al* (Wu *et al.*, 2009) have simulated and evaluated the performance of gated ICCD cameras to be applied in LRG-based underwater imaging applications.

### **Laser Line Scan (LLS) Methods**

LLS systems scan the environment with a narrow laser beam perpendicularly to the direction of the sensor support platform and sweeping out light rays as the vehicle moves. LLS techniques can use either continuous or pulsed laser reducing the backscatter effect by displacing the receiver from the laser source. Pulsed LLS can reduce the undesired scatter by time gating the receptor aperture to capture the light only at certain time intervals. Caimi *et al* (Caimi *et al.*, 2007) and Dalglish *et al* (Dalglish *et al.*, 2008) demonstrated that pulse-gated LLS provide a much better performance than previous continuous wave (CW) LLS configurations. CW-LLS systems, under certain conditions, are limited by multiple backscatter caused by an increase of turbidity or an increase of the illumination distance (Dalglish *et al.*, 2009).

LLS has lately been considered as the optimal technology for extended range underwater imaging.

### **Scattered Light Rejection using modulation/demodulation techniques**

Modulation/demodulation consist in displacing the frequency spectrum of a signal, and it can be used, for example, to discriminate useful components from noise, or to transmit several digital channels in an unique physical infrastructure. Coherent demodulation implies that the receiver is equipped with a Phase-Locked-Loop (PLL) that tracks the phase and the frequency of the received signal. The fact that sea water particles cause an important dispersion on the light (specially at high optical frequencies) has motivated many researches to question if coherent/non-coherent modulation/demodulation techniques could be efficient in underwater imaging sys-

tems. Illuminating with laser or infrared light (for example, at 99K MHz) has the advantage that the frequency, wavelength, phase or amplitude of the emitted light are known and can be demodulated in the receptor separating the signal spectrum from the scatter frequency components. Infrared light has been scarcely considered because it is absorbed by water at closer distances than laser. Other systems demonstrated that it is possible to enhance contrast and image quality at large distances by coherently modulating and demodulating the illuminating laser signal in phase (B-PSK or Q-PSK) (Cochenour *et al.*, 2007) (Laux *et al.*, 2007).

### SOME UNDERWATER IMAGING INFRASTRUCTURES

Surveying different existing imaging systems, such as underwater vehicles or visual infrastructures shall be convenient to learn from previous experiences and to plan an effective design, anticipating already identified problems. Many of the existing systems improve their features using several cameras for different purposes and/or various light sources:

1. Eye-in-the-sea: It is an unobtrusive deep-sea observatory and uses a LED which emits red light (wavelength 680nm) in combination with a low-light-level (LLL) camera (Widder, 2007).
2. (Rosenkranz *et al.*, 2008) Underwater imaging system designed for fisheries detection and observatory. A Gigabit ethernet high resolution camera is connected via optical fiber to the control computer. The environment is illuminated with strobe light to eliminate motion.
3. (Lam *et al.*, 2007): Underwater camera system for monitoring marine fauna in coral reefs. The system is provided with a wide angle infrared (IR) sensitive camera connected via optical fiber to a on-land controlling computer.
4. The submarine observatory NEPTUNE (pacific ocean) needs to integrate station nodes and static imaging systems to support ROVs in their surveillance tasks. Imaging platforms have been equipped with a high definition camera, and three different light sources: i) a 3 beam laser system to provide range information to the user, ii) two dimmable LEDs with more than 406 lumens of a equivalent power of 250 Watts, and a life of 50000 hours, and iii) a 150 Watts HID light to extend range of visualization ( Roston *et al.*, 2007).
5. Sedlazeck *at al* (Sedlazeck *et al.*, 2009) presented a 3D reconstruction system based on feature tracking. Images were provided by the ROV Kiel 6000, equipped with 3 cameras: i) a high definition camera, ii) a standard colour PAL still camera and, iii) a slave-mode controlled camera with automatic flash shot. The ROV is also equipped with a 250 Watts halogen lamp, another 70 Watts HID light and a 400 watts HMI dimmable focus.

6. In (Negahdaripour and Firoozfam, 2006) Negahdaripour and Firoozfam presented a vision system for automatic ship hull inspection, applicable to UAV but firstly tested with images provided by a ROV. The ROV was equipped with a stereo camera.
7. Negahdaripour *et al* (Negahdaripour *et al.*, 2007) explored the possibility and results of using optical-acoustic stereo imaging for 3D shape recovery of underwater targets. DIDSON (DIDSON, 2009) acoustic cameras provide acoustic images with such a high degree of reliability that they can be analyzed and processed in the same way as standard images.
8. The CSIRO Marine and Atmospheric Research in Australia (Shortis *et al.*, 2007) developed a ROV for sea bottom underwater map construction, fisheries study, detection and surveillance. The ROV was equipped with: i) two standard PAL cameras in stereo configuration for video recording to geolocate images with the vessel GPS, ii) a high resolution still camera for computing mosaicking and, iii) a forward-looking camera for obstacle detection and avoidance. Concerning to illumination, two 250 watts incandescent lamps were used for the video recording and two strobes for the still camera.
9. Recently, an underwater docking station was developed for enhancing the UAV REMUS (Allen *et al.*, 2006) performance. The vehicle incorporated several cameras for different purposes: i) one ethernet video camera to provide real-time information about the process of entering and leaving the docking station, and, ii) a periscope camera for the sea surface observation.

This camera was mounted in a housing that could be deployed and retracted above and below the sea surface.

10. Hercules (IFE, 2009) is a ROV specially designed for working in the deep sea, manipulating, recovering or digging in ancient shipwrecks. Hercules is equipped with one high definition video camera for monitoring the sea bottom and two still cameras for mosaicking tasks.
- 11 ARGUS is a ROV produced by Woods Hole Marine Systems, Inc, (Woods Hole Oceanographic Institution) which can operate independently or as a partner of other ROVs and it is equipped with cameras and HMI lighting for underwater image registration (WHMS, 2009).
- 12 Phantom DHD2+2 and Phantom HD2+2, (Deep Ocean Engineering) (DOE, 2009), are two ROVS designed for fisheries and scientific research, military missions, gas/oil pipes inspection or underwater filming, and specially suitable for deep water and strong currents. Both vehicles incorporate a high resolution PAL/NTSC colour camera with a wide angle lens, and two 250 watts halogen lamps to illuminate the area of inspection.

## POLARIZATION

A fraction of the light that passes through water is scattered back to the camera before reaching the object. This phenomenon, which is known as *backscatter*, significantly reduces the contrast in the resulting image. The effects of backscatter depend on the amount of water in the line of sight and, thus, on the distance to the object being observed. Moreover, the backscatter is magnified when artificial illumination is used (Treibitz and Schechner, 2009). As artificial illumination is a common requirement for sub-sea operation, backscatter happens to be an important problem in underwater robotics.

Fortunately, the media responsible for the backscatter behaves differently to the objects in the environment in front of polarized light. However, there is not a consensus in the research community regarding this subject. According to (Treibitz and Schechner, 2006) and (Treibitz and Schechner, 2009) some studies assume that objects in the scene preserve polarization whilst backscatter do not, and some other studies state that polarization is preserved only by the backscatter. In spite of these opposed points of view, polarization can be used to reduce the negative effects of backscatter because, either in one sense or another, backscatter behaves differently to the objects in the scene in front of polarized light.

This section focuses on the potential benefits of using polarization to increase contrast in underwater images. To this end, it first introduces some basic concepts, then surveys some relevant studies on the subject and finally shows some tests conducted in our laboratory.

### Basic Concepts

Light can be regarded as a wave that oscillates in an arbitrary direction perpendicular to its direction of motion. Polarization is, in this context, a property of light that indicates the direction of these oscillations. Light is said to be polarized if it oscillates in a single direction (*linear polarization*, Figure 4 left) or if it rotates as the wave travels (*circular and elliptical polarization*, Figure 4 right).

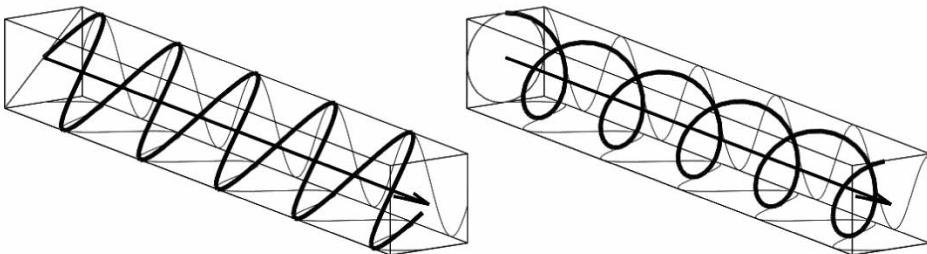


Figure 4: Illustration of linear polarization (left) and circular polarization (right).

Most of the light found in nature, as well as the light produced by most artificial light sources, is a superposition of waves oscillating in different planes. The *degree of polarization* (DOP) measures the correlation between the different oscillation planes. Accordingly, it is possible to classify light according to its degree of polarization, ranging from *unpolarized light* (no correlation) to *polarized light* (maximum correlation) through a continuum of *partially polarized* states.

Although uncommon, light with very high DOP can be found in nature. For example, according to (Schechner and Karpel, 2005), the sun light gets polarized in underwater environments when traversing the interface between air and water. Also, some animals, especially in the marine fauna, take advantage of polarization by perceiving it analogously to color vision in humans (Wolff, 1997).

A *polarizer* is a device that converts unpolarized or partially polarized light into polarized light. This is commonly accomplished by filtering out those waves not meeting some restrictions in their oscillation plane. That is why polarizers are commonly referred to as *polarizing filters*. The cost of this approach is a very important loss of light intensity. Off-the-shelf polarizing filters reduce the light intensity more than 50%.

Polarizing filters are classified as *linear* and *circular*. A linear polarizing filter lets pass through it only those light waves with a certain, linear, polarization. Circular polarizing filters convert unpolarized light to circularly polarized light. This is accomplished by firstly performing a linear filtering and then shifting 45 degrees one of the two orthogonal components of the linearly polarized light. Accordingly, if the goal is to filter a certain oscillation plane, linear and circular polarizers are equivalent. However, cameras having auto-focus, auto-exposure or TTL light measurement cannot properly operate with linearly polarized light. Thus, if a polarizing filter has to be mounted on a digital camera, it has to be a circular polarizing filter.

### Extended Range Using Polarization

The different behaviour of objects and backscatter in front of polarized light can be used to improve contrast in underwater imaging. Some studies exploit this idea in underwater environments where sun light is sufficient and no artificial illumination is required (Karpel and Schechner, 2004; Schechner and Karpel, 2004; Schechner and Karpel, 2005). These studies are based on the following two assumptions. First, that the interface between air and water partially polarizes the sun light. Second, that backscatter preserves polarization whilst the observed objects do not. The author's proposal is to attach a polarizing filter to the camera and capture two images of the same scene using orthogonal polarization angles. By properly combining the resulting two images, backscatter can be significantly removed.

Similar approaches have been proposed (Morgan et al, 1997; Treibitz and Schechner, 2009) to deal with those underwater environments where sun light is not sufficient. In these cases, the artificial light source is endowed with a linear polarizer so that the scene is illuminated with polarized light, similarly to the previous case.

The aforementioned approaches have some problems, that are clearly described in the provided references. The most important one, especially when using these techniques in underwater robotics, is the need for two images to filter out backscatter. On the one hand, this reduces the available frame rate to the half. On the other hand, as the underwater robot moves, the two images may not correspond to the same scene.

Other approaches, such as the *polarized light stripping* (Gupta *et al.*, 2008) or the *polarization vision* (Wolff, 1997) are also useful in order to remove backscatter at the cost of additional, expensive hardware in the first case, or the requirement of three images per scene in the second case.

## Housing

An important issue when designing an underwater imaging system involving polarization is related to the interface of the camera with the water, as it should have a minimum effect on the polarization. In (Karpel and Schechner, 2004) some details regarding this issue are provided.

First, the housing must guarantee that the only light going through the camera lens comes from the viewing port. Other light sources must be blocked. Second, the stress in the transparent port's material changes the polarization of the light that it transmits due to the so called *photoelastic* effect. In order to reduce this effect, glass ports should be used instead of plastic ones and, more importantly, the polarizer should be placed outside the port, in contact with water.

Regarding the port's shape, the optimal choice is a dome whose center coincides with the center of projection of the camera lens.

## Experimental Evaluation

In order to evaluate the advantages and drawbacks of using a polarization-based system in underwater scenarios, we have implemented the proposal in (Treibitz and Schechner, 2009) and tested it in a water tank in our lab. As stated previously, this proposal consists in attaching a polarizing filter to the artificial light source and another polarizing filter to the camera. Then, one image is taken using orthogonal states for both polarizers and a second image is obtained being both polarizers in a parallel state. By combining both images, the effects of backscatter can be reduced.

The water tank size is 1.5m x 0.4m x 0.45m and contains 240 l of water. The only light source during the experiments was a 3Watt LED lamp endowed with a HOYA linear polarizer. The images were taken using an Olympus E510 camera with a circular polarizer attached to it. A calibrated sheet, as well as some other objects, were placed inside water. Also, in order to check the effects of water turbidity, different amounts of milk were dropped into water. Figure 5 illustrates our experimental setup.



Figure 5: The experimental setup.

Some of the obtained results are shown in Figure 6, where the two images taken for each scene, as well as the image resulting of the descatter process, are shown. The figure shows the results for different levels of water turbidity. Next, some analysis is provided.

The first thing that has to be taken into account when evaluating the obtained results is that this technique requires a very simple and cheap hardware. Thus, the question we want to answer is not if polarization based

methods are better than other complex and expensive techniques such as laser based ones, because the answer is probably that they are not. The question we want to answer is if polarization methods provide sufficient benefits with respect to simply using a camera with no filters and an unpolarized light source.

The main problem that we have observed is that polarizing filters strongly attenuate the light and this influences the quality of the images. In most cases, low illumination introduces noise in the image as the CCD performs poorly under these conditions. Because of that, using polarizers makes necessary to use stronger light sources involving more power consumption, and this may be problematic for an autonomous vehicle.

As it can be observed in Figure 6, the reconstructed image contains less backscatter than the two original ones. However, a detailed analysis of the images shows that the resulting image has more noise and is saturated in some areas. This observation is consistent with (Treibitz and Schechner, 2009), where it is stated that keeping the camera's exposure time constant, which is usual in video acquisition, never improves the *signal to noise ratio* (SNR) of the resulting images. Moreover, they also show that even using automatic exposure and assuming optimal exposure times there is SNR gain only in rare cases. We have also observed that the algorithm's results strongly depend on two parameters, named *p<sub>scat</sub>* and *p<sub>obj</sub>*. These parameters denote the expected amount of polarization preserved by backscatter and objects in the scene respectively and may change from one scenario to another.

The authors propose a method to obtain these values from one image, however, the method requires human intervention to select some particular areas in the images.

Finally, a requirement of this proposal is to use two images per scene obtained from the same camera position. This requirement is especially problematic for two reasons. On the one hand, using two images per scene reduces the available frame rate to the half. On the other hand, if the camera is attached to a moving underwater robot, it is not possible to guarantee that both images have been obtained from the same camera position.

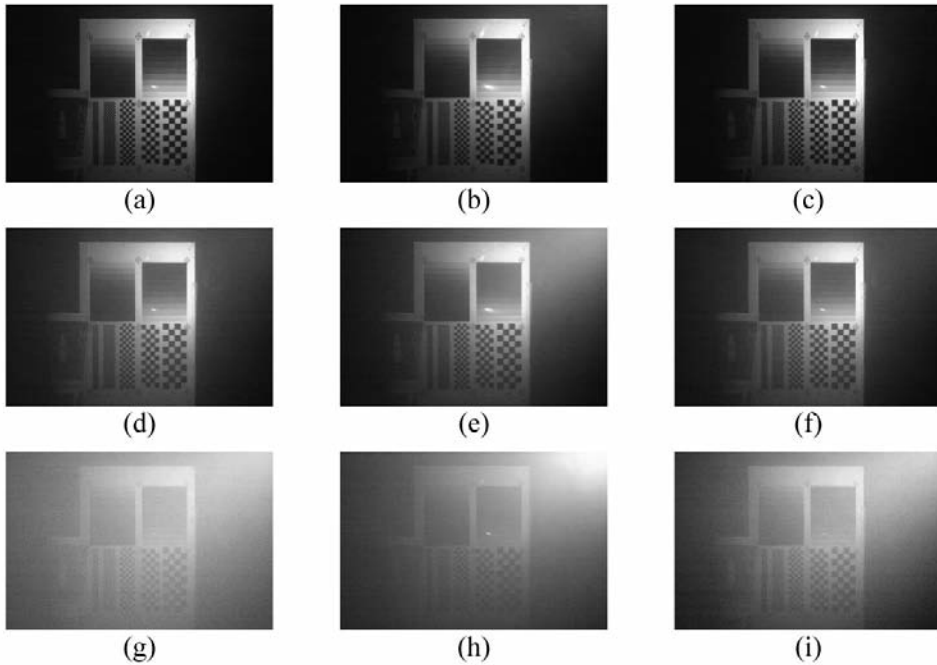


**Figure 6:** Some results using polarization. Left column: light and camera polarizers perpendicular. Central column: light and camera polarizers parallel. Right column: reconstructed image. First row: 10cc of milk. Second row: 20cc of milk. Third row: 50cc of milk.

As a conclusion, the studied approach is able to significantly reduce the negative effects of backscatter in the image formation at the cost of strongly reducing the light intensity and, thus, at the cost of reducing the SNR. Although this technique may be useful to obtain clear images using a stationary camera, additional problems appear when mounting it onto an underwater mobile robot. On the one hand, the proposed method to estimate the algorithm parameters requires human intervention and, thus, are not suitable for autonomous operation. On the other hand, as the robot is continuously moving, it is not possible to guarantee that the two required images are obtained from the same position.

## CONCLUSIONS

Due to the different interactions between water and light, sub-sea images have some special characteristics that have to be taken into account when designing an underwater optical imaging system. Aspects such as the illumination type or the camera's housing shape and material, which are generally not relevant in many terrestrial applications, become of crucial importance when going under water.

Additionally, if the imaging system has to be mounted on a ROV or an AUV, some additional constraints appear. In these cases, autonomy is very important and human intervention has to be reduced to the minimum. Thus, systems requiring some manual configuration during the image acquisition have to be avoided. Also, in AUVs that have no physical link with the support vessel, power consumption has to be considered. In these cases, power-demanding illumination systems should not be used.

This paper has surveyed different illumination techniques. Among the described approaches, the best way to improve the image quality while not dramatically increasing the AUV cost or power consumption, is to keep the light source and the camera as separated as possible. In this way, the volume of water where the emitted light and the camera's field of view intersect is reduced. This leads to a reduction of backscatter and, thus, to a higher contrast in the resulting image.

Also, the camera's housing has been analysed in this paper. The optimal shape is a dome whose center coincides with the center of projection of the camera lens. Also, in order to reduce the photoelastic effect, glass ports are preferred over those made of plastic materials. Finally, if some technique based on light polarization is used, the polarizing filter should be placed outside the dome, in contact with water, and special attention has to be paid to light sources not coming from the viewing port, as they have to be blocked.

Concerning to polarization, some studies have been surveyed. These studies are based on the assumption that backscatter behaves differently to the objects in the scene in front of polarized light. Some of the studies rely on the partial polarization produced when the sun light traverses the interface between air and water, whilst some other are meant to be used in areas where no sun light is available.

In both cases, the camera has to be endowed with a polarizing filter and the ability to switch it between two orthogonal states is needed. If images are taken by a human operator, this may be an easy task, but difficulties arise when the task has to be accomplished autonomously. Also, the requirement of two images per scene poses two problems. First, frame rate is reduced to the half. Second, obtaining two images of the same scene is difficult when the system is mounted on an AUV.

One of the surveyed polarization based methods has been tested in our lab. Results show some reduction of the backscatter effects in the image, meaning that the contrast is increased. However, due to the strong light attenuation produced by polarizers, the SNR is decreased. This reduction of the SNR reduces the performance of image analysis algorithms and, thus, it may lead to problems in autonomous systems.

To conclude, from the author's point of view, the best choice to improve image quality in underwater scenarios using an AUV, is to keep light source and camera as separated as possible and use a glass dome port. Polarization based techniques should be considered only when the vehicle is not moving and the resulting images are meant to be analysed off-line by human operators.

## ACKNOWLEDGEMENTS

This work is partially supported by DPI 2008-06548-C03-02, FP7- GA-2010-248497 and FEDER funding.

## REFERENCES

- Allen, B.; Austin, T.; Forrester, N.; Goldsborough, R.; Kukulya, A.; Packard, G.; Purcell, M. and Stokey, R. (2006). Autonomous docking demonstrations with enhanced Remus technology. In *Proceedings of IEEE OCEANS*, pp 1-6.
- Caimi, F.M.; Dalglish, F.R.; Giddings, T.E.; Shirron, J.J.; Mazel, C. and Chiang, K. (2007). Pulse versus cw laser line scan imaging detection methods: simulation results. In *Proceedings of IEEE OCEANS*, pp 1-4.
- Cochenour, B.; Mullen, L. and Laux, A. (2007). Phase coherent digital communications for wireless optical links in turbid underwater environments. In *Proceedings of IEEE OCEANS*, pp 1-5.
- Dalglish, F.R.; Caimi, F.M.; Britton, W.B. and Andren, C.F. (2009). Improved LLS imaging performance in scattering-dominant waters. In *International Society for Optical Engineering (SPIE)*, 73(17).
- Dalglish, F.R.; Caimi, F.M.; Britton, W.B.; Andren, C.F. and Wan, Y. (2008). Experimental comparison of pulsed-gated and continuous wave LLS underwater imagers. In *Proceedings of IEEE Ocean Optics XIX*.
- DIDSON (2009). Didson acoustic camera [online]. Available from: <http://www.soundmetrics.com/>.
- DOE (2009). Deep Ocean Engineering. Dhd2+2 ROV [online]. Available from: <http://www.deepocean.com/data.html>.
- IFE (2009). Institute for Exploration. Hercules ROV [online]. Available from: <http://www.mysticaquarium.org/ife/technology/340-hercules>.
- Funk, C.J.; Bryant, S.B. and Beckman, P.J. (1972). *Handbook of Underwater Imaging System Design*. Ocean Technology Department, Naval Undersea Center.
- Gilbert, G.D. and Pernicka, J.C. (1967). Improvement of underwater visibility by reduction of backscatter with a circular polarization technique. *Applied Optics*, 6(4), 741-746.
- Gordon, H.R. (1994). Modeling and simulating radiative transfer in the ocean, in: *Ocean Optics*, ed. *Oxford monographs on geology and geophysics*, Oxford University Press, 3-39.

- Gupta, M.; Narasimhan, S.G. and Schechner, Y.Y. (2008). On controlling light transport in poor visibility environments. In *Proceedings of IEEE Conference on Computer Vision and Pattern Recognition (CVPR)*, pp 1-8 .
- Han, H.; Zhang, X. and Ge, W. (2009). Performance evaluation of underwater range gated viewing based on image quality metric. In *Proceedings of Int'l Conference on Electronic Measurements and Instruments (ICEMI)*, volume 4, pp 441-444.
- He, S.; Li, L. and Zhou, Y. (2009). A new synchronization control circuit based on fpga for the laser range-gated imaging system. *OptoElectronic Letters*, 5(4).
- J. Horgan and D. Toal. (2009). Computer Vision Applications in the Navigation of Unmanned Underwater Vehicles, in *Underwater Vehicles*, In-Tech. 195-214,
- Jaffe, J.S. (1988). Underwater optical imaging: the design of optimal systems. *Oceanography*, 11(1), 40-41.
- Jaffe, J.S. (1990). Computer modeling and the design of optimal underwater imaging systems. *IEEE Journal of Oceanic Engineering*, 15(2), 101-111.
- Jaffe, J.S. (2007). Multi autonomous underwater vehicle optical imaging for extended performance. In *Proceedings of IEEE OCEANS*, pp1-4 .
- Karpel, N. and Schechner, Y.Y. (2004). Portable polarimetric underwater imaging system with a linear response. In *Proceedings of International Society for Optical Engineering (SPIE)*, volume 5432, pp 206-115.
- Kocak, D.M.; Dalgleish, F.R.; Caimi, F.M., and Schechner, Y.Y. (2008). A Focus on Recent Development and Trends in Underwater Imaging. *Marine Technology Society Journal*, MTSJ 42 (1), 52-67.
- Lam, K.; Bradbeer, R.S.; Shin, P.K.S. Kun, K.K.K. and Hodqson, P. (2007). Application of a real-time underwater surveillance camera in monitoring of fish assemblages on a shallow coral communities in a marine park. In *Proceedings of IEEE OCEANS*, pp 1-7.
- Laux, A.; Mullen, L. and Cochenour, B. (2007). I/q data processing techniques for the analysis of an amplitude modulated laser imaging system. In *Proceedings of Conference on Laser and Electro-Optics (CLEO)*, pp 1-2.
- Mobley, C.D. (1994). *Light and Water: Radiative Transfer in Natural Waters*. Academic Press, (CD Edition, 2004).
- Morgan, S.P.; Khong, M.P. and Somekh, M.G. (1997). Effects of polarization state and scatterer concentration on optical imaging through scattering media. *Applied Optics*, 36(7), 1560-1565.
- Narasimhan, S.G. and Nayar, S.K. (2005). Structured light methods for underwater imaging: Light stripe scanning and photometric stereo. In *Proceedings of IEEE OCEANS*, volume 3, pp 2610-2617.
- Negahdaripour, S. (1998). Revised Definition of Optical Flow: Integration of Radiometric and Geometric Cues for Dynamic Scene Analysis. *IEEE Trans. Pattern Analsis and Machine Intelligence*. (PAMI) 20 (9), 961-979

- Negahdaripour, S.; Zhang, H. and Han, X. (2002). Investigation of photometric stereo method for 3-d shape recovery from underwater imaging. *In Proceedings of IEEE OCEANS*, volume 2, pp 1010-1017.
- Negahdaripour, S. and Firoozfam, P. (2006). A rov stereovision system for ship-hull inspection. *IEEE Journal of Oceanic Engineering*, 31(3), 551-564.
- Negahdaripour, S.; Sekkati, H. and Pirsivash, H. (2007). Opti-acoustic stereo imaging: on system calibration and 3-d target reconstruction. *In Proceedings of IEEE Conference on Computer Vision and Pattern Recognition (CVPR)*, pp 1-8.
- Ortiz, A. (1998) Aplicación de técnicas de visión por computador a entornos submarinos. *Technical report- Universitat de les Illes Balears*.
- Ortiz, A. and Antich, J., (2009). Bayesian Visual Tracking for Inspection of Undersea Power and Telecommunication Cables, *Journal of Maritime Research*, Vol 6, Num 2 pp 83-98, 2009.
- Ortiz, A. and Oliver, G. (2006). Radiometric Calibration of Vision Cameras and Intensity Uncertainty Estimation. *Image and Vision Computing, (IVC)* 24 (10), pp 1137-1145.
- Ortiz, A. and Oliver, G. (2010). Analysis of Colour Channel Coupling from a Physics-based Viewpoint: Application to Colour Edge Detection, *Pattern Recognition*, 43(7), pp 2507-2520.
- Rosenkranz, G.E.; Gallager, S.M.; Shepard, R.W. and Blakeslee, M. (2008). Development of a high-speed, megapixel benthic imaging system for coastal fisheries research in alaska. *Fisheries Reseach*, 92(1), 340-344.
- Roston, J.; Bradley, C. and Cooperstock, J.R. (2007). Underwater window: High definition video on venus and neptune. *In Proceedings of IEEE OCEANS*, pp 1-8.
- Schechner, Y.Y. and Karpel, N. (2004). Clear underwater vision. *In Proceedings of the IEEE Computer Vision and Pattern Recognition (CVPR)*, volume 1, pp 536-543.
- Schechner, Y.Y. and Karpel, N. (2005). Recovery of underwater visibility and structure by polarization analysis. *IEEE Journal of Oceanic Engineering*, 30(3), 570-587.
- Sedlazeck, A.; Kser, K. and Koch, R. (2009). 3d reconstruction based on underwater video from rov kiel 6000 considering underwater imaging conditions. *In Proceedings of IEEE OCEANS*, pp 1-10.
- Singh, H.; Howland, J.; Pizarro, O. (2004). Advances in large-area photomosaicking underwater. *IEEE Journal of Oceanic Engineering, (JOE)* 29 (3).
- Shortis, M.R.; Seager, J.W.; Williams, A.; Barker, B.A. and Sherlock, M. (2007). A towed body stereo-video system for deep water benthic habitat surveys. *In Proceedings of the Eighth Conference on Optical 3-D Measurement Techniques*, volume 2, pp 150-157.
- Swartz, B.A. (1994). Laser range gate underwater imaging advances. *In IEEE OCEANS*, volume 2, pages 722-727.
- WHMS (2009). Woods Hole Marine Systems. Argus rov. <http://www.whmsi.com/>.
- Tan, C.S.; Sluzek, A.; Seet, G.L. and Jiang, T.Y. (2006). Range gated imaging system for underwater robotic vehicle. *In Proceedings of IEEE OCEANS*, pp 1-6.

- Taylor, G. and Kleeman, L. (2006). Shape Recovery Using Robust Light Stripe Scanning, in *Visual perception and robotic manipulation*, volume 26, 31-56.
- Treibitz, T. and Schechner, Y.Y. (2006). Instant 3descatter. In *Proceedings of the IEEE Computer Vision and Pattern Recognition (CVPR)*, volume 2, pp 1861-1868.
- Treibitz, T. and Schechner, Y.Y. (2009). Active polarization descattering. *IEEE Transactions on Pattern Analysis and Machine Intelligence*, 31(3), 385-399.
- Treibitz, T. and Schechner, Y.Y. (2009). Polarization: Beneficial for visibility enhancement ? In *Proceedings of the IEEE Conference on Computer Vision and Pattern Recognition (CVPR)*, pp 525-532.
- Weidemann, A.; Fournier, G.R.; Forand, L. and Mathieu, P. (2005). In harbor underwater threat detection/identificacion using active imaging. In *Proceedings of International Society for Optical Engineering (SPIE)*, volume 5780, 59-70
- Widder, E. (2007) . Sly eye for the shy guy. *Oceanography*, 20(4), 46-51.
- Wolff, L.B. (1997). Polarization vision: a new sensory approach to image understanding. *Image and Vision Computing*, 15, 81-93.
- Wu, L.; Shen, Y.; Li, G., Chen, C. and Yang, H. (2009). Modelling and simulation of range-gated underwater laser imaging systems. In *Proceedings of International Society for Optical Engineering (SPIE)*, volume 7382.
- Zheng, B.; Liu, B.; Zhang, H. and Gulliver, T.A. (2009). A laser digital scanning grid approach to three dimensional real-time detection of underwater targets. In *Proceedings of IEEE Pacific Rim Conference on Communications Computers and Signal Processing*, pp 798-801.



## **SIDECAN SONAR IMAGERY PROCESSING SOFTWARE FOR UNDERWATER RESEARCH AND EDUCATION PURPOSES**

**M. I. Zamanillo<sup>1</sup>, J. M. Zamanillo<sup>2</sup>, E. Revestido<sup>3</sup> and F. J. Velasco<sup>3</sup>**

Received 11 February 2011; in revised form 16 February 2011; accepted 20 March 2011

### **ABSTRACT**

Detailed submarine digital analysis of side scan sonar images significantly enhances the ability to assess seafloor features and artifacts digital images. These images are usually poor in their resolution if they are compared with optical images. There are commercial solutions that could solve this trouble, such as: the use of high resolution multibeam sidescan sonar, or the use of bathymetric sonar. Present work shows an economical solution to avoid this kind of problem by using digital image processing techniques under MATLAB environment. The application presented here is easy to use and has been developed under user friendly philosophy and could be operated for users at any level. Two types of sonar surveys, seafloor mapping and submerged target searches (buried or not), each require different processing methods for data analysis. This work is the first step and a general purpose tool for future lines of research in submerged objects recognition. Results are comparable in quality with commercial hardware solutions.

**Keywords:** SSS, single sidescan sonar, underwater, digital image processing, autonomous underwater vehicle, remotely operated vehicle.

<sup>1</sup> Professor, Electronics Technology, Systems and Automation Engineering Department (TEISA). University of Cantabria, Higher Technical Navigation School, C/Gamazo nº 1 39004 Santander (Cantabria), Spain. Email: isabel.zamanilloB@unican.es, Tel. +34 942 201331. <sup>2</sup> Professor, Communications Engineering Department (DICO). University of Cantabria. I+D+i Telecommunication Building, Plaza de la Ciencia, Av. de los Castros s/n, 39005 Santander (Cantabria), Spain. Email: jose.zamanillo@unican.es, Tel. +34943202219, Fax. +34942201488. <sup>3</sup> Professor, Universidad Electronics Technology, Systems and Automation Engineering Department (TEISA). University of Cantabria, Higher Technical Navigation School, C/Gamazo nº 1 39004 Santander (Cantabria), Spain. Email: franciscojesus.velasco@unican.es, Tel. +34942201368, Fax. +34942201303.

## INTRODUCTION

Digital images captured from the echoes of sidescan sonar onboard an unmanned undersea vehicle, are usually characterized for their low resolution. This is so because underwater, sound transmission is limited and this is most notable in useable ranges. The usable range of high frequency sound energy is greatly reduced by seawater, typically to around 50 to 150 m (Blondel, P. 2009). Low frequency sound energy is reduced at a much lesser rate with usable ranges of in excess of 250 m. achievable. Therefore, a tradeoff exists between higher resolution images produced by a high frequency side scan sonar and the longer range provided by a low frequency side scan sonar. In analyzing digital side scan sonar data numerous techniques have been demonstrated to correct and enhance the imagery as well as aid in interpretation (Lurton, X. 2002) (Medwin H. and Clay C.S. 1998)).

The collaboration of two research groups from different departments of the University of Cantabria have been necessary in the development of low cost and flexible software for digital processing of sidescan sonar images under MATLAB environment by using digital filtering and advanced signal processing techniques. Some of these techniques are already used in DVB digital video systems and broadcasting, with excellent results (Hardie, R.C. and Barner, K.E. 1996).

## MEASUREMENT TOOLS AND ENVIRONMENT

Advances in the fields of underwater technologies (Bellingham J.G. et al., 1994), robotics (Ishoy A., 2000), acoustical positioning (Marani, G., 2009), (Palomeras N. et al., 2010), remote sensing (Lillesand, Thomas M. and Kiefer, Ralph W. 1994), submarine guidance (Antich J., Ortiz A. and Oliver G., 2005) and digital processing imagery (Padmavathi, G. et al. 2010) have led to the development of Autonomous Underwater Vehicles (AUVs) and reached unimaginable levels only few years ago. Unlike other types of research can be carried out inside a laboratory or in the field, measurement tools used in this work must be adapted to a hostile environment as is the marine environment. These abilities have been enabled better and precise researches in several fields, such as: biological (Dahms, Hans-Uwe and Hwang, Jiang-Shiou, 2010), geological (Drury, Stephen A., 2001), zoological (Cheung, W.W.L. et al., 2009), natural resources (Wang Q. and Wang X., 2010), archeological (Bowens A., 2009) and military (Von Alt C., et al., 2001). These characteristics have led to the design of underwater vehicles with a built-in propulsion system, which has increased the possibilities of movement in the underwater environment. This is the situation of UUVs (Unmanned Underwater Vehicles) which are divided into two different categories:

- ROVs (Remotely Operated Vehicles), can be towed by a boat from the surface at moderate speeds.
- AUVs (Autonomous Underwater Vehicles), which are propelled by electric motors and governed autonomously remotely from the surface, from a ship or from land.

With these systems, the researcher can move relatively quickly to a few meters from the sea floor, following the topography of the same and recording video images to find a place or object of interest. The problem presented by these vehicles is that the image quality is degraded in terms of depth, and optical systems that capture images need powerful lighting systems, which in the case of autonomous vehicles (AUVs) without power connection through the umbilical wire to the surface is not feasible and sidescan digital sonar images are used against optical ones. Figure 1 (a) and 1 (b) show the ROV and AUV recently acquired by the University of Cantabria, and used in this work. Figure 1 (a) shows the ROV, model Seaeeye Falcon from the Swedish company SAAB, this vehicle is an auxiliary rescue vehicle equipped with an articulated arm. It is possible to use optical image recording underwater since it has powerful illuminators fed from the surface. This vehicle lacks of a sonar device (installation will be considered in the future) and this is the reason that direct comparison of optical images and the acoustic images is not available at this point.

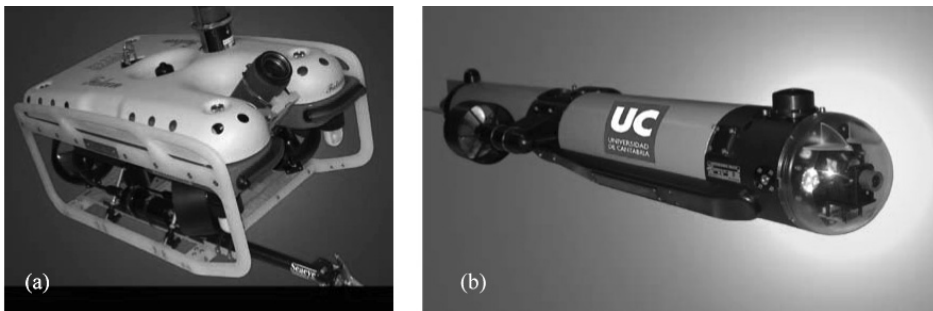


**Figure 1:** ROV and AUV owned by the University of Cantabria. (a) ROV, model Seaeeye Falcon from SAAB company. (b) AUV, model C'Inspector from Kongsberg company.

Figure 1 (b) shows the AUV, model C'Inspector from the Norwegian company Kongsberg, this is an autonomous vehicle equipped with a high speed optical fiber data connection of 1Km length. The vehicle can be used for inspection tasks in the background and detection of submerged objects and also it has been equipped with a. Tritech SeaKing Sidescan Sonar with 675 kHz of operating frequency and chirp modulation. This device has a narrow beam and shorter range (100m) for more detailed images of closer targets. Technical characteristics of this sonar are shown in Table I. Chirp side scan sonar utilizes pulse compression techniques to produce long transmission pulses and achieve long range without a resultant decrease in across-track resolution. The commercial implementation of Chirp side scan sonar is in a single beam configuration. Underwater, sound transmission is limited and this is most notable in useable ranges. The usable range of high frequency sound energy is greatly reduced by seawater, typically to around 50 to 100m (Blondel, P. 2009). Low frequency sound energy is reduced at a much lesser rate with useable ranges of in excess of 200m achievable.

**Table I:** Technical Characteristics From Tritech Seaking Sidescan Sonar.

Characteristics	Value
Operating Frequency	675 kHz (chirp modulation)
Horizontal Beam width (-3dB)	1° 0.5°
Vertical Beam width (-3dB)	50°
Weight in air/water	5.3kg/2.7kg
Maximum operating depth	4000 m
Power Requirements	18-36V@12VA
Control Connector	Tritech Sonar Connector
Transmitter Source Level	200 dB re 1 $\mu$ P @ 1 m
Transmitter Pulse Length	50 - 200 $\mu$ s
Receiver Sensitivity	> 2 $\mu$ V rms
Gain Control Range	80 dB
Display Dynamic Range	40 dB (Software Configurable)
Data Sampling Rates	5 - 200 $\mu$ s
Data Resolution	4-8 bits (Software Configurable)
Software	Tritech Seagnet Display Software or low level language commands
Data file format	Proprietary Tritech "V4Log"
Communication Protocols	Arcnet, RS-232
Communication data rates	RS232 hasta 115.2 kbaud, Arcnet 156 ó 78 kbaud

Therefore, a tradeoff exists between higher resolution images produced by a high frequency side scan sonar and the longer range provided by a low frequency side scan sonar. Unfortunately, the AUV C'Inspector vehicle is not capable of providing quality optical images below 1m in depth because the lack of external illuminators.

It is necessary to remark to refine and debug the software presented in this paper authors have been used some images from the sidescan sonar of C'Inspector taken in several measurement campaigns carried out in the Bay of Santander. But, most of the sonar images have been used to test and refine the algorithms of digital processing implemented in the software proceeds from free image libraries without copyrights from different Internet sites.

## SIDESCAN SONAR OPERATION AND ACOUSTIC SCATTERING THEORY

Single sidescan sonar devices transmit two beams, one on each side as it is shown in Fig.2. These beams are narrow along-track to get a high resolution, and wide across-track to cover as much range as possible. The distance from the sonar to a

point on the seabed or target is called the slant range. It should not be confused with the ground range, between this point the point immediately below the sonar. The angle of incidence of the incoming acoustic wave is a key factor in understanding how it will scatter. Most of the energy is reflected in the specular direction. Some will be reflected along other angles (scattering angles, distributed along the main refec-tion angle). Depending on the seafloor or the submerged target, some energy will be lost in the seabed. A very small portion, several orders of magnitude lower, might be reflected back toward the imaging sonar also known as backscatter (Blondel and Murton, 1997). The seabed reverberation area is mainly constituted by background noises (Zhang Xiao-wei, Zheng Xiong-bo and Shen Yang, 2010).

**Figure 2:** Definitions of basic geometric parameters used in sidescan sonar imagery.

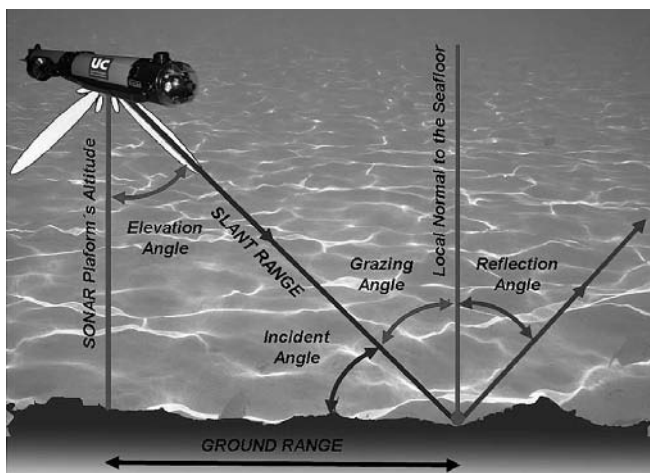
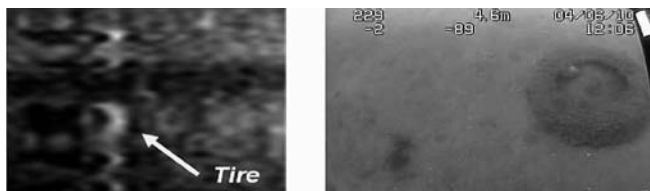


**Figure 3:** Comparison between a sidescan sonar image and the photograph of a tire in the Bay of Santander.



(a) Sidescan sonar image with noise of a tire in the Bay of Santander.

(b) Photograph image of the same tire made with the ROV

influences of the noise, it is very important to remove noises of sonar images, as it is shown in Fig. 3 (a) for a grayscale sidescan image. Fig 3 (b) shows a photograph of the same tire on a sandy seafloor.

The brightness of sonar image is related to the ratio between the echoes to the noise, if a comparison with ordinary optical images is made, sonar images are low frequency images and they have less detail, and the background noises of sonar images are high-frequency impulse noises with larger amplitudes relative to the multiple echoes from the target area. Because of the complexity of the underwater environment, the gray level or monochrome color of sonar image from the target area is usually smaller than that of background noise. To improve the visual effects and reduce the

## SIDESCAN SONAR ACQUISITION SOFTWARE

In present communication authors have been taking into account the geometrical requirements shown in the prior section with the aim to get the best quality sonar digital images. But, the sidescan sonar acquisition software has been provided by the sonar manufacturer of the device and it has several limitations as shown below. The standard file format use by the applications is the Trittech's proprietary format V4LOG which is not compatible with usual image processing tools that generally use standard types of video and static image formats, to load the file such as: AVI (Audio Video Interleave) or TIFF (Tagged Image File) formats for motion images and static ones. Although, the application add the calibration grid, to the image file, which is a serious limitation when the image is post-processed using digital techniques. This is because the export filter makes a screen capture or rasterization (this actuates like a flat bed scanner) of the image presented in the screen. To avoid this kind of problems now we are working a new in-house control software using the low level commands of the sidescan sonar.

During the first step of the research, our main effort has been focused on maximizing the quality of the original image provided by the commercial control software, so we used a, uncompressed TIFF storage format. We do not use any other most popular and compact graphic formats with uses compression such as JPG (Joint Experts Group) to avoid the introduction of additional errors or compression artifacts prior processing the image.

## IMAGE EASY SONAR SOFTWARE

The interpretation of sonar images has traditionally been performed visually by trained interpreters (Blondel, P. 2009); this feature presents the distinct advantage of using the skill of the human interface to limits which are often unattainable by computers. But there are also many disadvantages to a purely visual interpretation. First of all, it is a subjective procedure: two interpreters with different experience, or different skills, are likely to get different interpretations for some features and details, depending on their experience of the sonar used or of the environment studied. Visual interpretation is also time-consuming, and a longer amount of time spent on analysis does not ensure higher objectivity. As a result of this, present work has been focused in the use of existing techniques applied in other areas of image digital processing to the problem of sidescan sonar image processing. As a result of our research, a simple and powerful software tool called *ImageEasySonar*, has been developed. The application has been programmed under the friendly user philosophy and could be operated by users at any level and would be used in educational and training purposes. Although, the software could be running in different hardware platforms such as: PC, Apple Macintosh, UNIX and, Linux machines because it has been write under MATLAB environment. Another advantage consists in source code

can easily modified by the programmer. In addition, through integrated MATLAB tool guide is possible to develop professional applications with elements such as: pull-down menus, pop-up menus, dialog boxes, alerts, etc. without the person responsible for coding should make further efforts to create such objects. All these features, combined with mathematical optimization routines and processing accompanying the MATLAB software package has enabled that the first version of software *ImageEasySonar* presented here has been operative in a relatively short time.

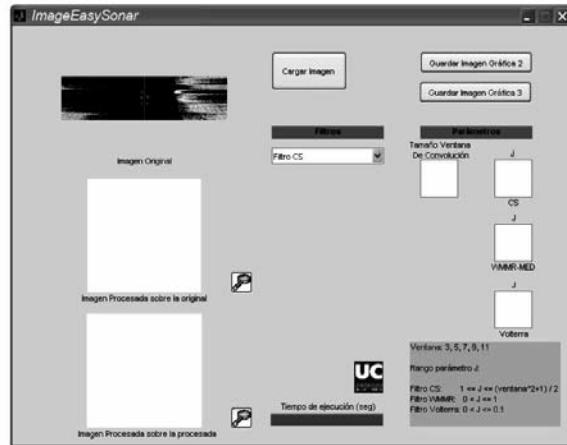


Figure 4: Aspect of the main interface of ImageEasySonar software.

## DIGITAL ALGORITHMS AND FILTERS USED IN IMAGE EASY SONAR SOFTWARE

The spatial filtering operation techniques are applied to a digital image and highlight or reduce details in order to simplify visual interpretation or provide further processing. These techniques included in the image enhancement toolbox of MATLAB, improve edge detail images and thus refocus digitally the scene digitally to reduce or eliminate noise patterns in digital video before making a DVB transmission and they are considered as local operations in digital image processing, in the sense of changing the value of each pixel in accordance with the values of the pixels that surround it, transforming it comes to original levels so that they resemble or differ more than those for neighboring pixels (Parker, J.R., 1996). The image enhancement algorithms are applied to remotely sensed images in order to improve the appearance of an image for the human visual analysis or occasionally for further computer analysis (Lee Y. and Fam A., 1987). A possible classification of spatial filters based on its linearity, being able to distinguish between linear and nonlinear filters. Within the first section we can distinguish the spatial filters according to their spatial frequency. CS filters (Comparison and Selection), (Lee Y. and Fam A, 1987), WMMR-MED (Weighted Majority of M values with Minimum Range), (Longbotham, H. and Eberly, D., 1993), Volterra (Taiho Koh and Powers, E., 1985) and EDGE (Canny, J. 1986), (Hardie, R.C, Barner, K.E. 1996) , among others discussed in this paper correspond to the group of non-linear enhancement filters. In addition to the aforementioned filtering tech-

niques, it has been implemented in the program 14 additional filters from the image processing MATLAB toolbox. The user of ImageEasySonar can select among 17 different image process techniques, which are widely detailed in the literature (Canny, J. 1986), (Corinthios, M., 1999), (Longbotham, H. and Eberly, D., 1993), (Mitra, S.K., et al., 1991), (Jensen, John R. 1996), (Zhuo, S. Guo D. and Sim, T., 2010).

The Comparison and Selection (CS) filter is one of the simpler enhancement filters (Lee Y. and Fam A, 1987). As an example, we give a brief explanation about this filters works. The first step is to choose the color space to apply the transformation, if grayscale is chosen the mathematical transformation is apply to one layer. If RGB space is chosen it is necessary to apply separately the technique layer by layer (Red layer, Green layer and Blue layer) as it is shown in figure 5(a) and Fig 5 (b). Values are in the integer range from 0 up to 255. This feature expands by other tree the computation time.

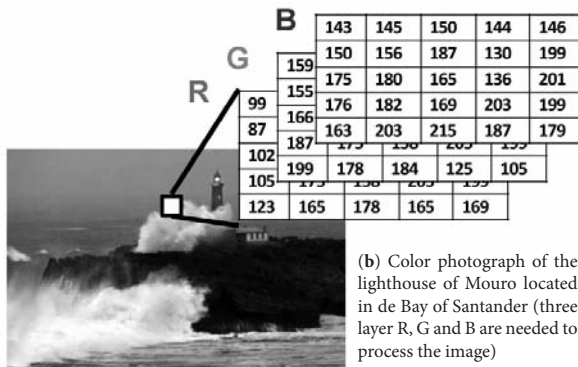
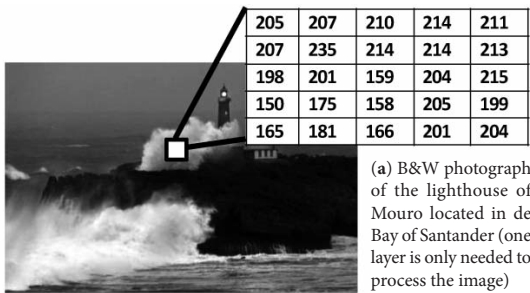


Figure 5: The color space is an important election to apply spatial digital filtering.

The second step consist in properly choose the geometry (linear, square, circular, etc) and size (3x3 pixels, 5x5 pixel, 9x9 pixels or 11x11 pixels), of the movable exploring window or kernel, which size makes more visible the edges as shown in Fig. 6 (c), or soften as it is shown in figure 6 (b). Third step consist to properly fix the J parameter of the algorithm, this parameters fixed the distance (in pixels) from the mean of all numerical values of the kernel renumbered from reordered from the minimum to the maximum according with the following.

The output  $Y_k$  of the CS filter with parameter J at time k is defined through the input values  $X_k-N, \dots, X_k+N$ , in a window of length  $2N+1$ , for a positive integer N by:

$$Y_k = \begin{cases} X_k^{(N+1-J)}, & \text{if } \mu_k \geq M_k \\ X_k^{(N+1+J)}, & \text{otherwise} \end{cases} \tag{1}$$

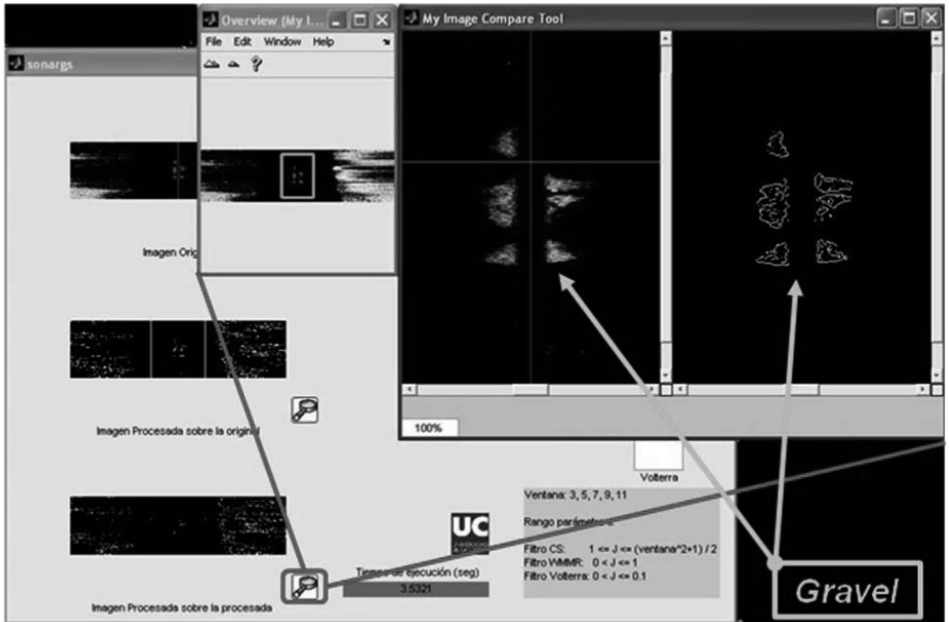
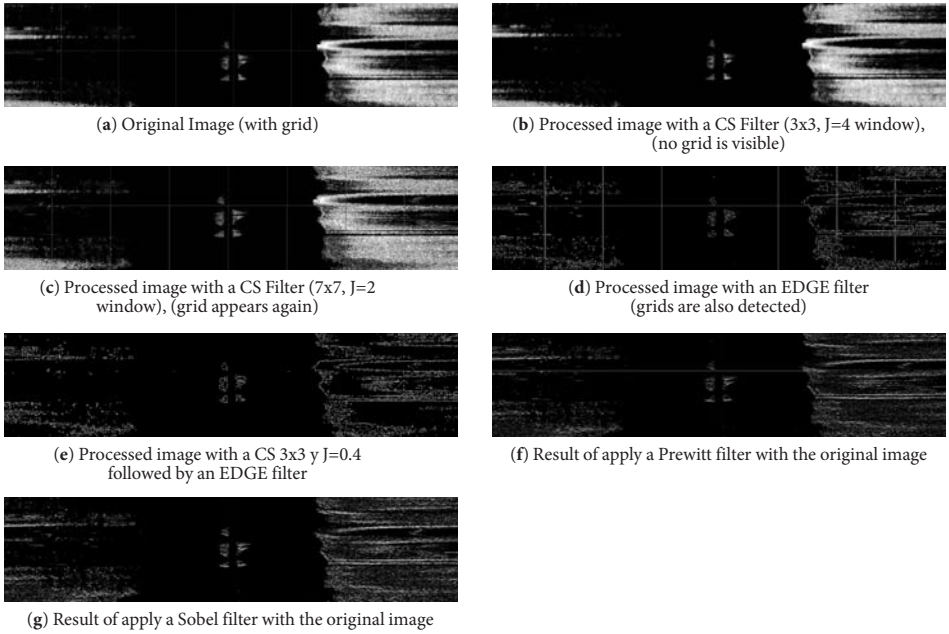
where  $X_k^{(i)}$  is the  $i$ th smallest sample inside the window,  $\mu_k$  and  $M_k$  are the sample mean and median, respectively, and  $J$  is an integer satisfying  $1 \leq J \leq N$ .

When  $J = N$ , the CS filter selects either the minimum or the maximum value in the window depending on the data. For the case of  $J = 0$ , this filter reduces to the well investigated median filter. Since CS filters are nonlinear, the superposition property does not hold in its general form. (Lee Y. and Fam A., 1987). The CS filter ranks the values in the filter window or kernel in numerical order, and calculates the mean value. Parameter  $J$  identifies a pair of rank numbers (measured inward from the top and bottom of the rank list) whose corresponding raster values provide the two possible filter output values. If the center cell value is less than the window mean, the lower output value is assigned, and if it is greater than the mean, the higher output value is used. The CS filter sharpens blurred edges while smoothing non-edge areas. The sharpening effect increases with lower values of Parameter  $J$  (which move the filter output values farther from the mean).

Some of the results obtained when applying digital filtering techniques just been discussed and depicted in Figure 6. For brevity the mathematical expressions used in each filtering technique are not shown here and we have ignored many of the results obtained for other images. Another interesting feature of the application is that user can apply several different digital filters on the same image and visualize graphically, original image and up to two different transformations before save them into the hard disk An important parameter the execution time of each digital filtering process, which is dependent on the selected parameters in the application as shown in Figure 6 (b) and Figure 6 (c) obtained as the digital processing from the image shown in Figure 6 (a).

Figure 6 (d) shows the result of applying the algorithm edge (it is noticeable that the calibration grid is visible) to the image, while filtering when combined CS plus edge filtering, result not only removes the grid also shows in detail the edges of the processed image. The edge detection class is designed to detect and highlight boundaries between image areas that have distinctly different brightness. The output raster is a grayscale image of the edges, with the cell brightness proportional to the difference in neighboring cell brightness in the original image. The resulting image can be used as the basis for additional image interpretation and analysis, such as image segmentation.

Filtering techniques based on the Prewitt filters and/or Sobel shown in Figure 6 (f) and Figure 6 (g) require a lower computational cost than the above-mentioned CS, and EDGE WWMED. In our case, the result not only gives different color to the original image but it gives an appearance of high-relief, or false 3D. Results are similar results to those obtained with more expensive hardware. As for future work, authors wish to apply these techniques in real-time time or at least “quasi-real” time in this part of the research the main goal has been the computational speed versus quality processing.



(h) Aspect of the Zoom tool of ImageEasySonar

**Figure 6:** Aspect of the interface and results of digital processing sidescan sonar images using ImageEasySonar softwar.

The hardware and software characteristics used in this study, are presented here:

- PC compatible with  $\mu$ P AMD Athlon64 X2 Dual Core @ 3.01 GHz y 2 GB RAM DDR memory.
- Operative System Windows XP Professional v2002 with Service Pack2.
- MATLAB R2009b 7.9.0.

CPU computation time is less than 5% with about 40 processes running at that time and increasing from 50 to 55% during the processing of the filter applied. The memory usage during the process of computing including loading the program itself in any case not exceeds 90 MBytes. Figure 6 (h) shows the zoom tool included in the application that allows seeing the details more clearly, even compared to the initial image. The novelty of the work presented here is the use of these techniques designed for static and DVB video optical captured images to “acoustically” ones from low resolution single sidescan sonar.

## CONCLUSIONS

It has developed an application software that allows processing images from a sidescan sonar by using techniques of post-digital signal processing, some of them already used in DVB digital video systems. The intuitive interface to use has been programmed under user-friendly, and WYSIWYG (What you see is what you get) philosophies and could be operated for users at any level for research or educational purposes. Furthermore, the application allows the overlapping of different filtering techniques and improving the image quality on the same box or frame. By applying the Prewitt and Sobel filters is possible to get an approximate high relief profile of the seafloor without the need of acquires expensive hardware like: multibeam side-scan sonar or a slow scan by bathymetric sonar.

## ACKNOWLEDGMENTS

Authors would like to thank the Scientific and Technical Services Research (SCTI), of the University of Cantabria under the supervision of Vicerrectorado de Investigación y Transferencia Tecnológica, and the Regional Government of Cantabria for the logistical and financial support without this work has not been realized.

**REFERENCES**

- Antich, J. et al. (2005). "A PFM-based control architecture for a visually guided underwater cable tracker to achieve navigation in troublesome scenarios". *Journal of Maritime Research*, Vol. II, No. 1, pp. 33-50.
- Bellingham, J.G. et al. (1994): A second generation survey AUV, in *Proc. Autonomous Underwater Vehicle Technology*, July pp. 148-155.
- Blondel, P. (2009): *The Handbook of Sidescan Sonar*. Springer/Praxis, Heidelberg, Germany/Chichester, U.K., 316 pp.
- Blondel, P. and B.J. Murton (1997): *Handbook of Seafloor Sonar Imagery*. Wiley/Praxis, Chichester, U.K.
- Bowens, A. (2009): *Underwater Archaeology: The NAS Guide to Principles and Practice Second Edition*, Blackwell Publishing, UK, 220pp.
- Canny, J. (1986): A Computational Approach to Edge Detection, *IEEE Transactions on Pattern Analysis and Machine Intelligence*, Vol. PAMI-8, No. 6, pp. 679-698.
- Cheung, W.W.L.; Lam, V.W.Y.; Sarmiento, J.L.; Kearney, K.; Watson, R. and Pauly, D. (2009): Projecting global marine biodiversity impacts under climate change scenarios. *Fish and Fisheries*, Wiley. Vol. 10, pp. 235-251.
- Corinthios, M. (1999): *Signals, Systems, Transforms, and Digital Signal Processing with MATLAB*. CRC Press, pp. 1316.
- Dahms, Hans-Uwe and Hwang, Jiang-Shiou, (2010) :Perspectives of underwater optics in biological oceanography and plankton ecology studies. *Journal of Marine Science and Technology*, Vol. 18, No. 1, pp. 112-121
- Drury, Stephen A. (2001): *Image Interpretation in Geology (3rd ed.)*. Chapter 5, *Digital Image Processing*. New York: Routledge. pp. 133-138.
- Hardie, R.C.; Barner, K.E. (1996): Extended permutation filters and their application to edge enhancement. *IEEE Transactions on Image Processing*, Vol. 5, No. 6, Jun, pp.855-867
- Hardie, R.C. and Boncelet, C., (1993): LUM filters: a class of rank-order-based filters for smoothing and sharpening, *IEEE Transactions on Signal Processing*, Vol. 41, pp. 1061-1076.
- Hardie, R.C. and Boncelet, C.G., (1995): Gradient-based edge detection using nonlinear edge enhancing prefilters, *IEEE Transactions on Image Processing*, Vol.4 (11), 1572-1577.
- Ishoy, A. (2000): How to make survey instruments "AUV-friendly", in *Proc. MTS/IEEE Int. Conf. OCEANS*, pp. 1647-1652.
- Jensen, J. R., (2005): *An Introductory Digital Image processing: A remote sensing perspective Image enhancement*, Prentice-Hall, UpperSaddle River N.J. 526 pp.
- Jensen, John R. (1996): *Introductory Digital Image Processing: a Remote Sensing Perspective (2nd ed.)*. Chapter 7, *Image Enhancement*. Upper Saddle River, NJ: Prentice-Hall. pp. 153-172.

- Lee Y. and Fam A, (1987): An edge gradient enhancing adaptive order statistic filter. *IEEE Transactions on Acoustics, Speech, and Signal Processing* Vol.35, pp. 680-695
- Lillesand, Thomas M. and Kiefer, Ralph W. (1994): *Remote Sensing and Image Interpretation* (3rd ed.). Chapter 7, *Digital Image Processing*. New York: John Wiley and Sons. pp. 585-618.
- Lim, Jae S.,(1990): *Two-Dimensional Signal and Image Processing*, Englewood Cliffs, NJ, Prentice Hall, pp. 478-488.
- Longbotham, H. and Eberly, D., (1993): The WMMR filters: a class of robust edge enhancers, , *IEEE Transactions on Signal Processing* Vol. 41, pp. 1680-1685.
- Lurton, X. (2002): *An Introduction to Underwater Acoustics*. Springer/Praxis, Heidelberg, Germany/Chichester, U.K., 380 pp.
- Marani, G. (2009): Advances in autonomous underwater intervention for AUVs, in *Work Shops and Tutorials, 2009 IEEE International Conference on Robotics and Automation*. Kobe, Japan.
- Medwin, H. and Clay, C.S. (1998): *Fundamentals of Acoustical Oceanography*. Academic Press, London, 712 pp.
- Mitra, S.K.; Li, H.; Lin, I.-S. and Yu, T.-H. (1991): A new class of nonlinear filters for image enhancement, *Acoustics, Speech, and Signal Processing*, 1991. ICASSP-91., 1991 International Conference on 4, 2525-2528.
- Padmavathi, G.et al. (2010): Comparison of Filters used for Underwater Image Pre-Processing. *IJCSNS International Journal of Computer Science and Network Security*, VOL.10 No.1, January, pp.58-65.
- Palomeras, N. et al.,(2010): Distributed Architecture for Enabling Autonomous Underwater Intervention Missions, in *Proceedings Of the 4th Annual IEEE International System Conference*. San Diego, USA.
- Parker, James R., (1996): *Algorithms for Image Processing and Computer Vision*, New York, John Wiley & Sons, Inc., pp. 23-29.
- Poularikas, A.D. and Ramadan, Z.M. (2006): *Adaptative Filtering Primer with MATLAB*. Taylor & Francis. CRC Press.
- Russ, J.C. (2007): *The Image Processing Handbook*. 5th Edition. CRC Press.pp.817.
- Taiho Koh and Powers, E., (1985): Second-order Volterra filtering and its application to nonlinear system identification, *IEEE Transactions on Acoustics, Speech, and Signal Processing*, Vol. 33, pp. 1445-1455.
- Thurnhofer, S. and Mitra, S.K., (1996): A general framework for quadratic Volterra filters for edge enhancement, *IEEE Transactions on Image Processing*, Vol. 5 pp. 950-96.
- Urlick, R.J. (1996): *Principles of Underwater Sound*, Third Edition. Peninsula Publishing, Los Altos, CA, 444 pp.
- Uvais Qidwai and C.H. Chen: *Digital image processing, An algorithmic approach with MATLAB*. Chapman and Hall Textbooks in computing. CRC Press ISBN 978-1-4200-7950-0.

- Von Alt, C., et al. (2001): Hunting for mines with REMUS: A high performance, affordable, free swimming underwater robot, in Proc. MTS/IEEE Int. Conf. OCEANS, pp. 117-122.
- Wang, Q. and Wang, X. (2010): Interferometric Fiber Optic Signal Processing Based on Wavelet Transform for Subsea Gas Pipeline Leakage Inspection. International Conference on Measuring Technology and Mechatronics Automation (ICMTMA 2010), pp. 501-504.
- Zhang Xiao-wei; Zheng Xiong-bo and Shen Yang, (2010): Sidescan sonar image de-noising algorithm in multi-wavelet domain. Computer Application and System International Conference on Modeling (ICCASM 2010), Vol: 2, pp. 367-371.
- Zhuo, S.; Guo D. and Sim, T. (2010): T. Robust Flash Deblurring, IEEE Conference on Computer Vision and Pattern Recognition (CVPR), pp. 2440-2447.



## INSTRUCTIONS FOR AUTHORS

<http://www.jmr.unican.es>

### Description

Journal of Maritime Research (JMR) publishes original research papers in English analysing the maritime sector international, national, regional or local. JMR is published quarterly and the issues—whether ordinary or monographic—include both theoretical and empirical approaches to topics of current interest in line with the editorial aims and scope of the journal.

The objective of JMR is to contribute to the progress, development and diffusion of research on the maritime sector. The aim is to provide a multidisciplinary forum for studies of the sector from the perspective of all four of the following broad areas of scientific knowledge: experimental sciences, nautical sciences, engineering and social sciences.

The manuscripts presented must be unpublished works which have not been approved for publication in other journals. They must also fulfil all the requirements indicated in the 'Technical specifications' section. The quality of the papers is guaranteed by means of a process of blind review by two scientific referees and one linguistic reviewer. Although the journal is published in print format, the processes of submission and reception of manuscripts, as well as revision and correction of proofs are all done electronically.

### The publication process

#### *Submission and acceptance of manuscripts*

Papers should be sent via the journal's web site at <http://www.jmr.unican.es>, following the guidelines indicated for the submission of manuscripts by authors. Submitting the manuscript involves sending electronically via the web site three different types of information: general information about the article and the authors, an abstract and the complete paper.

The general information about the article and the authors, as well as the acknowledgements, is to be introduced by means of an electronic form, in which the following data are requested:

- Title of the paper. Subtitle.
- Field of the manuscript presented (Experimental Sciences, Engineering, Nautical Sciences or Social Sciences) and sub-field.
- E-mail of the author to whom correspondence should be addressed.
- Personal data of each author including name, professional category or position, institution or organisation, postal address and e-mail.
- Acknowledgements, if included, should be no longer than 150 words without spaces between paragraphs.

The manuscripts submitted which are in line with the aims and scope of JMR will be submitted to a blind review process. The objective is to assess the scientific quality (two referees) and ensure that the text is linguistically acceptable (one reviewer). Only those works which are considered adequate from a scientific point of view will be reviewed linguistically. Manuscripts

which do not pass the linguistic filter will be admitted with the condition that the author make linguistic and stylistic modifications as indicated.

Authors will be informed of the acceptance, rejection and/or modifications required no later than four months after the receipt of the manuscript. Once the paper has been accepted, authors can check on the status of their article via the web site. Any doubts or questions should be addressed to the Editor at [jmr@unican.es](mailto:jmr@unican.es)

### Copyright

After manuscripts have been definitively accepted, the authors must complete the copyright agreement assigning the copyright to JMR so that it can be published.

### Proofs

Once the copyright transfer agreement has been completed, the Editors will assign the paper to an upcoming issue of JMR and proofs will be sent as a PDF file to the author who has corresponded with JMR throughout the reviewing process. The corrected proofs must be returned by e-mail to the Editor of JMR within 96 hours of receipt.

### Reprints

Once the paper has been published, the authors will be sent a total of 12 free reprints, which will be sent the postal address of the corresponding author. Authors may also request, via the JMR web site <http://www.jmr.unican.es>, a maximum of 10 complete journals at 50% of the cover price.

### Style and technical specifications

Manuscripts should be sent to JMR's web site in a format that is recognisable to Microsoft Word (.doc) in any of its versions for Windows. The maximum length of manuscripts is 23 double-spaced pages (approximately 7000 words) including the abstract, references and appendices. Manuscripts will be submitted using a specific application of the electronic form used to send personal data. The page layout should follow these guidelines:

- Size: DIN A4 (29 cm by 21 cm)
- Margins, 3 cm: top, bottom, left, and right.
- Font: Times New Roman, normal style, 12-point type.
- Double spacing should be used for all the paper except for the references which are to be single-spaced.
- Notes, when necessary, are to be placed at the end of the paper and numbered in their order of appearance in the text. Mathematical derivations should not be included in these endnotes.

The abstract is to be presented on one page and should include the following information:

- Title and subtitle of the paper
- Field and sub-field of the work presented.
- Abstract, which is to be no longer than 200 words, and should have no spaces between paragraphs.

- Key words (between 3 and 5) which will be used for computerised indexing of the work, in both Spanish and English.
- The complete work should be no longer than 23 pages (about 7000 words) and should be structured as is shown below.

The first page will contain the same information as the summary:

- Title of the paper, as specific and brief as possible, and subtitle if desired.
- Field and sub-field of the work presented.
- Abstract of 200 words.
- Key words.

The rest of the article:

- Introduction or Problem
- Methods
- Development (application and results)
- Conclusions
- Endnotes
- References. Only those included in the article in alphabetical order.
- Appendix containing a condensed version of the article in Spanish. This is to be 3 or at most 4 pages in length (approximately 1000-1200 words) with the following sections: abstract, methods and conclusions.

The body of the article is to be divided into sections (bold, upper-case), subsections (bold, italics) and optionally into sub-subsections (italics), none of which are to be numbered. Insert line spaces before and after the title of each section, subsection and sub-subsection. Symbols, units and other nomenclature should be in accordance with international standards.

## References

The Harvard System is to be used, following the guidelines indicated below.

The way in which *bibliographic citations* are included in the text will depend on the context and the composition of the paragraph and will have one of the following forms:

- One author: Farthing (1987); (Farthing, 1987); (Farthing, 1987 pp. 182-5)
- Several authors: Goodwin and Kemp (1979); Ihere, Gorton y Sandevar (1984); Ihere et al.(1984); (Ihere et al., 1984)

The *bibliographic references* are to be arranged in alphabetical order (and chronologically in the case of several works by the same author), as is indicated in the following examples:

### Books

Farthing, B. (1987) *International Shipping*. London: Lloyd's of London Press Ltd.

### Chapters of books

Bantz, C.R. (1995): Social dimensions of software development. In: Anderson, J.A. ed. *Annual review of software management and development*. Newbury Park, CA: Sage, 502-510.

### Journal articles

Srivastava, S. K. and Ganapathy, C. (1997) Experimental investigations on loop-manoeuvre of underwater towed cable-array system. *Ocean Engineering* 25 (1), 85-102.

### Conference papers and communications

Kroneberg, A. (1999) Preparing for the future by the use of scenarios: innovation shortsea shipping, *Proceedings of the 1<sup>st</sup> International Congress on Maritime Technological Innovations and Research*, 21-23 April, Barcelona, Spain, pp. 745-754.

### Technical Reports

American Trucking Association (2000) *Motor Carrier Annual Report*. Alexandria, VA.

### Doctoral theses

Aguter, A. (1995) *The linguistic significance of current British slang*. Thesis (PhD).Edinburgh University.

### Patents

Philip Morris Inc., (1981). *Optical perforating apparatus and system*. European patent application 0021165 A1. 1981-01-07.

### Web pages and electronic books

Holland, M. (2003). *Guide to citing Internet sources* [online]. Poole, Bournemouth University. Available from: [http://www.bournemouth.ac.uk/library/using/guide\\_to\\_citing\\_internet\\_sourc.html](http://www.bournemouth.ac.uk/library/using/guide_to_citing_internet_sourc.html) [Accessed 1 November 2003]

### Electronic journals

Storchmann, K.H. (2001) The impact of fuel taxes on public transport — an empirical assessment for Germany. *Transport Policy* [online], 8 (1), pp. 19-28 . Available from: <http://www.sciencedirect.com/science/journal/0967070X> [Accessed 3 November 2003]

### Equations, tables, Illustrations.

*Equations* are to be written with the Microsoft Word Equation Editor using right-justified alignment. They should be numbered consecutively using Arabic numerals within parentheses.

*Tables* should be inserted in the appropriate point in the text using Microsoft Word. They should be numbered consecutively with Arabic numerals and a concise title should be centred at the top of the table. The source is to be indicated at the bottom on the left. Any symbols used should be explained.

*Illustrations* are to be inserted in the appropriate point in the text using Microsoft Word. All illustrations (graphs, diagrams, sketches, photographs, etc.) will be denominated generically Figures and are to be numbered consecutively using Arabic numerals with the title centred at the top. The source is to be indicated at the bottom on the left. Photographs must be in black and white with a quality of at least 300 ppp.

